AD-A070 102 AIR FORCE INST OF TECH WRIGHT-PATTERSON AFB OHIO SCH--ETC F/G 20/4
AN EXPERIMENTAL EVALUATION OF A LASER VELOCIMETER BY THE STUDY --ETC(U)
JUN 79 N G CERULLO

UNCLASSIFIED AFIT/GAE/AA/79J-1 NL

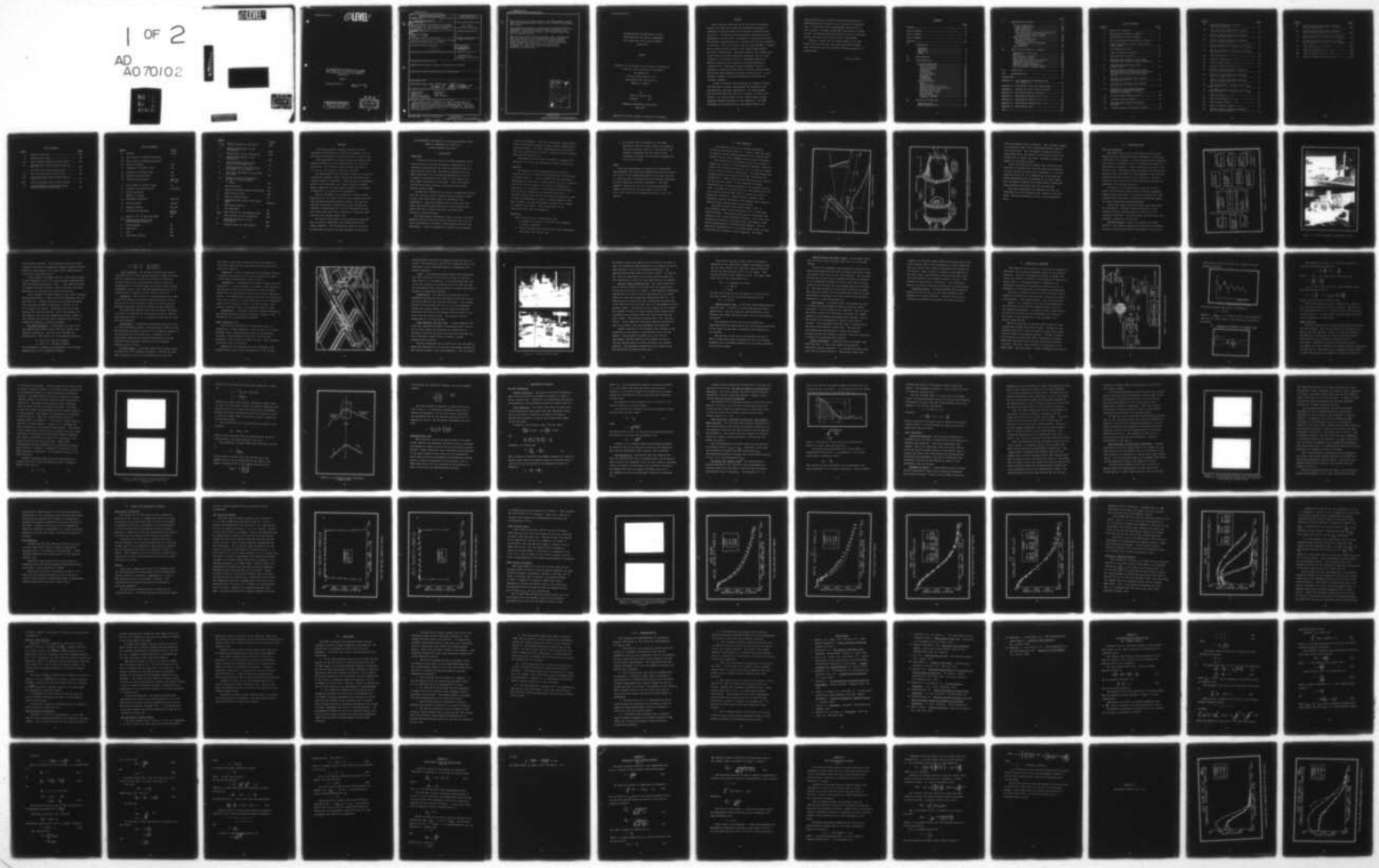

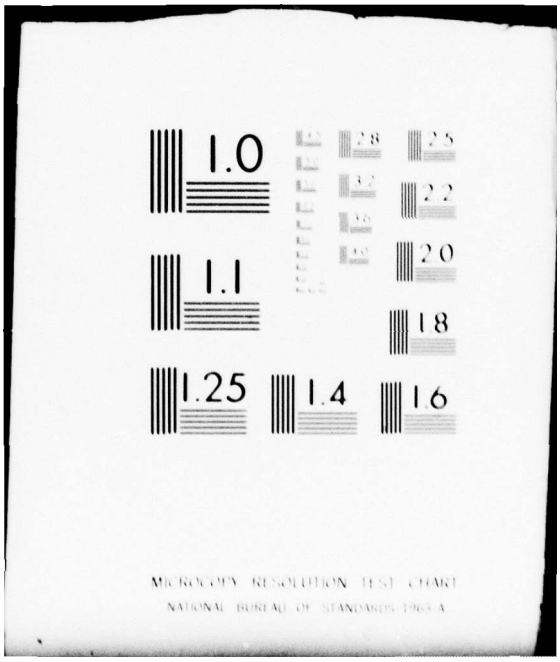
1.0
1.1
1.25
1.4
1.6
2.8
2.5
2.2
2.0
1.8
MICROCOPY RESOLUTION TEST CHART
NATIONAL BUREAU OF STANDARDS-1963-A

ED

LEVEL II

AD A070102

DDC
RECEIVED
JUN 20 1979
B

DISTRIBUTION STATEMENT A

AFIT/GAE/AA/79J-1

LEVEL II

AN EXPERIMENTAL EVALUATION OF A LASER VELOCIMETER BY THE STUDY OF TURBULENCE IN A PLANE FREE JET AT HIGH SUBSONIC VELOCITIES

THESIS

AFIT/GAE/AA/79J-1 Nino G. Cerullo
Captain CAF

DISTRIBUTION STATEMENT A
Approved for public release;
Distribution Unlimited

DDC
RECEIVED
JUN 20 1979
B

UNCLASSIFIED

SECURITY CLASSIFICATION OF THIS PAGE (When Data Entered)

REPORT DOCUMENTATION PAGE	READ INSTRUCTIONS BEFORE COMPLETING FORM
1. REPORT NUMBER (14) AFIT/GAE/AA/79J-1	2. GOVT ACCESSION NO. / 3. RECIPIENT'S CATALOG NUMBER
4. TITLE (and Subtitle) (6) AN EXPERIMENTAL EVALUATION OF A LASER VELOCIMETER BY THE STUDY OF TURBULENCE IN A PLANE FREE JET AT HIGH SUBSONIC VELOCITIES.	5. TYPE OF REPORT & PERIOD COVERED M.S. Thesis
	6. PERFORMING ORG. REPORT NUMBER
7. AUTHOR(s) (10) Nino G. Cerullo Capt CAF	8. CONTRACT OR GRANT NUMBER(s) (9) Master's Thesis,
9. PERFORMING ORGANIZATION NAME AND ADDRESS Air Force Institute of Technology (AFIT/EN) Wright Patterson AFB, OH 45433	10. PROGRAM ELEMENT, PROJECT, TASK AREA & WORK UNIT NUMBERS
11. CONTROLLING OFFICE NAME AND ADDRESS (12) 135p.	12. REPORT DATE (11) June 1979 / 13. NUMBER OF PAGES 132
14. MONITORING AGENCY NAME & ADDRESS(if different from Controlling Office)	15. SECURITY CLASS. (of this report) Unclassified / 15a. DECLASSIFICATION/DOWNGRADING SCHEDULE

16. DISTRIBUTION STATEMENT (of this Report)

Approved for public release; distribution unlimited

17. DISTRIBUTION STATEMENT (of the abstract entered in Block 20, if different from Report)

18. SUPPLEMENTARY NOTES

Approved for public release; IAW AFR 190-17.

31 MAY 1979 JOSEPH P. HIPPS, Major, USAF
Director of Information

19. KEY WORDS (Continue on reverse side if necessary and identify by block number)

experimental	Turbulence
evaluation	Free Jet
Laser Velocimeter	High Subsonic
Hot Wire Anemometer	

20. ABSTRACT (Continue on reverse side if necessary and identify by block number)

This research was conducted in order to experimentally evaluate the Laser Velocimeter by comparing the results to those obtained by means of a Hot Wire Anemometer. The means used for this evaluation was a 10 x 1 cm free jet exhausting into stationary air.

DD FORM 1 JAN 73 1473 EDITION OF 1 NOV 65 IS OBSOLETE

UNCLASSIFIED

SECURITY CLASSIFICATION OF THIS PAGE (When Data Entered)

012 225

The velocities of interest were in the high subsonic range and all measurements were taken at 25, 50 and 75 cm from the exit plane.

The parameters measured or calculated were mean velocities, turbulence intensities, Reynold's Shear Stresses, time microscale, spatial microscale, time integral scale, and spatial integral scale.

The results of this research indicate that, although the Laser Velocimeter is an accurate and reliable system, its range of operation is limited in high velocities and/or turbulence intensities. It was also found that, as specified, this system not only required no "seeding" but would also function with a filter installed in the set-up.

Accession For
NTIS GRA&I ☑
DDC TAB ☐
Unannounced ☐
Justification
By
Distribution/
Availability Codes
Dist. | Avail and/or special
A

AFIT/GAE/AA/79J-1

AN EXPERIMENTAL EVALUATION OF A LASER VELOCIMETER BY THE STUDY OF TURBULENCE IN A PLANE FREE JET AT HIGH SUBSONIC VELOCITIES

THESIS

Presented to the Faculty of the School of Engineering
of the Air Force Institute of Technology
Air University
in Partial Fulfillment of the
Requirements for the Degree of
Master of Science

by

Nino G. Cerullo, BSc
Captain CAF

Graduate Aeronautical Engineering

June 1979

Approved for public release; distribution unlimited.

Preface

This study was conceived out of the need to critically evaluate the Laser Velocimeter by measuring velocities in turbulent motion and comparing the results to available data and theory. The Malvern Laser Velocimeter represents a major advancement in this field. Measurement of velocities has been successfully accomplished with a conventional hot wire anemometer in the past. The very design of the hot wire anemometer requires that an obstruction be placed in the flow thereby causing artificial disturbances. This fact, added to the random nature of the flow, its three-dimensional properties, and its high frequency of fluctuation, makes it extremely difficult to measure accurately the properties and characteristics of turbulent flow. The Malvern Laser Velocimeter offers a technique of measuring velocities in turbulent motion without the obvious error-inducing qualities of the hot wire. I will attempt to compare the results achieved by using the two different systems.

I wish to thank my thesis advisor, Dr. Harold E. Wright, who conceived the study, who acquired the equipment, and provided many invaluable suggestions. His encouragement and enthusiasm certainly went far to dispel the fear of the unknown. Mr. William Baker and Mr. Harold "Leroy" Cannon provided valuable assistance in the Laboratory. The AFIT workshops in the persons of Mr. Carl Shortt and Mr. Ron

Ruley provided crisis response and made modifications to modifications with a smile so as to allow me to finish on time. I would also like to acknowledge the work of Lt. (Dr.) George D. Catalano, AFFDL/FXM, and express my thanks to him. He worked nights and weekends in order to make the system functional which helped my work immeasurably.

Finally, I would like to express thanks to my wife, Stella, who for the past years but specifically during this research period, has provided unflagging support and encouragement.

Nino G. Cerullo

Contents

		Page
Preface		ii
List of Figures		vi
List of Tables		ix
List of Symbols		x
Abstract		xii
I.	Introduction	
	Background	1
	Approach	2
	Objectives	2
	Scope	3
II.	Test Apparatus	4
III.	Instrumentation	8
	Hot Wire Anemometer	8
	Hot Wire Sensors	8
	1015C Correlator	11
	3721A Correlator	12
	Voltmeters	12
	Oscilloscope	12
	DC Power Supply	12
	Manometers	13
	Thermometer	13
	Cathotometer	13
	Laser Velocimeter	13
	Laser	15
	Beam Splitter	15
	Phase Modulator Drive Unit	15
	Receiver Photon Detection Unit	17
	Photomultiplier Tube	18
	PM Tube Power Supply	19
	Osciiloscope	19
	Digital Correlator	19
	Frequency Counter	20
IV.	Principle of Operation	21
	Phase Modulator	24
	Photomultiplier Tube	29

Page

V. Experimental Procedure 30

Hot Wire Anemometer 30
Sensor Calibration 30
Test Conditions 30
Data Acquisition 31
Mean Velocities, Turbulence Intensities, and Reynold's Shear Stresses 32
Microscale and Integral Scale 32
Laser Velocimeter 34
Traversing Mechanism 34
Alignment of Optics 34
Mean Velocities and Turbulence Intensities 36
Data Reduction 39

VI. Results and Discussion of Results 40

Experimental Limitations 40
Results 40
Exit Velocity Profiles 41
Axial Velocity Decay 44
Mean Velocity Similarity Profiles 44
Turbulence Intensity Profiles 50
Reynold's Shear Stresses 53
Time and Spatial Microscales 53
Time and Spatial Integral Scales 54

VII. Conclusions 56

VIII. Recommendations 59

Bibliography 61

Appendix A: A Two-Dimensional Turbulent Free Jet - Theory 64

Appendix B: Calculation of the Jet Spread Angle 71

Appendix C: Theoretical Axial Velocity Profile 73

Appendix D: The Autocorrelation Function 75

Appendix E: Experimental Results at M = 0.4 78

Appendix F: Experimental Results at M = 0.6 88

Appendix G: Experimental Results at M = 0.8 98

Appendix H: Experimental Data 108

Vita 119

List of Figures

Figure		Page
1	Flow Field Schematic	5
2	Experimental Apparatus Schematic	6
3	Instrumentation Block Diagram	9
4	Hot Wire Anemometer Experimental Set-Up	10
5	Laser Velocimeter Set-Up in the Forward Scatter Mode	14
6	LV Experimental Set-Up	16
7	Laser Velocimeter Operation	22
8	Autocorrelation Function	23
9	Autocorrelation Function with Phase Modulator and Without at High Turbulence ...	26
10	Principle of Laser Velocimetry - Doppler Model	28
11	Autocorrelation Function (a) at Low Velocities and Low Turbulence Intensities (b) with Fine Screen Mesh and Paper Filter	37
12	Hot Wire and LV Nozzle Exit Velocity Profile at M = 0.4	42
13	Hot Wire and LV Nozzle Exit Profile at M = 0.6	43
14	Attenuation of the Autocorrelation Function as Velocity/Turbulence Intensity Increases	45
15	Hot Wire Axial Velocity Profile	46
16	LV Axial Velocity Profile	47
17	Hot Wire Mean Velocity Similarity Profiles	48
18	LV Mean Velocity Similarity Profiles	49

Figure		Page
19	Hot Wire Turbulence Intensity Similarity Profiles	51
20	Hot Wire and LV Turbulence Intensity at M = 0.4 and 25 cm	79
21	Hot Wire and LV Turbulence Intensity at M = 0.4 and 50 cm	80
22	Hot Wire and LV Turbulence Intensity at M = 0.4 and 75 cm	81
23	Hot Wire Reynold's Stresses $(u'v')/U^2_{cen}$ at M = 0.4	82
24	Hot Wire Reynold's Stresses $(u'w'/U^2_{cen})$ at M = 0.4	83
25	Time Microscale M = 0.4	84
26	Spatial Microscale M = 0.4	85
27	Time Integral Scale M = 0.4	86
28	Spatial Integral Scale M = 0.4	87
29	Hot Wire and LV Turbulence Intensity at M = 0.6 and 25 cm	89
30	Hot Wire and LV Turbulence Intensity at M = 0.6 and 50 cm	90
31	Hot Wire and LV Turbulence Intensity at M = 0.6 and 75 cm	91
32	Hot Wire Reynold's Stresses $(u'v'/U^2_{cen})$ at M = 0.6	92
33	Hot Wire Reynold's Stresses $(u'w'/U^2_{cen})$ at M = 0.6	93
34	Time Microscale M = 0.6	94
35	Spatial Microscale M = 0.6	95
36	Time Integral Scale M = 0.6	96
37	Spatial Integral Scale M = 0.6	97
38	Hot Wire and LV Turbulence Intensity at M = 0.8 and 25 cm	99

Figure		Page
39	Hot Wire and LV Turbulence Intensity at M = 0.8 and 50 cm	100
40	Hot Wire and LV Turbulence Intensity at M = 0.8 and 75 cm	101
41	Hot Wire Reynold's Stresses ($u'v'/U^2_{cen}$) at M = 0.8	102
42	Hot Wire Reynold's Stresses ($u'w'/U^2_{cen}$) at M = 0.8	103
43	Time Microscale at M = 0.8	104
44	Spatial Microscale at M = 0.8	105
45	Time Integral Scale at M = 0.8	106
46	Spatial Integral Scale at M = 0.8	107

List of Tables

Table		Page
I	Görtler Curve Data	109
II	Tollmien Curve Data	110
III	Axial Velocity Theoretical Curve Data	111
IV	Hot Wire Exit Velocity Profile Data at M = 0.6	112
V	Hot Wire Axial Velocity Decay Data	113
VI	Hot Wire Similarity Profiles Data	114
VII	Laser Velocimeter Exit Profile Data at M = 0.6	115
VIII	Laser Velocimeter Axial Velocity Decay	116
IX	Laser Velocimeter Similarity Profile and Turbulence Intensity Data	117

exit velocity profiles. This particular sensor was chosen

List of Symbols

Symbol		Units
E	Voltage	volts
$\bar{K}_i$	Unit Vector in Incident Direction	
$\bar{K}_s$	Unit Vector in Scattered Direction	
f_o	Doppler Frequency	cps
f_i	Frequency of Incident Light	cps
f_s	Frequency of Scatter Light	cps
f_d	Doppler Frequency Shift	cps
g_c	Gravitational Constant	$\frac{Kgm - m}{N - sec^2}$
λ_o	Wave Length of Inicdent Light	μm
K	Constant of Proportionality	m/sec/volt
m	Fringe Visibility	
n	Number of Fringes	
P_a	Atmospheric Pressure	Kgm_f/cm^2
P_o	Total Pressure	Kg_f/cm^2
P_c	Chamber Pressure	Kg_f/cm^2
R	Universal Gas Constant	$\frac{N - m}{Kg_m - °K}$
r_o	Radius ($1/e^2$) of the Laser Beam	mm
R( )	Dimensionless Value of the Autocorrelation Function	
S	Fringe Spacing	μm
T	Time Delay	sec
t	Time	sec
U	Local Mean Velocity	mps

Symbol		Units
U_{cen}	Maximum Velocity in the Plane	mps
u'	Velocity Fluctuation in the X-direction	mps
W	Mean Velocity in the Z-direction	mps
w'	Velocity Fluctuation in the Z-direction	mps
X	Axial Coordinate Axis in the Direction of Primary Flow	cm
Y	Coordinate Axis in the Horizontal Plan Normal to the X-axis	cm
Y_o	Jet Nozzle Half-Width at the Nozzle Exit Plane	cm
$Y_{1/2}$	Distance from the Centreline of the Jet to the Point where $U = \frac{1}{2}U_{cen}$	cm
τ	Time Microscale	sec
λ	Spatial Microscale (Taylor Microscale)	cm
Γ	Time Integral Scale	sec
Λ	Spatial Integral Scale	cm
θ	Convergence Half Angle of the Laser Beams	degrees
η	Turbulence Intensity	
b	Jet Half-Width	cm
U_{cor}	Mean Velocity in the Potential Core	mps
V	Mean Velocity in the Y-direction	mps
v'	Velocity Fluctuation in the Y-direction	mps
$\bar{V}$	Velocity Vector of the Particle	mps

Abstract

This thesis provides methods and results of the experimental evaluation of the Laser Velocimeter (LV) by the study of turbulence in a plane free jet 1 cm by 10 cm.

The measurements of primary interest were those taken across the width of the jet downstream at 25, 50 and 75 jet widths. The velocity range of concern was that of M = 0.4, M = 0.6, and M = 0.8 at the jet exit.

The measurements taken were mean velocities, turbulence intensities, Reynold's shear stresses and microscale and integral scales of turbulence. Both the hot wire anemometer and the laser velocimeter were used in order to provide proper comparison of results under conditions as constant as possible in all areas of the experiment.

The jet was found to be classical in nature and the consistency of the results using the two systems show that both provided extremely accurate results. Not only did the Laser Velocimeter system function well without any "seeding" as advertised, but it also functioned with the fine screen mesh and filters installed to remove all dust particles and increase sensor life.

The relative efficiency of each system was evaluated and its relative advantages and disadvantages became readily apparent. The LV system was found to be limited at high flow velocities and high turbulence intensities.

AN EXPERIMENTAL EVALUATION OF A LASER VELOCIMETER BY THE STUDY OF TURBULENCE IN A FREE JET AT HIGH SUBSONIC VELOCITIES

I. Introduction

Background

A device such as the Laser Velocimeter measuring local flow velocities in harsh enviromnents, characteristic of aerospace propulsion systems, would be extremely useful in many research activities. One distinct advantage of the Laser Velocimeter over the Hot Wire Anemometer is that it is capable of measuring flow fields in areas where a hot wire cannot physically be positioned. Laser Velocimeters are now being used to measure successfully flow fields between turbine blades.

Conventional systems such as hot wire anemometers interact with the flow and locally introduce flow disturbances which in some cases cause doubt about the validity of the measurements. Harsh environments such as those with high impact and thermal loads contribute to high failure rates. Aside from their relative fragility, they also lose accuracy at high velocities.

The Laser Doppler Velocimeter, due to its use of optical measuring devices, does not interact with the flow, does not create disturbances, nor does it suffer damage from the flow environment. Since its inception in 1964, it has undergone

method possible and still be compatible with the free jet

extensive development. The Laser Velocimeter system used in this investigation is devoid of many inherent limitations of previous systems. One major improvement has been the fact that this system does not require "seeding" but will function with normal laboratory air.

The potential of the Laser Velocimeter is practically unlimited in the area of aeronautical research activities.

Approach

The approach to this investigation was to use an existing set-up of a classical two-dimensional jet developed by Shepard (Ref 12). It was intended that the turbulence measurements carried out by Shepard would serve as a reference. The use of hot wire results as a basis for comparison is meaningful as its accuracy in this application has proven to be very good in comparison to classical predictions. A thorough investigation of the flow field was carried out with the hot wire anemometer in order to support Shepard's data and, secondly, the Laser Velocimeter was used in an attempt to reproduce the results. The effectiveness of the Velocimeter would then be documented.

Objectives

The objectives of the investigation were

1. To compare the results of the hot wire anemometer to those of Shepard;
2. To map the same flow field with the Laser Velocimeter and compare the results; and

3. To evaluate the effectiveness of the Laser Velocimeter and its claims, within the bounds of this investigation; that is, to verify the "non-seeding" requirement and the ability of the instrument to measure all the other parameters by the hot wire system.

Scope

The only measurements of interest were those which would document the turbulence parameters of the flow field at 25, 50 and 75 jet widths downstream of the nozzle exit and at three different velocities using the constant temperature hot wire anemometer and Laser Velocimeter. The high subsonic velocities at the jet exit produced Reynold's numbers (based on the jet exit width) of 8.75×10^4, 12.6×10^4, and 16.5×10^4 respectively at M = 0.4, 0.6, and 0.8.

II. Test Apparatus

The apparatus used was the existing apparatus constructed by Shepard (Ref 12). Figure 1 shows the planes of primary interest where measurements were taken by both systems, the hot wire anemometer and the Laser Velocimeter.

Test conditions were selected in order to be able to compare the results to those obtained by Shepard. Therefore, nozzle exit velocities of Mach 0.4, 0.6, 0.8 and test planes of 25, 50 and 75 cm were investigated. The above conditions provided similar exit velocities of 140, 200 and 260 mps respectively. These velocities were maintained very closely by the judicious control of the compressor discharge conditions and a vernier adjustment at the apparatus control valve. The data of interest were that which would yield the exit velocity profile, mean velocity similarity profiles, turbulence intensities, Reynold's shear stresses, time microscale, spatial microscale, time integral scale, spatial integral scale, and the axial velocity decay.

Initially the set-up was used as shown in Fig. 2. At an advanced stage of the experiment, the 3 cm deep shot bed was removed. The heaters which were not being used were removed as they created unneeded turbulence. The orifice was removed and replaced by two plates with 5 mm diameter holes and with approximately 37 percent area blockage. The two plates were separated by a 0.3 cm thick rubber insert in order to minimize any turbulence present upstream. The nozzle

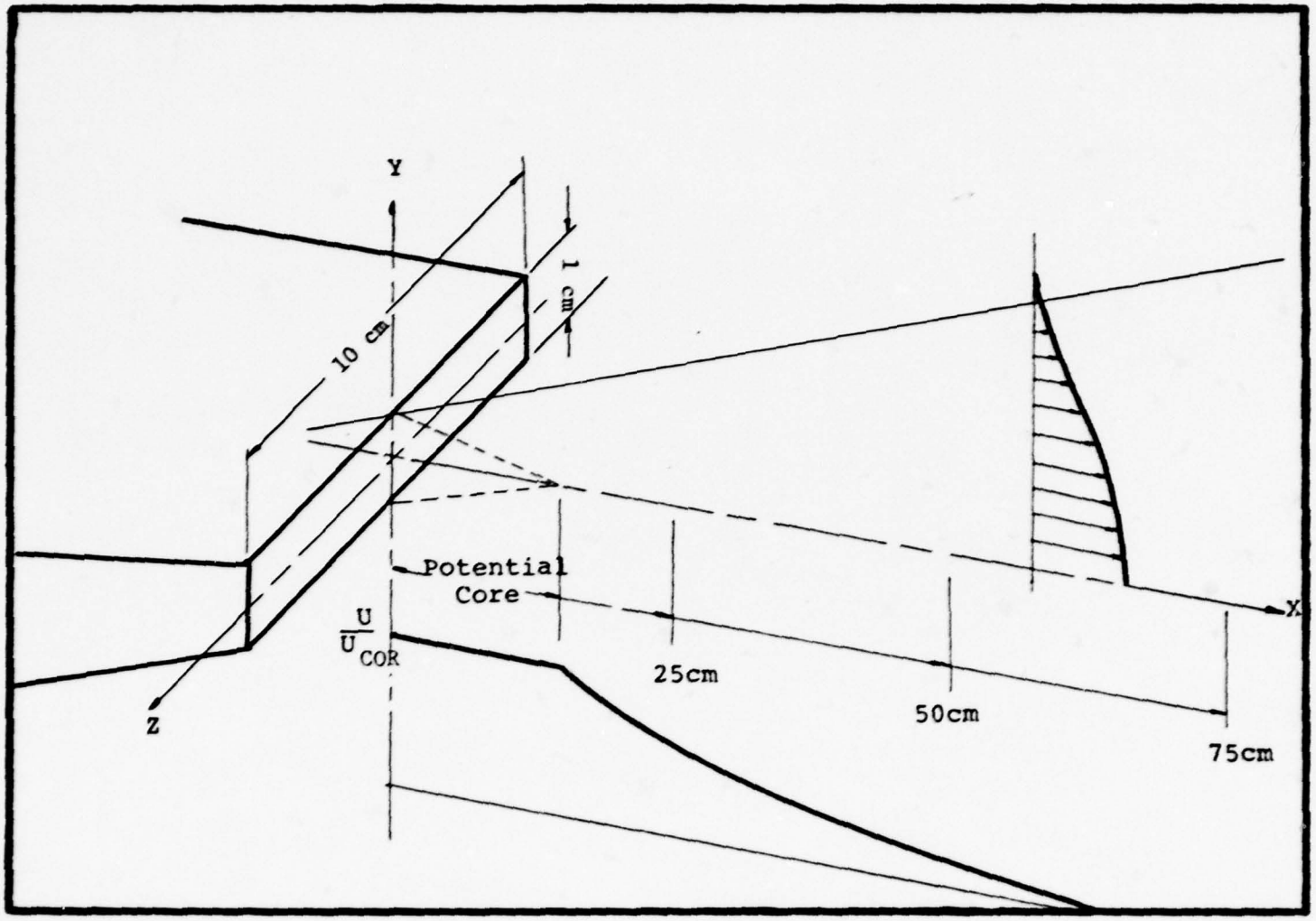

Figure 1. Flow Field Schematic

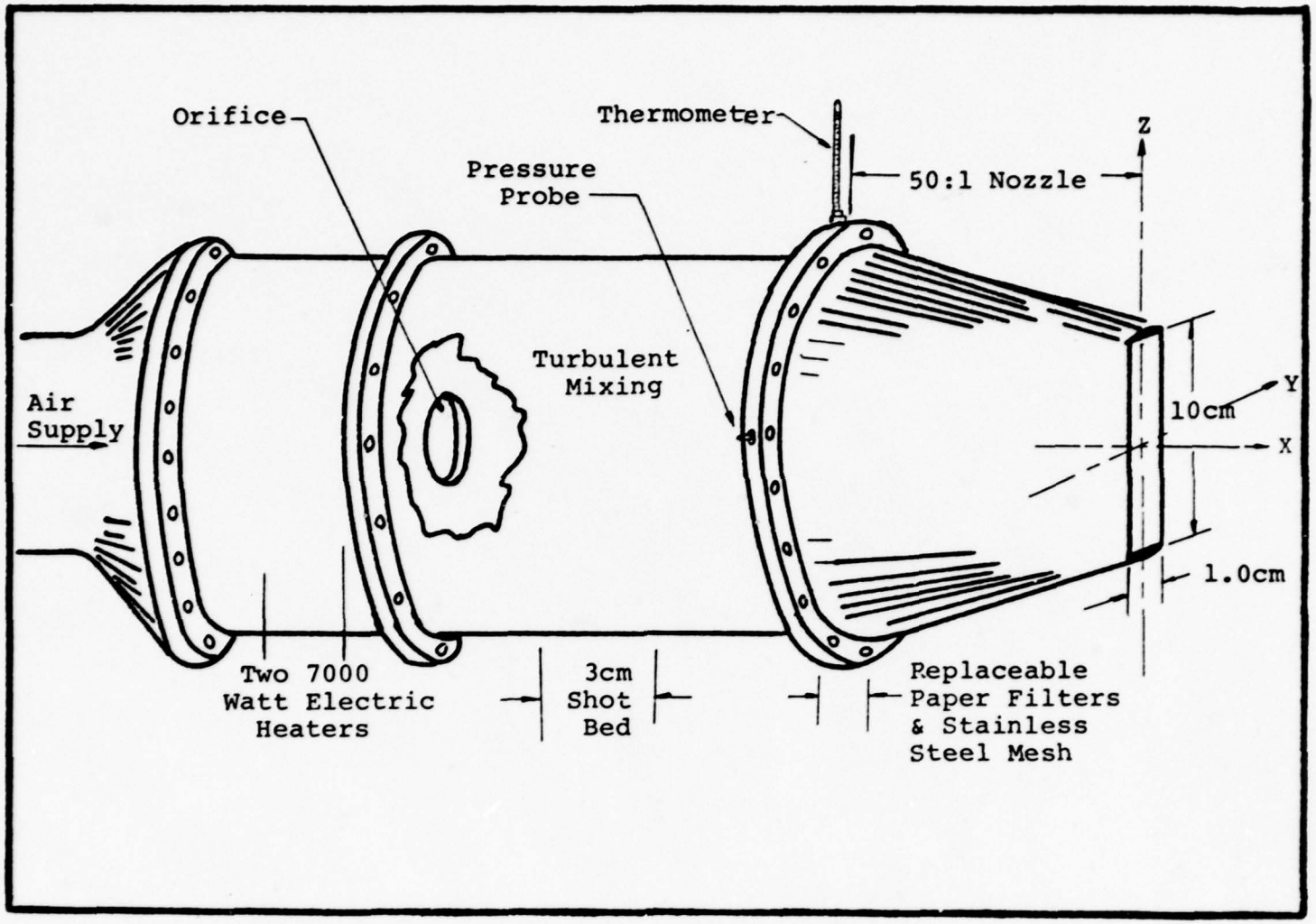

Figure 2. Experimental Apparatus Schematic

filter arrangement was not modified. This included a number of replaceable paper filters sandwiched between layers of fine screen mesh. This arrangement cleaned the flow of particulate matter and reduced the possibility of hot wire failure due to foreign particles. The mesh provided the support for the paper filters.

Since the shot bed was removed some arrangement was required to straighten the flow and reduce the turbulence so as to satisfy the nozzle exit requirements. A circular honeycomb section 27 cm in diameter and 10 cm thick was placed approximately 15 cm upstream of the first flange. This arrangement produced the desired results without the large pressure drop experienced with the shot bed.

The nozzle arrangement was designed such that low turbulence and a thin boundary layer resulted in the exit plane. This was achieved by a 50 to 1 area contraction ratio.

III. Instrumentation

Hot Wire Anemometer

The central piece of the instrumental set-up was the Thermo-Systems, Incorporated (TSI) Anemometer in conjunction with the hot wire sensors. A block diagram of the instrumentation system is included as Fig 3 to indicate how signals are processed and displayed. Figure 4 provides a pictorial view of the set-up. The hot wire sensors provide the unlinearized signals to the two channels of the anemometer where they are processed and then directed to the linearizer. From the linearizer they go to the TSI 1015C correlator and then are displayed on DC and RMS voltmeters.

To arrive at the autocorrelation function for this study an unlinearized signal directly from the anemometer bridge circuit was routed to the Hewlett-Packard (HP) 3721A correlator and from there to the HP 3720A Spectrum Display for visual observation and photographing.

The DC power supply and oscilloscope were used mainly for calibration. The power supply was used as a very accurate reference voltage source in order to set the linearizer constants. The oscilloscope was used to set the frequency response of the hot wire.

Hot Wire Sensors. Single wire sensors, TSI Model 1214-T1.5, were used to measure mean velocities to determine the axial velocity decay and for the mapping of the nozzle

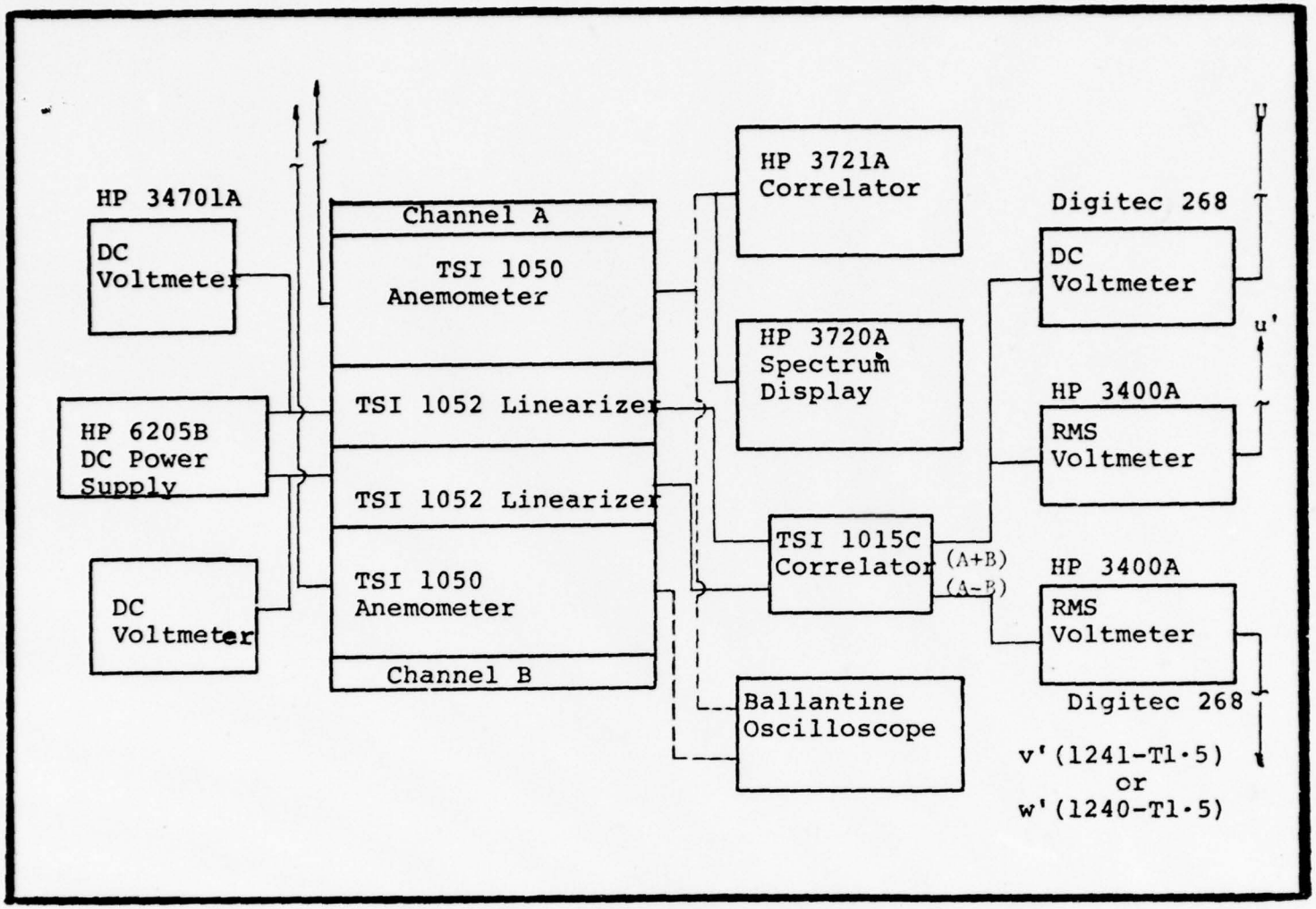

Figure 3. Instrumentation Block Diagram

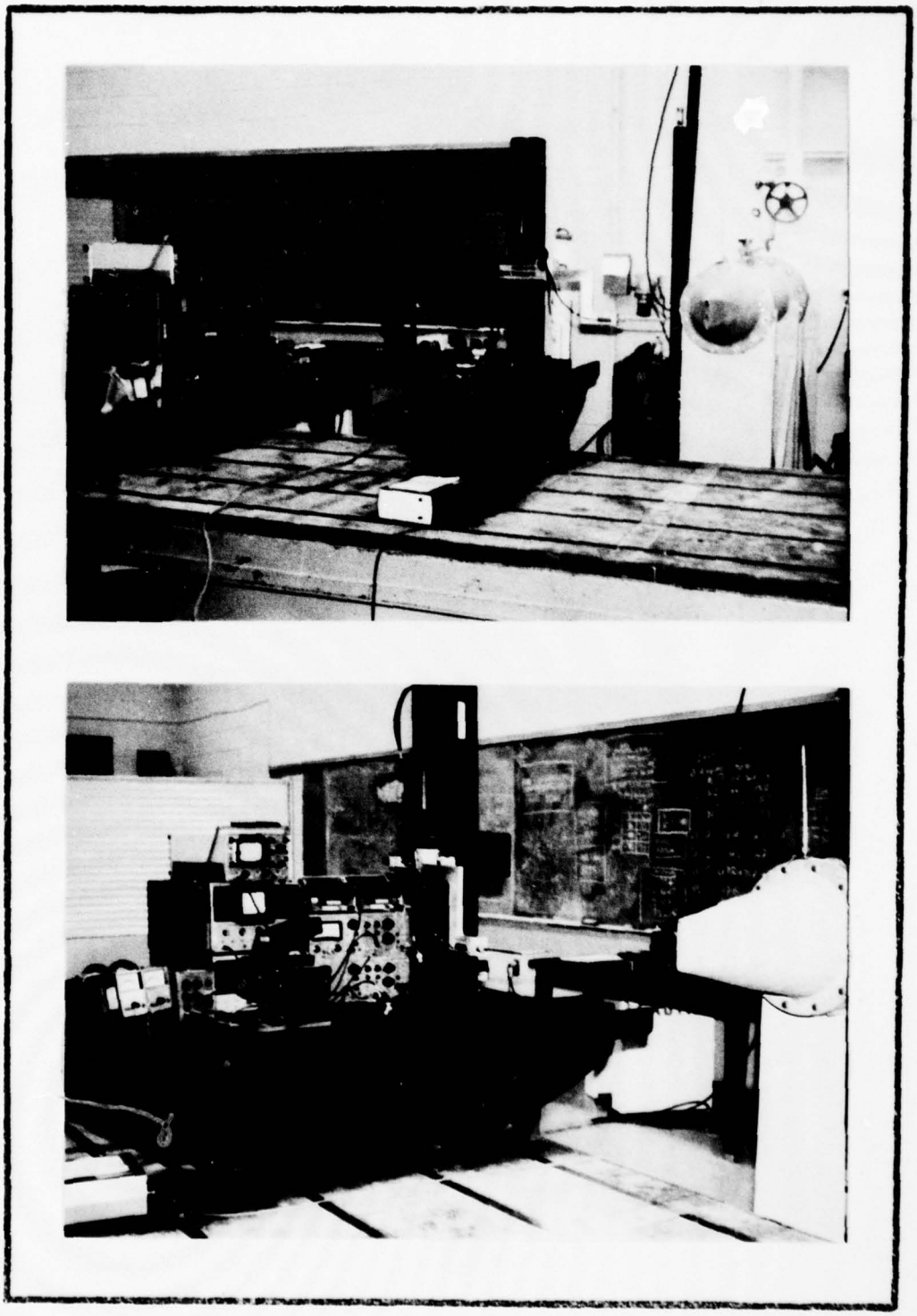

Figure 4. Hot Wire Anemometer Experimental Set-Up

exit velocity profiles. This particular sensor was chosen because it provided an acceptable frequency response and also because it was durable in the high velocity ranges present very close to the nozzle exit.

X-wire sensors, TSI Model 1241-T1.5, were used to obtain at mean velocities (U) in the axial direction simultaneously with fluctuating velocities u' and v'. This sensor was used in conjunction with an elbow in order to provide the proper orientation for measuring the required velocities.

X-wire sensors, TSI Model 1240-T1.5, were used to measure fluctuating velocity w' which could not be measured with the TSI 1241-T1.5. Although both the X-wire sensors performed well they were extremely susceptible to failure at the M = 0.8 and 25 cm station. Invariably both failed upon reaching the centre of the jet. Of the two sensors, the TSI 1240-T1.5 was the more susceptible possibly because it was oriented such that the vortex shedding from the sting created the greatest vibrational stresses.

TSI 1015C Correlator. A correlator was used to add and subtract the voltage outputs from the channel A and channel B linearizers. The sum of the voltages was proportional to the velocity in the streamwise direction.

$$U = K(A + B) \quad \text{from DC voltmeter}$$

$$u' = K(A + B) \quad \text{from RMS voltmeter}$$

The difference of voltages was proportional to velocities perpendicular to the streamwise direction.

U	Local Mean Velocity	mps

x

$V = K(A - B)$ DC voltmeter

$v' = K(A - B)$ RMS voltmeter

3721A Correlator. An HP 3721A correlator was used in conjunction with a 3720A spectrum display in order to process hot wire signals and calculate the correlation function. It then displayed the autocorrelation function which was photographed by a Polaroid camera for analysis and to provide a permanent record. The 3721A was connected directly to the bridge output of Channel A of the 1241-T1.5 hot wire.

Voltmeters. Two Digital D. C. millivoltmeters were used during the calibration and data collection process; one to monitor the 10 volts reference voltage for setting the TSI linearizer constants and one for measuring mean velocities.

Two 3400A RMS voltmeters were used to measure linearized AC output; one measured the fluctuating velocity u' and the other measured either v' or w' depending on the hot wire used and its orientation.

Oscilloscope. A Ballantine oscilloscope was used in the hot wire calibration process. The oscilloscope along with the RMS voltmeters provided a picture of the frequency response of the particular hot wire being used. A widening of the oscilloscope response and violent fluctuations in the RMS voltmeter would indicate instability in the frequency response of the hot wire.

DC Power Supply. An HP Model 6204B dual DC power supply was used to set the linearizer constants. The unit was also used to produce artificial flow velocities by using the

DC voltage so that the hot wires would not be exposed to high flow velocities for long periods of time required for calibration (Ref 12).

Manometers. A 100 inch Merriam fluid manometer was used to measure the pressure at the nozzle entrance and, hence, to determine the Mach number at the jet exit.

Thermometer. A thermometer was used to measure the total temperature. It was positioned in a region of the flow where the velocity of the air was negligible so that the total temperature was approximately equal to the static temperature (Fig 2). The temperature was required only for the calculation of the exit velocities to ensure that they were in approximate range and to be used as a check. For this reason, a more accurate instrument such as a thermocouple was not used.

Cathotometer. A Gaertner Scientific Company cathotometer was used to position the hot wire sensor to within $\pm$ .005 millimeters in all coordinate directions.

Laser Velocimeter (LV)

The LV set-up consisted of a helium-neon laser, a beamsplitter, a phase modulator, a lens of 50.8 cm, a 200 mm telephoto lens, a photomultiplier tube, an oscilloscope, a counter, a phase modulator drive unit, and a digital correlator. The LV set-up is shown in Fig 5. Fig 6 provides a pictorial view of the set-up.

Unseeded air was used and the LV was operated in the forward scatter mode as this was deemed to be the easiest

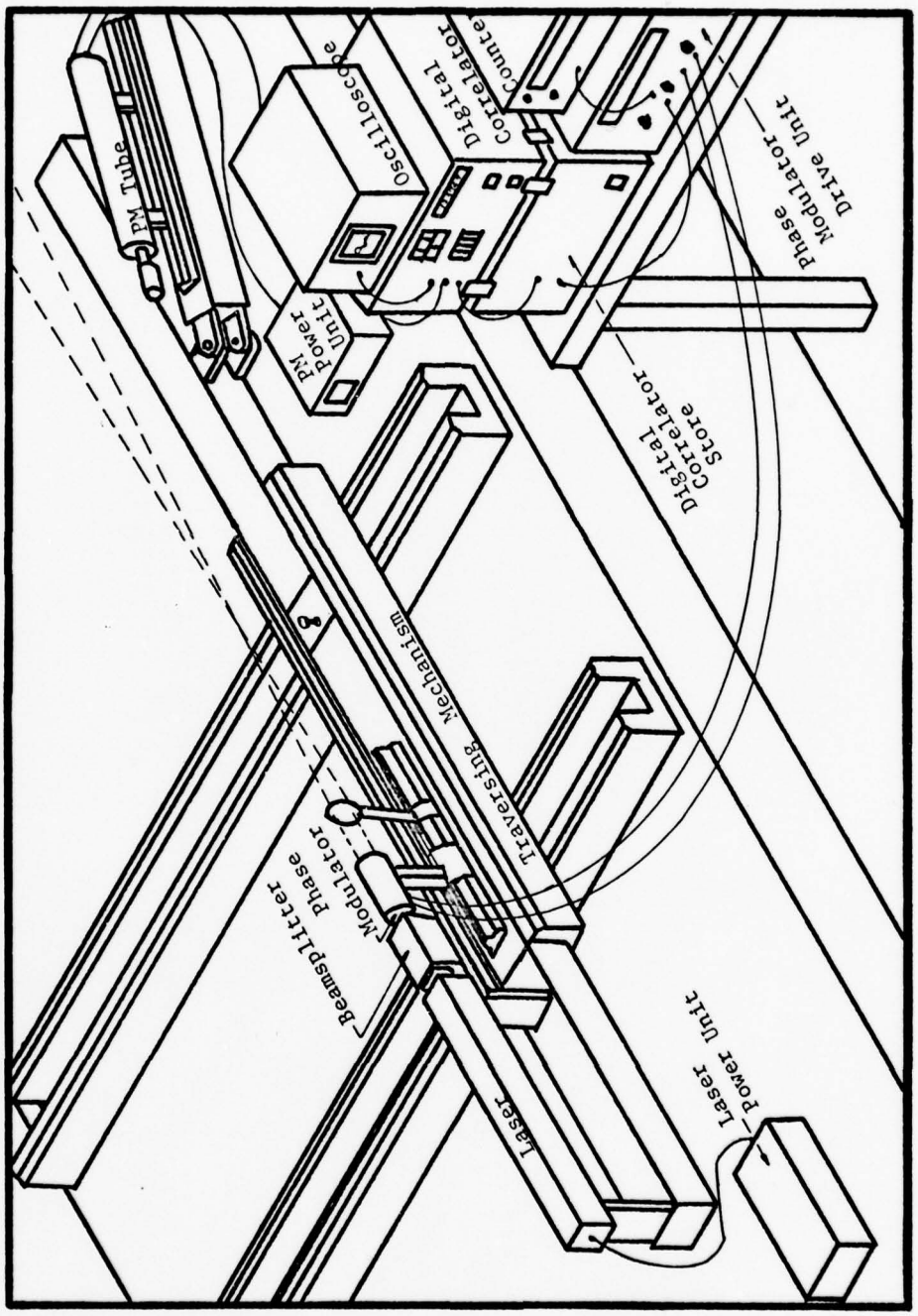

Figure 5. Laser Velocimeter Set-Up in the Forward Scatter Mode

method possible and still be compatible with the free jet set-up. The functions of each of the components used in the experiment will be described briefly to demonstrate the system capability.

Laser. A 15 mW Spectra Physics Model 124A helium-neon gas laser and Model 255 DC exciter was used to provide a laser beam of 1.1 mm diameter. It was positioned such that it was well outside the influence of the jet and such that the beam pointed away from areas where it might inadvertently impinge on unsuspecting personnel.

Beamsplitter. The function of the Malvern RF 307 Transmitter Beamsplitter and polarization unit was to split the laser beam into two beams of equal power. Two variable controls were provided; the first to vary the separation between the outgoing beams, and the second provided the continuous variation of the distance from the laser to the point where the beams crossed. The distance could be varied from 15 cm to many meters.

Phase Modulator and Drive Unit. A phase modulator and drive unit type Malvern K9023 in conjunction with a lens of 50.8 cm focal length was used when the combination of turbulence intensity and high velocities were such that the asic velocimeter system failed to produce a useful autocorrelation function.

The main requirement was to ensure that the two parallel beams were separated by 2 cm and that they passed through the two crystals present in the phase modulator. This can easily

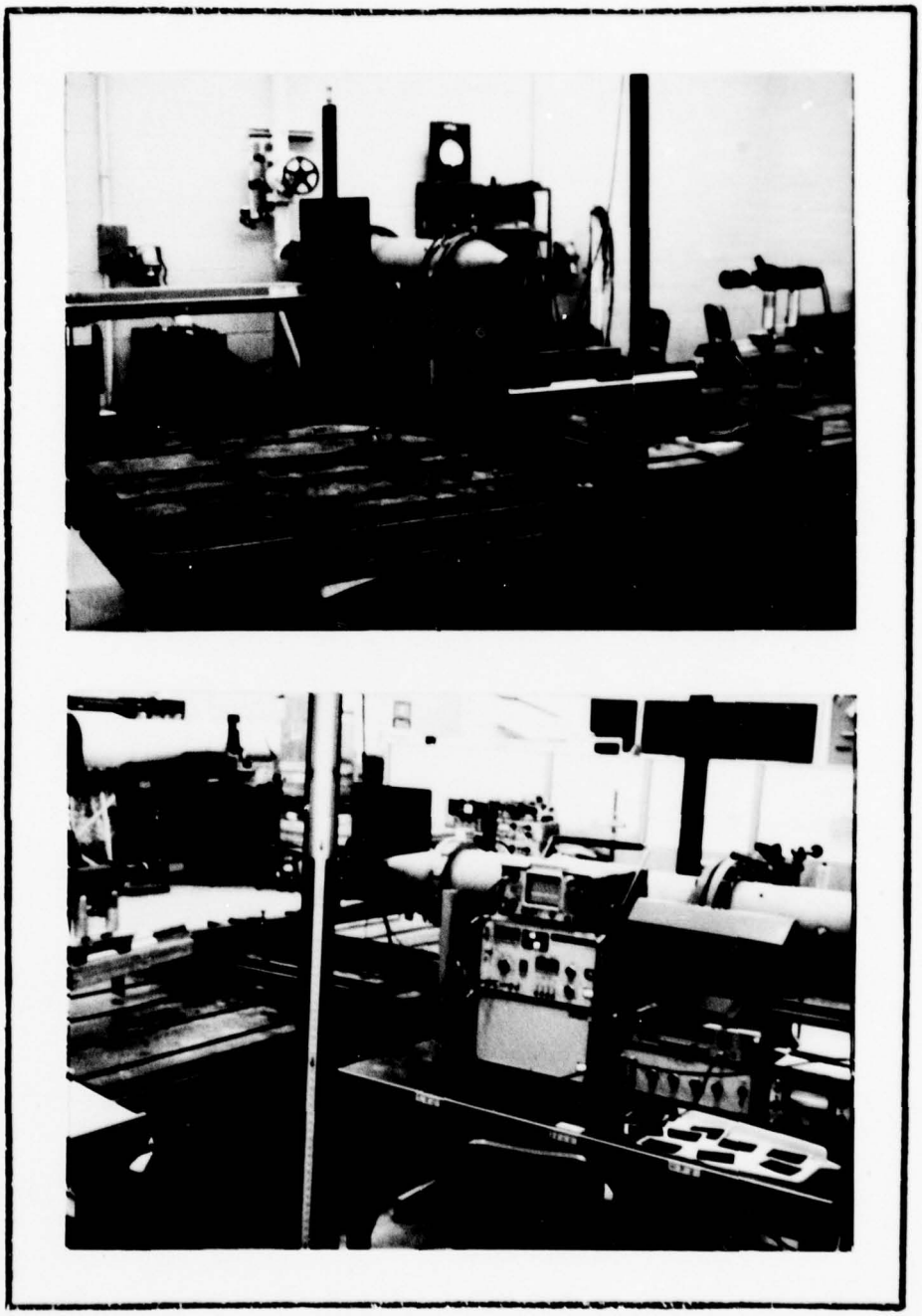

Figure 6. LV Experimental Set-Up

be checked visually by looking into the beams at an angle as they pass through the phase modulator or by looking at the two beams against a wall or any transparent material. Two sharply defined beams should be plainly visible. If they are not, then the adjustments on the phase modulator allow for fine adjustments to align the two beams and the two crystals.

Receiver Photon Detection Unit. The lenses used were a 200 mm Vivitar telephoto lens along with two spacers and a 105 mm lens with the 2.5 cm spacer. These specific lens/spacer combinations were used to permit installation of the photo-multiplier tube well outside the influence of the jet. Its function was to collect the light scattered by the particles in the flow and focus the light onto an interchangeable pinhole aperture system. The function of the pinhole was to regulate the diameter of the flow control volume being observed while eliminating any scattered light from areas other than the focal volume. The apertures provided were a 100, 200 and a 400 μm. It was found that the 400 μm aperture provided the best results and it was used throughout the experiment.

Another provision on the telephoto lens allowed for the regulation of the amount of light allowed entry into the pinhole. The procedure followed was to turn off all unnecessary overhead lighting and to adjust the lens so that the maximum amount of light impinged on the pinhole aperture. This procedure produced the best results given the relatively low powered laser used.

The size of the focal volume could be calculated depending on the combination telephoto lens/spacers used. For the high velocity low turbulence intensity flow the 105 mm lens was used along with a 2.5 cm spacer. This set-up provided a focal length of 35 cm. The focal volume (FV) size was then calculated to be

$$FV = 3 \times \text{Diameter of Pinhole}$$
$$= 3 \times 400\ \mu m$$
$$= 1.2\ mm$$

For the 200 mm lens and the two spacers (2.5 and 6.5 cm), the focal length was 54 cm and the resulting FV was

$$FV = 0.72\ mm$$

Photomultiplier Tube. An EMI 9863 KB/100 photomultiplier tube was used. It contains a narrow band optical filter, dynode chain, high gain amplifier and discriminator which amplifies and shapes the pulse signal for use by the digital correlator.

The purpose of the PM tube was to eliminate the amplitude modulation and maintain only the frequency modulation of the signal in the form of scattered light impinging on its cathode.

This portion of the set-up was the most critical in that it could very easily be damaged and that the focusing procedure was so extremely important for the proper operation of the entire system.

Photomultiplier Tube Power Supply. An EMI power supply type PM 25B was used to provide 1850 Volts to the PM tube cathode.

The hot wire anemometer was susceptible to many factors which would damage the wire such as turning the power on when the selector switch was in the "run" position. The LV system PM tube was the only portion which was extremely susceptible to its inadvertent exposure to direct laser light or bright lights of any kind when the high voltage supply was switched on. This fact combined with the flow's inability to damage the laser beam allowed for the optimum time required to take measurements as opposed to the hot wire which was extremely susceptible to harsh flow conditions.

Oscilloscope. An AN/USM-425(V)1 oscilloscope was used to display the autocorrelation function from the digital correlator. Once the function was displayed, then, by using the channel selector on the digital correlator the channel numbers of the maximums and minimums were obtained (Fig 8). The contents of the appropriate channels could also be obtained. This information was then used to calculate mean velocities and turbulence intensities. This specific oscilloscope was used because it allowed for external triggering which was required in order to allow the correlator to display the autocorrelation function.

Digital Correlator. A Malvern digital correlator type K7023 was used. It was a high speed (50 nanosecond resolution) digital correlator. It received the output pulse train from the photon detector. These pulse trains bunch

together as a particle passes through the bright areas of the fringe pattern, that is, the probability of photon detection from the particle will follow the intensity distribution of the fringes. Then, in order to extract the periodicity of the pulse train, the correlator multiplied the pulse train with many different time delayed versions of itself. This process is called digital correlation. The correlation function can then be visually displayed on the oscilloscope.

Frequency Counter. A Hewlett-Packard 5325B Universal Counter was used to arrive at the exact frequency shift produced by the phase modulator. The exact value of the frequency was required to calculate the actual velocity.

IV. PRINCIPLE OF OPERATION

The purpose of this section is to provide an abbreviated description of the Laser Velocimeter system and its working equations. The basic information necessary to operate the Malvern LV system is contained in the appropriate instruction manual (Ref 9). The manual presents a combination of background information on operating principles as well as procedures to be followed for the operation of the equipment.

The basic principle of the LV is that velocities can be computed by knowing the time taken for a particle to travel a known distance. This known distance is the fringe spacing.

Figure 7 is a schematic of the set-up and demonstrates the function of each piece of equipment used to arrive at the required measurements. It shows two laser beams crossing at the point at which the flow measurements are required. The result of the intersection of the two beams is an optical fringe pattern.

Particles contained in the flow cause flashes of light as they pass through the optical fringes. Flashes of light caused by particles in the flow result in pulse train bursts from the output of the photon detector. In order to extract the periodicity of the pulse train, the digital correlator multiplies the pulse train with many time-delayed versions of itself. The form of the output of the correlator is as shown below. The time delay, τ, which is measured with crystal

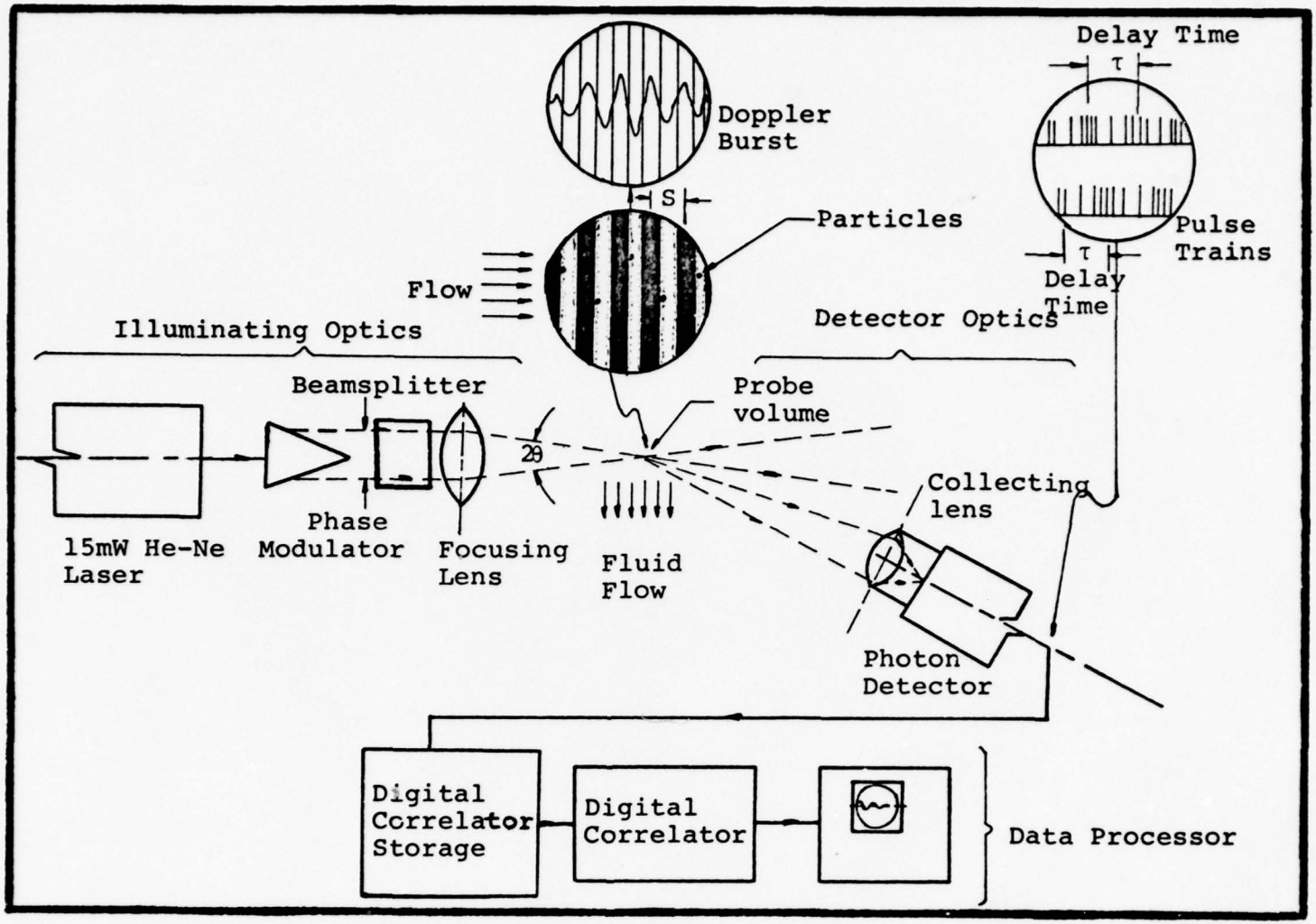

Figure 7. Laser Velocimeter Operation

clock accuracy defines the time for a particle to pass through one fringe

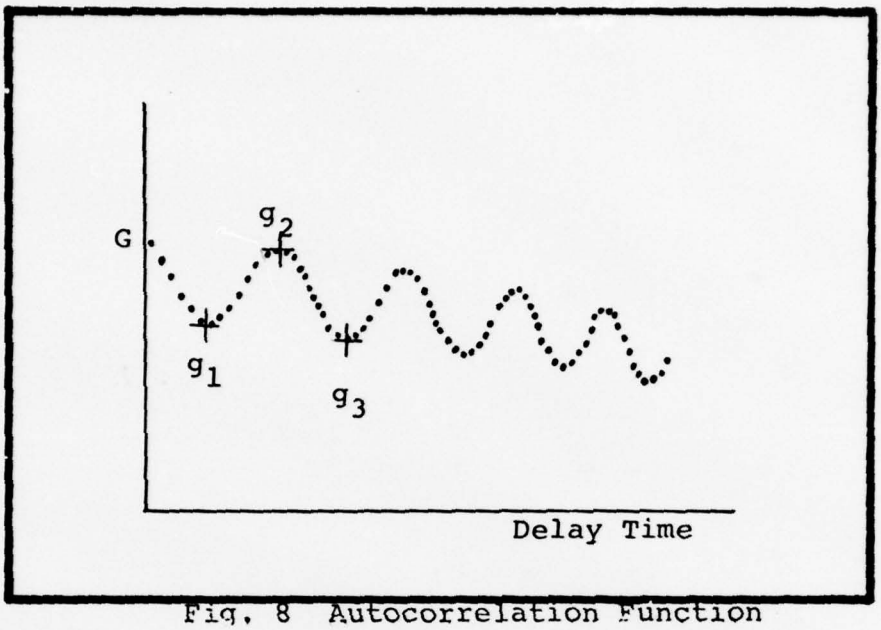

Fig. 8 Autocorrelation Function

The spacing between the fringes is defined as

$$S = \frac{L}{D} \frac{\lambda_o}{\mu}$$

where $\frac{L}{D} = \frac{1}{2 \sin\theta}$, $\lambda o = 0.6328$ μm, and μ is the refractive index of air. The velocity U can therefore be calculated as follows

$$U = \frac{S}{(\text{Channel no. of peak} - 3) \times \text{sample time}}$$

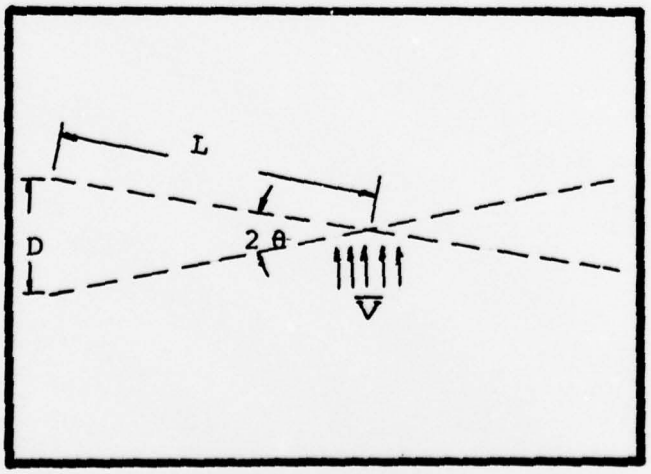

The turbulence intensity (η) can also be calculated from the autocorrelation function

$$\eta = \frac{1}{2\pi} \left[(R - 1) + \frac{1}{n^2} \right]$$

where $n = \frac{r_o}{S}$, r_o is the $1/e^2$ laser beam radius and

$$R = \left(\frac{g_2 - g_1}{g_2 - g_3} \right)$$

g_1, g_2, and g_3 are the values of the autocorrelation function as shown in Fig 8.

$$V_t = V_o \left[1 - \eta^2 - \frac{1}{m^2 n^2 \pi^2} \left(1 + \frac{m^2}{2} \right) \right]$$

where m is the fringe visibility factor.

Since the multiplying factor is essentially a factor of one, the above calculation was not performed. Note that if m is approximately one, if η is small (which would frequently be true), and if η is large, then, the second and third term in the parenthesis are very small.

Phase Modulator

The flow conditions of interest provided many difficulties for the LV system. The flow was either very turbulent or it was of very high velocity. Either of these two conditions attenuated the autocorrelation function such that neither mean velocities nor turbulence intensities could be calculated. Therefore, to extend the operating range of the system, the phase modulator and focusing lens were introduc-d into the set-up. The result was a translation of the fringes in space thus allowing the apparent turbulence intensity to

be increased or decreased. The phase modulator's function was to apply a suitable voltage to two electro-optical crystals so as to affect the phase of a light beam passing through the crystals. The phase modulator drive unit applies a suitable sawtooth voltage to the optical crystals (whose magnitude is controlled). The phase of one outgoing beam is advanced, while the phase of the other beam is retarded. The result is that the fringes are moved spatially by a certain amount of a fringe spacing. This amount is controlled by an adjustment on the drive unit. When the relative phase of the two outgoing beams is changed by π, the optical fringes spatially move half a fringe spacing. A change of 2π increases the spatial movement by one complete fringe spacing. The movement of the fringes may be with the flow or against the flow, hence, increasing or decreasing the differential Doppler frequency and enabling the direction of flow to be determined or the actual mean velocity to be calculated. Under normal circumstances the phase modulator is not required to measure mean velocities. However, to determine flow direction, the phase modulator is essential. Fig 9 shows the effect of the phase modulator.

A system of moving particles such as dust particles in a moving fluid will cause the scattered light to undergo a Doppler shift (Fig 9):

$$f_d = \bar{v} \cdot \bar{k}_s \qquad (1)$$

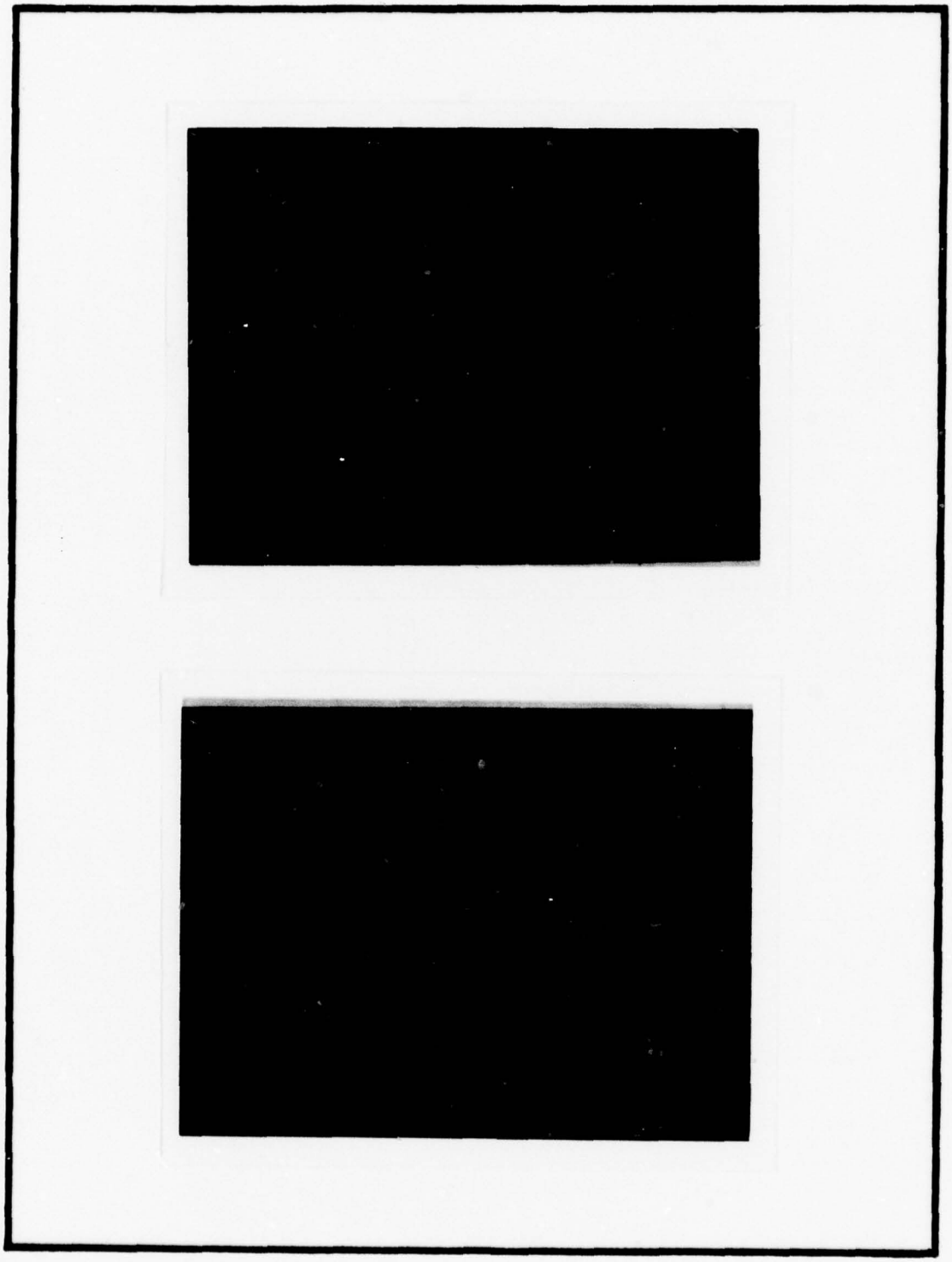

Figure 9. Autocorrelation Function with Phase Modulator and without at High Turbulence Intensities

where $\bar{k}_s$ is the scattering vector whose magnitude is given by

$$k_s = \frac{4\pi}{\lambda_o} \sin\theta \text{ therefore,}$$

$$f_d = \frac{2U \sin\theta}{\lambda_o}$$

Equation (1) shows a particularly significant result; that is, that the relationship between the Doppler frequency shift and the velocity is a linear one, whereas the relationship between the bridge voltage and velocity of a hot wire is not a linear one except when a linearizer is used to render the relationship linear.

The introduction of the phase modulator produces a new frequency

$$f_d' = (f_d \pm \Delta f)$$

where the plus and minus signs are determined by the drive/invert switch on the phase modulator drive unit.

This frequency f_d' would induce some local mean velocity U_i

$$U_i = \frac{f_d' \lambda o}{2 \sin\theta}$$

To calculate the actual local mean velocity U_{loc}, the induced velocity must be multiplied by the ratio of the Doppler frequency shift to the induced frequency shift

$$U_{local} = U_i \left(\frac{f_d}{f_d'} \right)$$

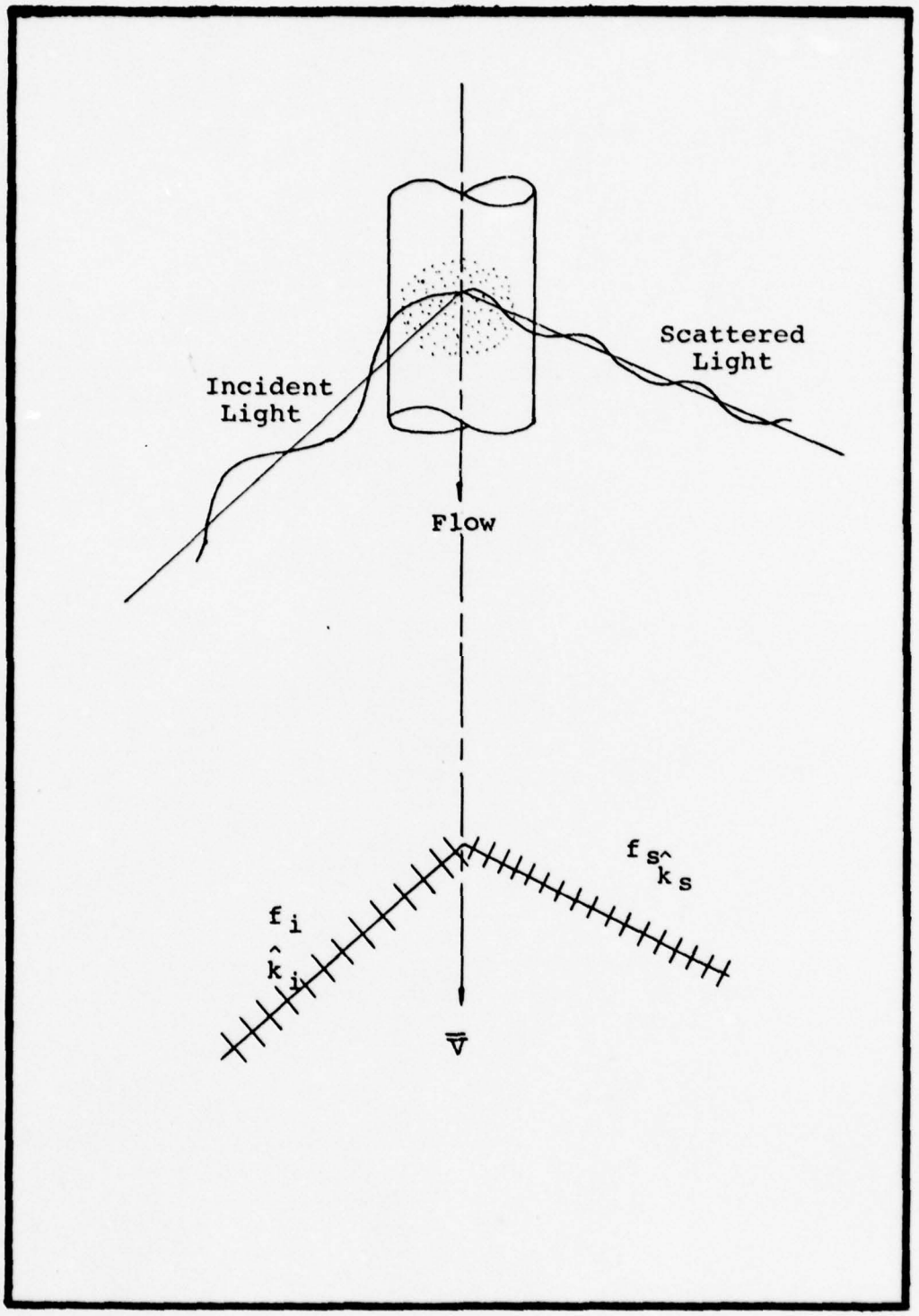

Figure 10. Principle of Laser Velocimetry
Doppler Model

To calculate the turbulence intensity, the same procedure applies

$$\eta = \frac{u}{U_i \left(\frac{f_d}{f'_d} \right)} = \frac{u}{U_{loc}}$$

But this turbulence intensity is based on the local mean velocity. So that these velocimeter values can be plotted and compared to the hot wire values, which were non-dimensionalized by the centreline velocities at the appropriate station, the following transformation must be made

$$\eta = \left(\frac{u}{U_{loc}} \right) \cdot \left(\frac{U_{loc}}{U_{cen}} \right)$$

Photomultiplier Tube

When particles in the flow scatter light in the focal volume, photons are deflected, and they in turn are detected and absorbed at random intervals by the electrically charged cathode. These absorptions create individual photo-electrons at the photo-cathode surface which are then processed by the PM tube electronic arrangements and recorded as discrete pulses of charge corresponding to each particle (Fig 7). These pulse trains are then digitized by the correlator in order to arrive at the autocorrelation function.

V. Experimental Procedure

Hot Wire Anemometer

Sensor Calibration. The sensor calibration procedure is most critical and must be followed religiously in order to obtain accurate data. Basically, the calibration was carried out according to the procedures outlined by Shepard (Ref 12).

Test Conditions. The nozzle exit velocities which were in the compressible flow regime hence the applicable tables (Ref 8) were used to calculate the number of inches of Merriam fluid required to achieve the required Mach number at the exit plane.

If Mach 0.4 was required, then, from the tables

$$\left(\frac{P_a}{P_o}\right) = 0.89562 \quad \text{and} \quad \left(\frac{T_e}{T_o}\right) = 0.96899$$

but

$$\frac{P_o}{P_a} = \left(\frac{P_c + P_a}{P_a}\right) = \left(\frac{P_c}{P_a} + 1\right)$$

Therefore, it follows that

$$P_c = \left(\frac{P_o}{P_a} - 1\right) P_a \qquad (2)$$

Now, in order to translate this chamber pressure into inches of Merriam fluid (where the specific gravity of Merriam fluid is 2.95) eq (2) was multiplied by the appropriate factors to obtain at

$$P_c = \left(0 \cdot 536\right) P_a$$

where P_a is the atmospheric pressure in inches of mercury. It is to be noted that the temperatures and pressures measured in the calming chamber were considered to be under stagnation conditions due to the relatively low velocities at this point.

The number of inches required for M = 0.6 and M = 0.8 were arrived at by a similar method.

The velocities at the exit were then calculated by using the definition of Mach number

$$M_e = \frac{V_e}{a} \qquad (3)$$

where

$$a = \sqrt{\gamma g_c R T_e}$$

By substituting (3) into (2) and using the required constants the velocity at the exit was calculated to be:

$$V_e = 1.3\sqrt{T_c}$$

Pressure in the calming chamber was maintained constant by adjusting the air by-pass valve such that the compressors were running continuously under constant load conditions.

Data Acquisition. The sensors used were mounted such that the required data could be acquired easily and accurately. Since the hot wire anemometer is by its very nature an intrusive system, the degree of disturbance was minimized by designing the support such that the support structures were not in the immediate area of the measurement station but downstream of it.

Sensor vibration affected the durability of the hot wire, especially the X-wires, and also the degree of fluctuation of the meters. For these reasons, the sensor support was also designed to minimize vibrational effects. However, these effects were not entirely eliminated.

The majority of the data was acquired by means of X-wires, however, the single wire was used to probe areas where the velocities were beyond the capabilities of the X-wires, that is, for the nozzle exit velocity profile and the axial velocity decay at M = 0.8.

Mean Velocities, Turbulence Intensities, and Reynold's Shear Stresses. The velocities were directly proportional to the voltage outputs from the hot wire sensors, therefore, all the parameters required were taken directly from the DVM and RMS voltmeters. The voltages were not changed to velocities except as a check, at known positions, to ensure that the output was correct.

The non-dimensionality of mean velocities was achieved by dividing either by U_{cor} or U_{cen}. Turbulence intensities were obtained by dividing the RMS velocities by U_{cen}. Non-dimensional Reynold's Stresses were arrived by multiplying u' by v' or w' and dividing by U^2_{cen}.

Microscale and Integral Scale. The autocorrelation function produced by the correlator was photographed by a Polaroid camera and later used to calculate the microscale and integral scale of turbulence. The microscale (τ) is

simply the time for the smallest eddies produced by the jet to pass the hot wire sensor. It was determined by the method outlined by Hinze (Ref 7) and Shepard (Ref 12):

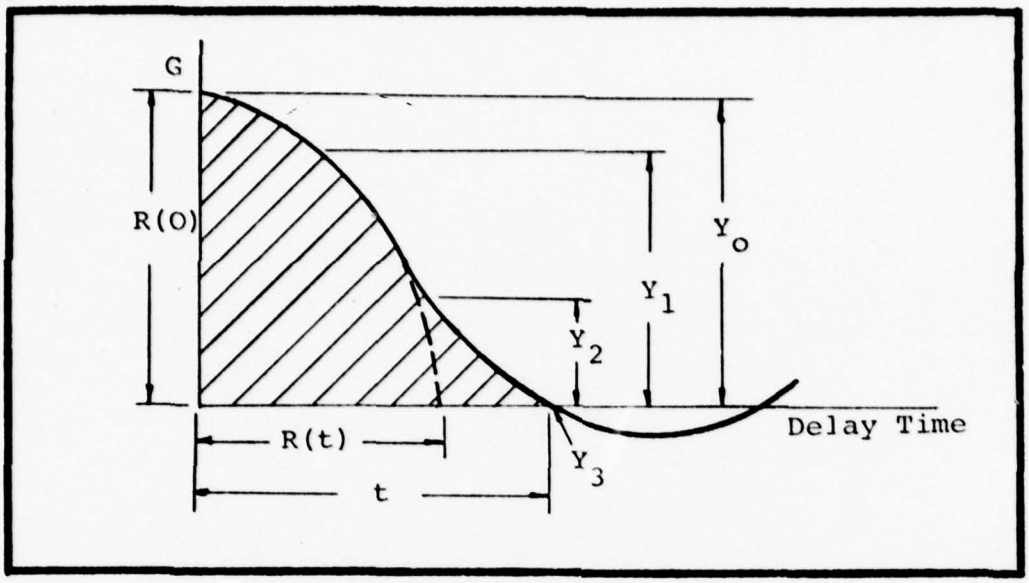

$$\tau = \frac{t}{\sqrt{1 - \frac{R(t)}{R(o)}}}$$

$$= \frac{t}{0.316}$$

where t is defined as the time for the autocorrelation function to first cross the time axis.

To determine the approximate size of the eddies, a transformation from time, t, to distance, x, can be made using Taylor's hypothesis (Ref 7).

$$\frac{\partial}{\partial t} = U\frac{\partial}{\partial x}$$

This allows the time microscale to be transformed to the Taylor microscale (λ) or spatial microscale. This microscale

provides the length of the smallest eddies to pass the sensor. This hypothesis, however, is only valid if the flow is isotropic turbulent flow.

The time integral scale (Γ), which gives the average time of the eddies passing the hot wire sensor, was calculated by measuring the area under the autocorrelation curve using Simpson's rule (Fig 8), and letting

$$Y_o = 1.0 \text{ and } Y_3 = 0.0$$

therefore

$$I = \frac{t}{3}\left(Y_o + 4Y_1 + 2Y_2 + Y_3\right)$$

Taylor's hypothesis was again used to calculate the spatial integral scale, Λ, which provides the average size of the eddies that pass the sensor.

Laser Velocimeter

Traversing Mechanism. The traversing mechanism was designed so as to be able to traverse the jet and measure the required flow parameters. Four main requirements were imposed: that it be relatively rigid, that every portion of the LV system be fixed relative to one another, that it prevent any errant light from entering the photomultiplier tube during the experiment, and that it could easily and accurately be moved from one station to another in the measurement plane of interest.

Alignment of Optics. It was necessary before any data could be collected to ensure that the optical components were properly aligned. Firstly, the two beams exiting the

beamsplitter were positioned 2 cm apart and parallel and then made to pass through the crystals of the phase modulator (if the phase modulator was being used). Secondly, the two beams were focused on the centreline of the jet, and lastly, the focal volume was focused onto the pinhole aperture in the photomultiplier tube. All these steps were critical and erroneous data would result if not carried out properly.

Since the focal volume could not be placed exactly at the centre of the jet visually, a method to find the centreline with the focal volume was developed. A velocity survey of the jet (both sides) in the Y direction was carried out and the velocity profile plotted. Since the jet was assumed symmetrical, the velocity profile could then be folded such that the two sides matched. This allowed the positioning of the centreline of the jet to within 1 mm. The $Y_{1/2}$ value was also found from these plots.

Since the beam pairs at the intersection point are not easily visible, a transparent object such as heavy white paper can be placed at the approximate intersection. The easiest means of focusing the resulting image onto the pinhole was to move the photomultiplier tube laterally and then to rotate it until the image was visible in the window. Then the reflex mirror was rotated such that the image could then be viewed through the x10 magnification eyepiece and final adjustments made on the photomultiplier table. The optimum distance from the beam crossing was the one that

offered the sharpest image of the beam pairs onto the PM tube pinhole aperture.

If the focusing procedure did not produce the required results something more well-defined, such as a meter stick, was placed at the centreline of the jet and the PM tube positioned approximately at the focal length of the combination telephoto lens/spacers. Then, when a number on the meter stick was focused, a return to the original procedure usually yielded the required results.

In order to arrive at the best autocorrelation function, that is, one that would produce the required information at different velocities and turbulence intensities, a certain amount of expertise was required in the dialing in of the appropriate sample time and frequency shift on the phase modulator drive unit. The inability to arrive at an autocorrelation function would frequently indicate a misalignment of the optics.

Mean Velocities and Turbulence Intensities. The mean velocities of interest ranged from the low subsonic to the high subsonic and from laminar flow to very turbulent flow. This LV system was incapable of handling these wider ranging limits. At low velocities and/or low turbulence intensities, the autocorrelation function was excellent (Fig 10).

As previously discussed, suitability of the LV to measure velocities depends mainly on the value of the fringe spacing, S, which itself depends on the value of $\frac{L}{D}$.

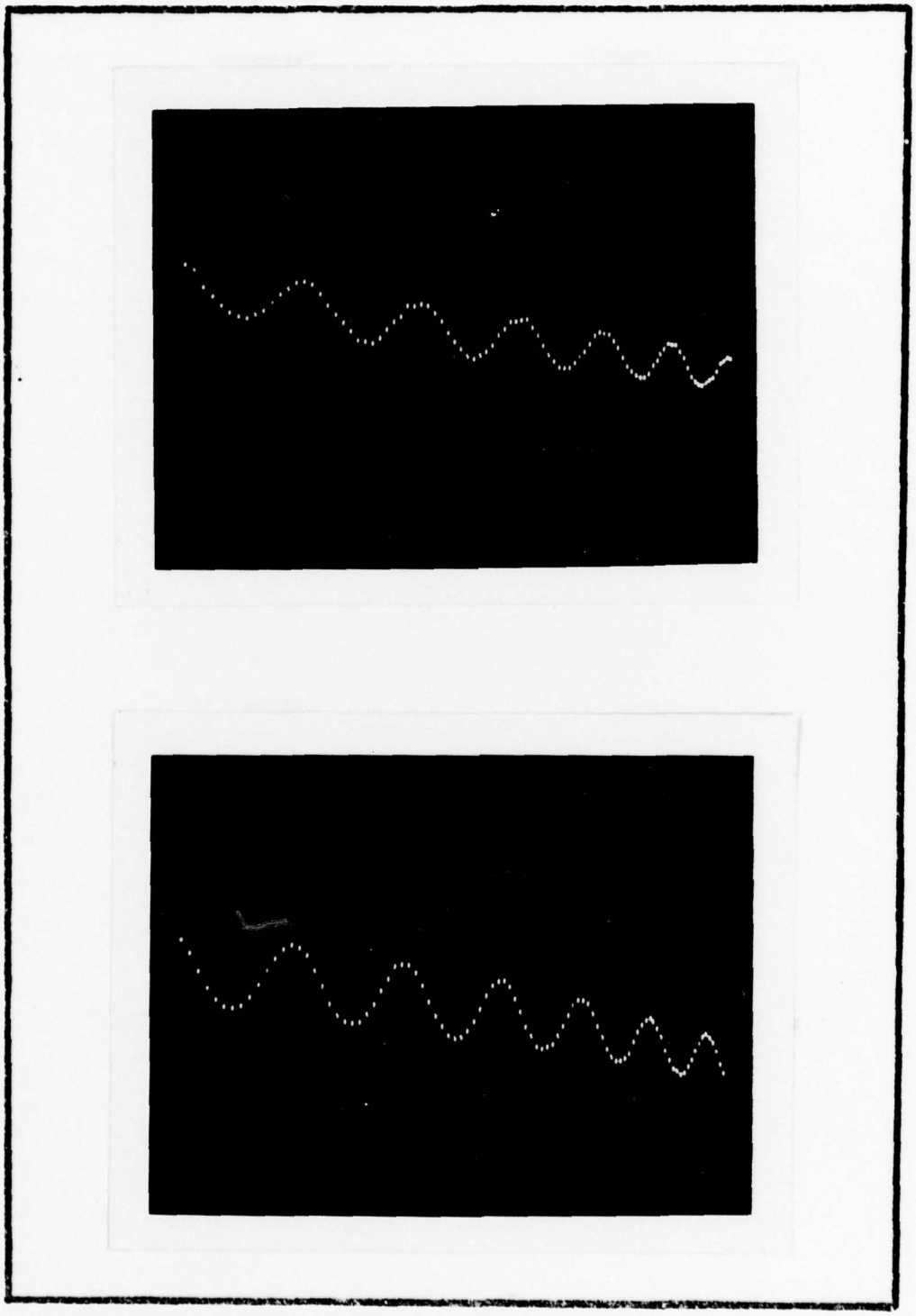

Figure 11. Autocorrelation Function (a) at Low Velocities (<10m/sec) and Low Turbulence Intensities; (b) with Fine Screen Mesh and Coffee Filters

The larger the value of $\frac{L}{D}$, the larger the value of S (very few fringes), hence, the larger the velocity limit. Therefore, to arrive at the axial velocity decay and the exit velocity profile the value of S = 62.4μm was used. In order to arrive at the mean velocity similarity profiles and turbulence intensities, the phase modulator was used.

The non-seeding requirement was also investigated thoroughly as this LV system boasted that only normal laboratory air need be used for the equipment to function properly. As opposed to the hot wire anemometer whose requirement is for extremely clean air to increase the longevity of the wire, the LV system thrives on dust particles. As previously explained, a paper filter and fine wire mesh arrangement was present in the nozzle area of the jet. When an attempt was made to use the LV with the same arrangement, no correlation function was obtained. The paper filters and fine wire mesh were removed and all subsequent measurements were made without them. The assumption was that the filtering system was not compatible with the LV system.

Once a certain amount of dexterity with the equipment was gained, then another attempt was made to introduce the filtering arrangement to see its effect. This time a well-defined autocorrelation function was achieved with both filters in (Fig 11).

Velocity measurements were only made in the X-direction. Velocity measurements in the Y and Z directions would have

required major modifications to the traversing mechanism. Measurements in the Y direction could have been made simply by rotating the beamsplitter, however, the beamsplitter produced two beams not symmetrical about the centreline of the laser. Therefore, the rotation of the beamsplitter would have resulted in measurements in a slightly different position in the flow and, hence, not valid for comparison purposes.

Data Reduction

In order that the data acquired could be easily and visually scanned for validity, computer programs were developed prior to the running of the experiment. These programs reduced the data and plotted it in the shortest possible time.

Therefore, large amounts of data could easily be handled by using the CDC 6600 computer and Calcomp Plotter and produce a quick indication of trends.

Some data of interest is presented in Annex H. All other data and computer programs are held in Rm 142 of the Air Force Institute of Technology School of Engineering, Wright-Patterson Air Force Base, Dayton, Ohio.

VI. Results and Discussion of Results

Experimental Limitations

The central aim of this study was not to study the behaviour of the jet but to evaluate the Malvern LV system by comparing its results with those of the hot wire system. To accomplish that aim, a duplication of all data garnered by the hot wire system was attempted with the LV system. Moreover, a comparison of the two systems would also evaluate the efficiency and accuracy of the hot wire anemometer.

To maintain the study within a defined time frame, certain parameters were chosen as being ideal for evaluation purposes and also for comparison to the results of Shepard. Not all parameters were within the capability of the LV system. Lower subsonic velocities would have allowed better comparisons as these velocities would have been well within the limits of the LV.

Results

Some overall comparative results are presented within the following pages but others which were more specifically defined results are presented in Appendices E, F, and G. Some appropriate data are presented in Annex H. The remaining data and computer programs are available as previously explained.

All data was non-dimensionalized as shown on the appropriate plots. The method used wat that used by Shepard

so that a proper comparison with his results could be accomplished.

Exit Velocity Profiles

The exit velocity profile obtained with an X-wire at M = 0.4 was a completely flat profile (Fig 12). The LV profile superimposed here was done at M = 0.6. When carried out with a single wire and at M = 0.6, the "top hat" profile of Fig 13 was clearly in evidence. Fig 13 also shows that the LV results agree relatively well with the hot wire results except that the LV was sensing velocities well past the end of the jet exit. There are three possible explanations for this occurrence. One is that the spatial resolution of the system is not good at high values of fringe spacing, S. At high values of S, the two beams intersect not at a single point but within a length of approximately 20 cm and this distance increases as the angle between the beams is decreased. The focusing procedure is no longer exact. Another factor which undoubtedly contributed was the crude traversing mechanism considering the relatively small jet exit width. Lastly, at high velocities, even with the laminar flow at the exit, the autocorrelation function was so attenuated (Fig 14) that the information required to produce mean velocities is concentrated within the first 6 or 7 channels of the correlator where the first 3 channels are monitoring channels only. Hence, the small differences in velocity expected as the jet

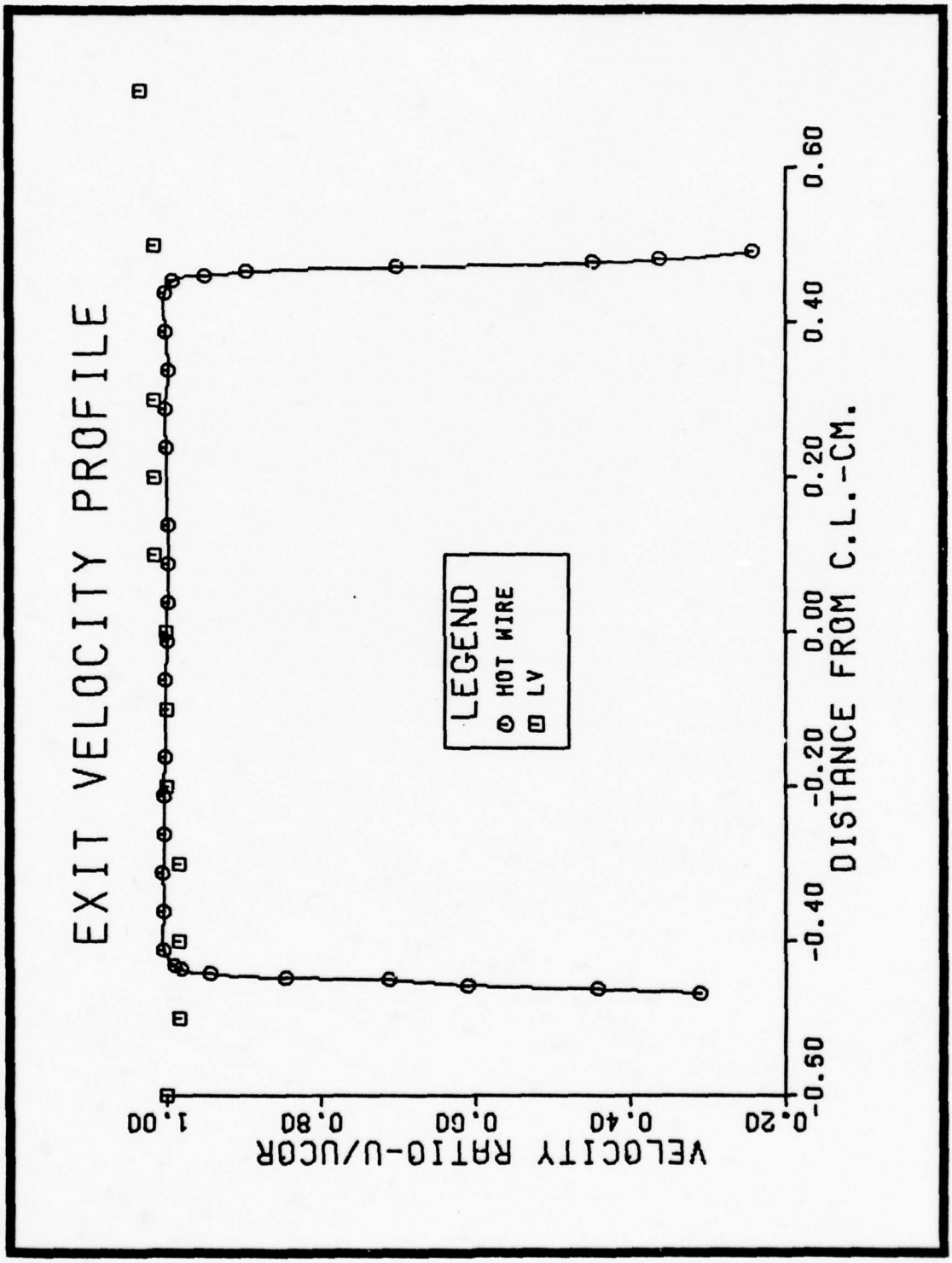

FIG.12 HOT WIRE AND LV NOZZLE EXIT PROFILE

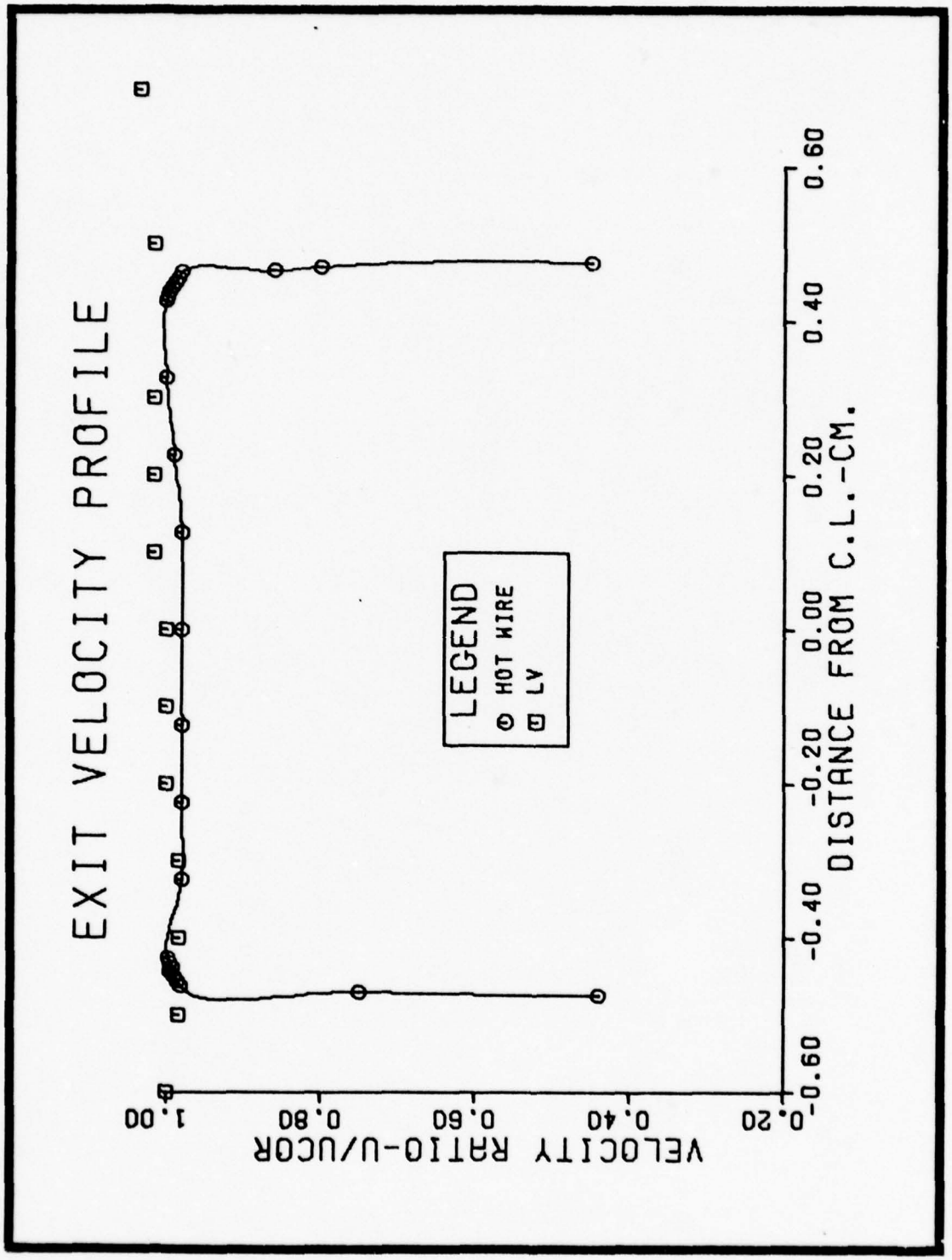

FIG.13 HOT WIRE AND LV NOZZLE EXIT PROFILE

is traversed are only fractions of one channel. These readings are only accurate to $\pm .5$ channels. There are a total of 99 channels which produce the autocorrelation functions and are displayed in Fig 8.

Axial Velocity Decay

Figs 15 and 16 show that the hot wire and LV results agree extremely well with the theoretical curve as calculated in Annex B and with each other. Whereas the hot wire results do not demonstrate too much of a change in the length of the potential core from one Mach number to another, the LV shows very clearly that the potential core increases in length as the Mach number is increased to a maximum of 8 cm at M = 0.8. This is shown by Fig 16 and is greater than the value of approximately 5 jet widths usually quoted in literature.

Mean Velocity Similarity

When measurements in a free jet are made across the jet at points where the flow is fully isotropic turbulent, the mean velocities present at different stations in the flow will all reduce to the same curve if properly non-dimensionalized. In order to compare the results to theoretical curves developed by Tollmien and Görtler (Ref 2), the velocities and distances from the centreline were non-dimensionalized by dividing by U_{cen} and $Y_{1/2}$ respectively.

Fig 17 shows that the hot wire results agree well with the Tollmien curve at distances close to the centreline and compare quite well with the Görtler curve at large

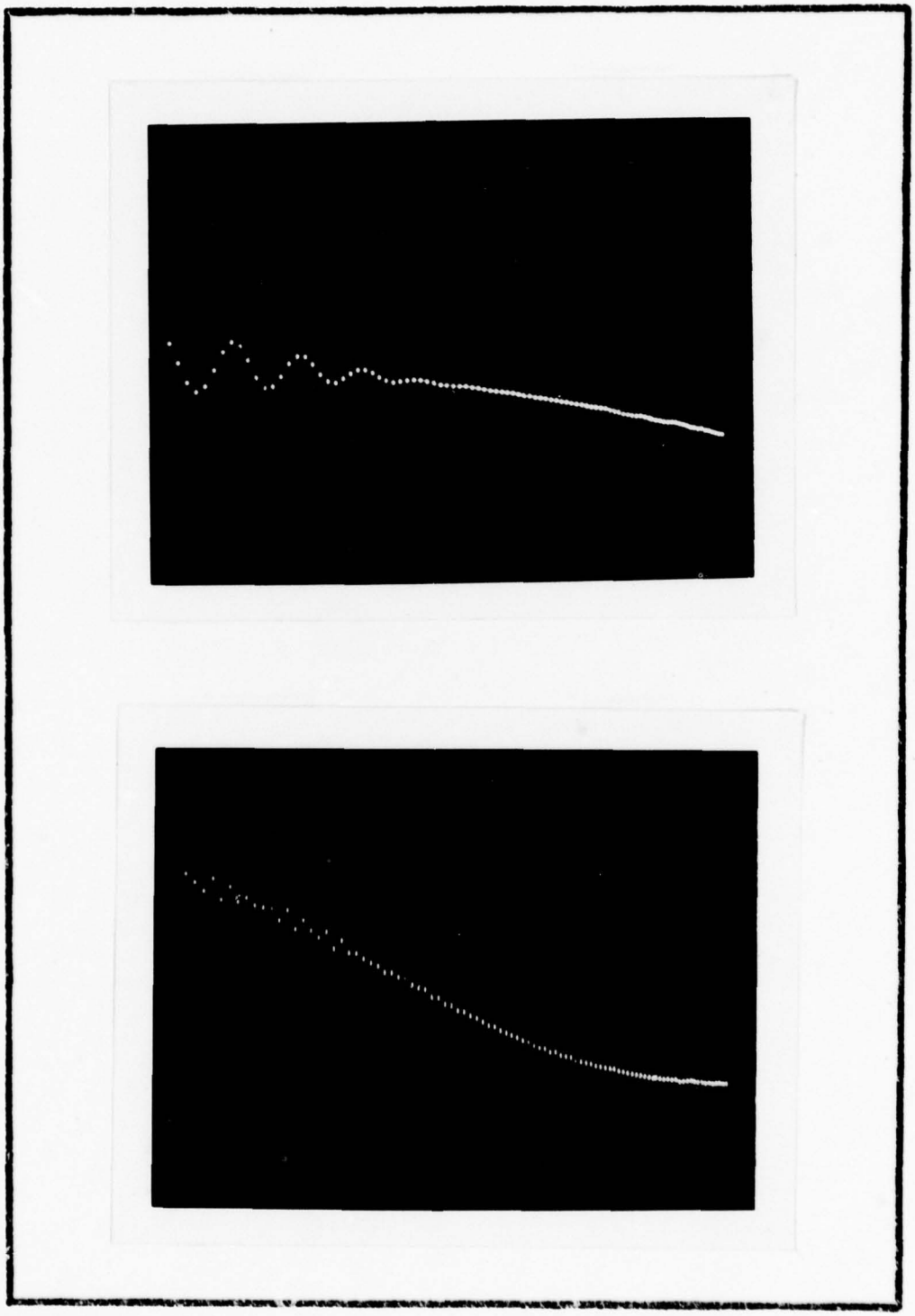

Figure 14. Attenuation of the Autocorrelation Function as Velocity or Turbulence Intensity Increases

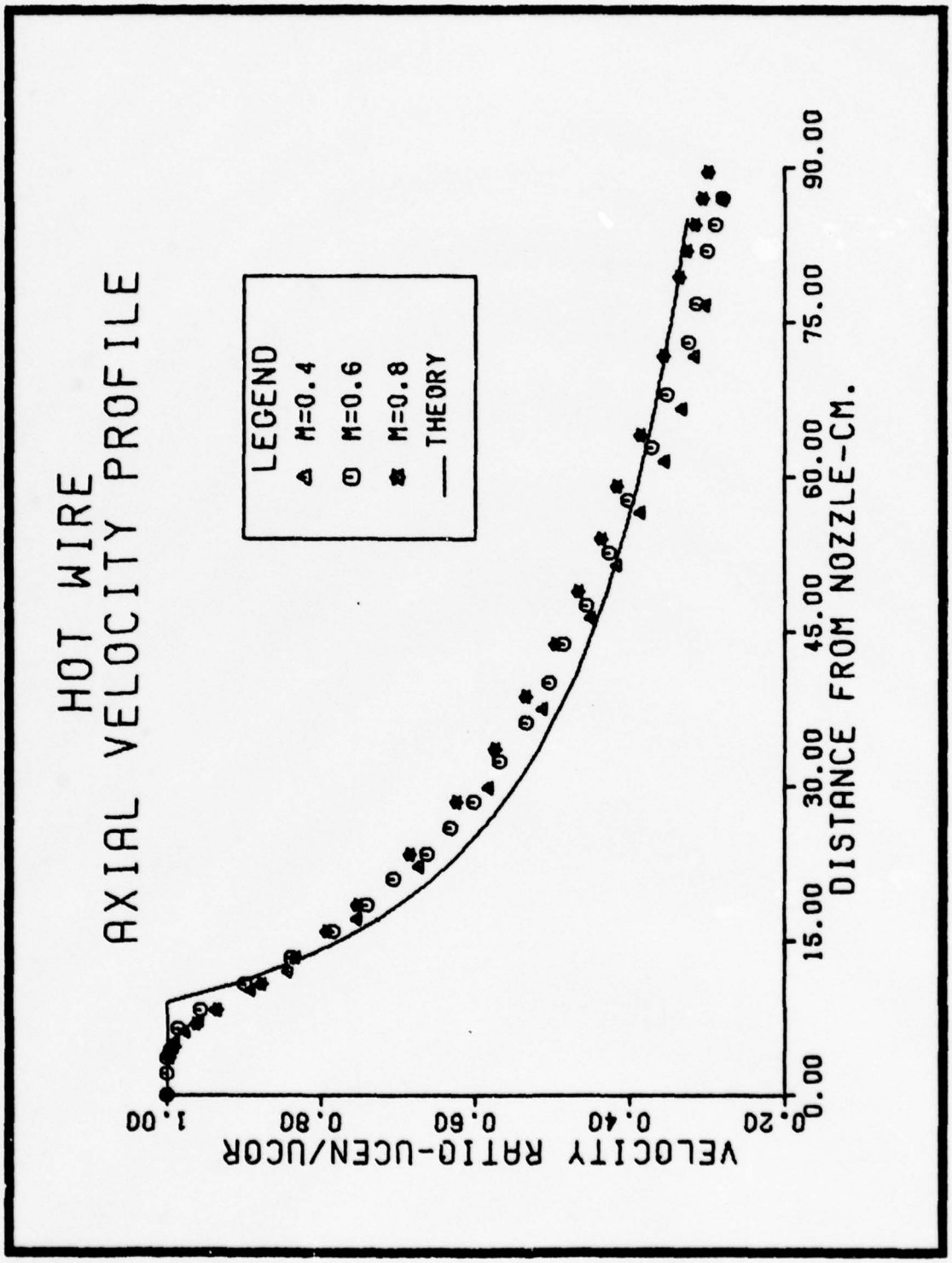

FIG. 15 HOT WIRE AXIAL VELOCITY PROFILE

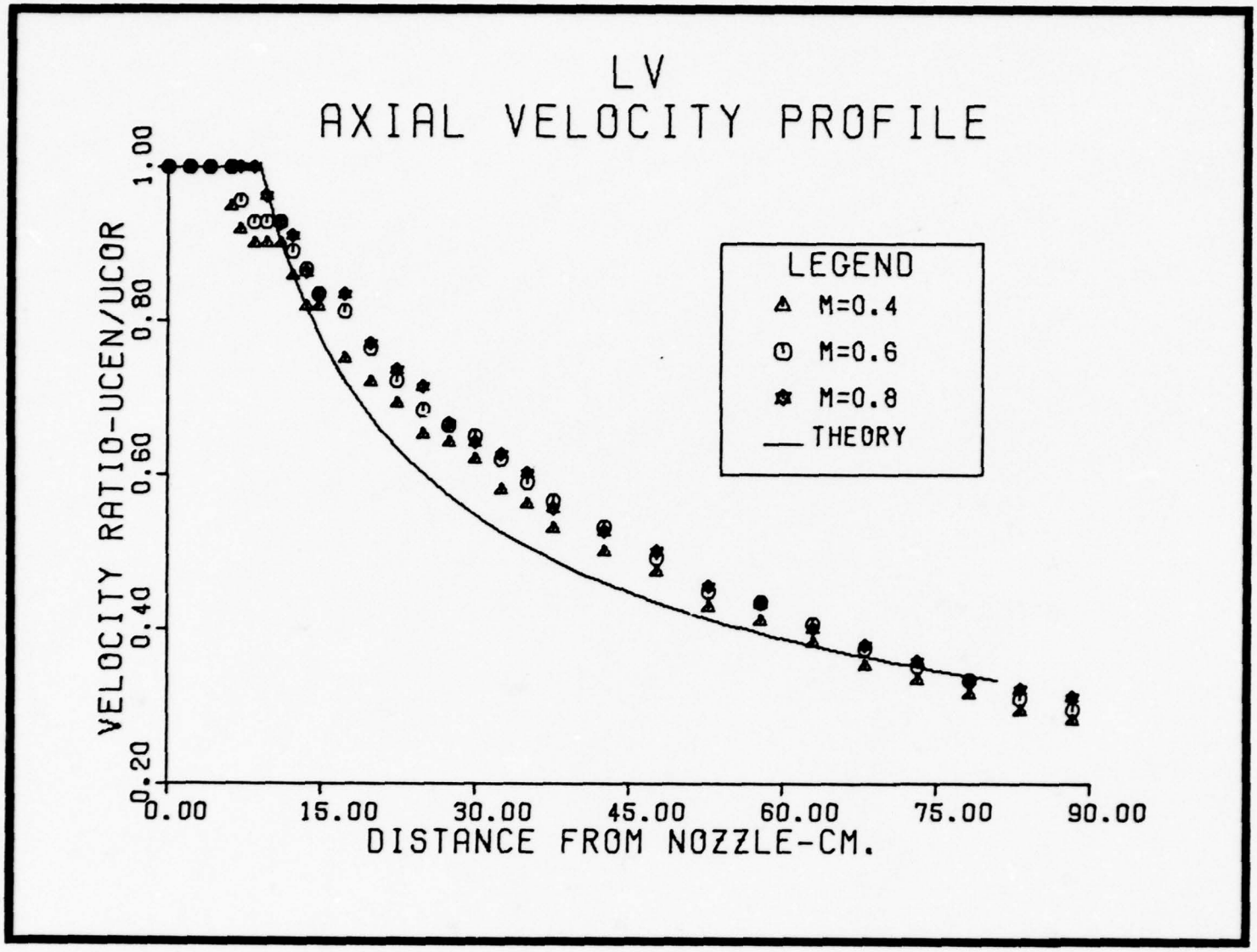

FIG.16 LV AXIAL VELOCITY PROFILE

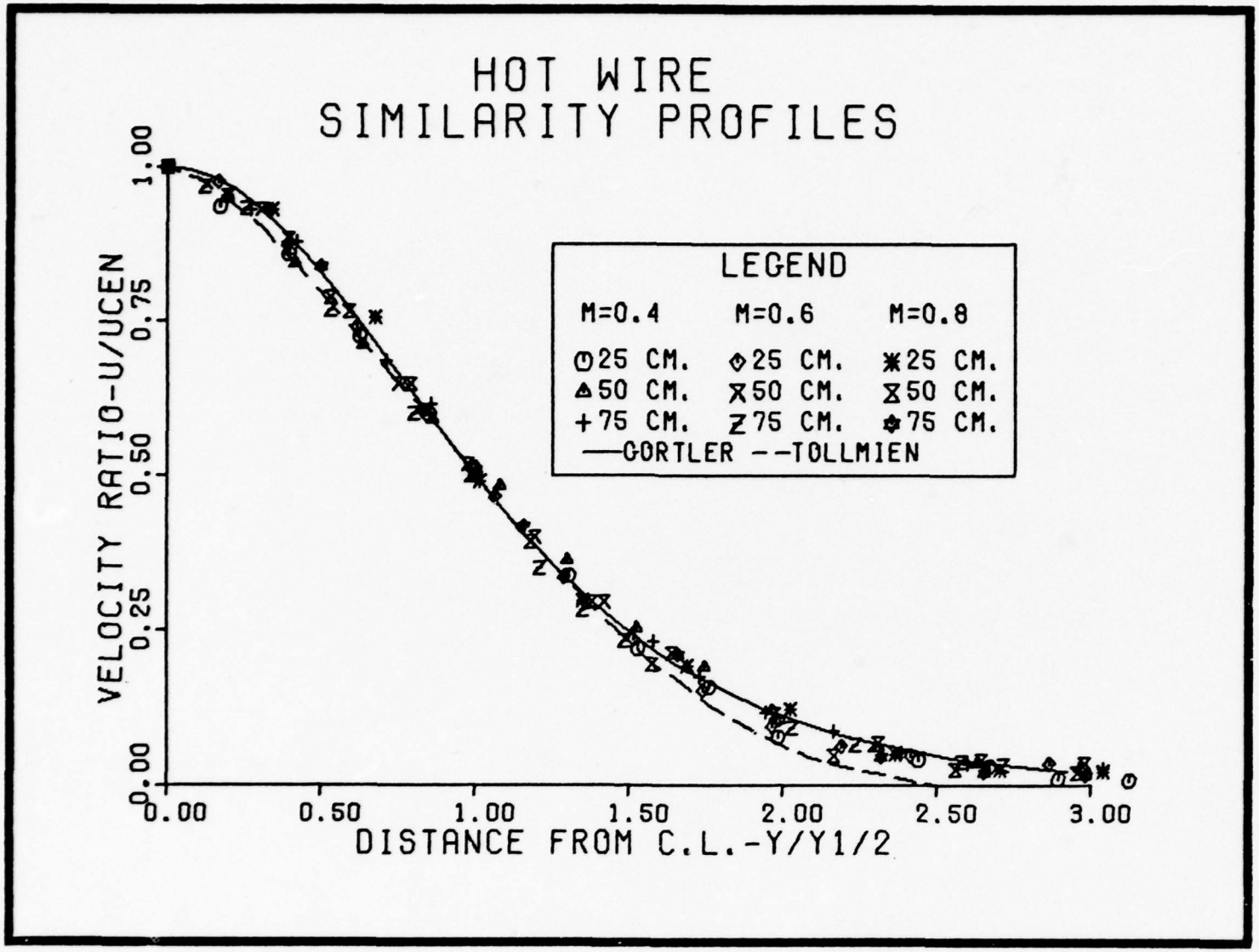

FIG.17 HOT WIRE MEAN VELOCITY SIMILARITY PROFILES

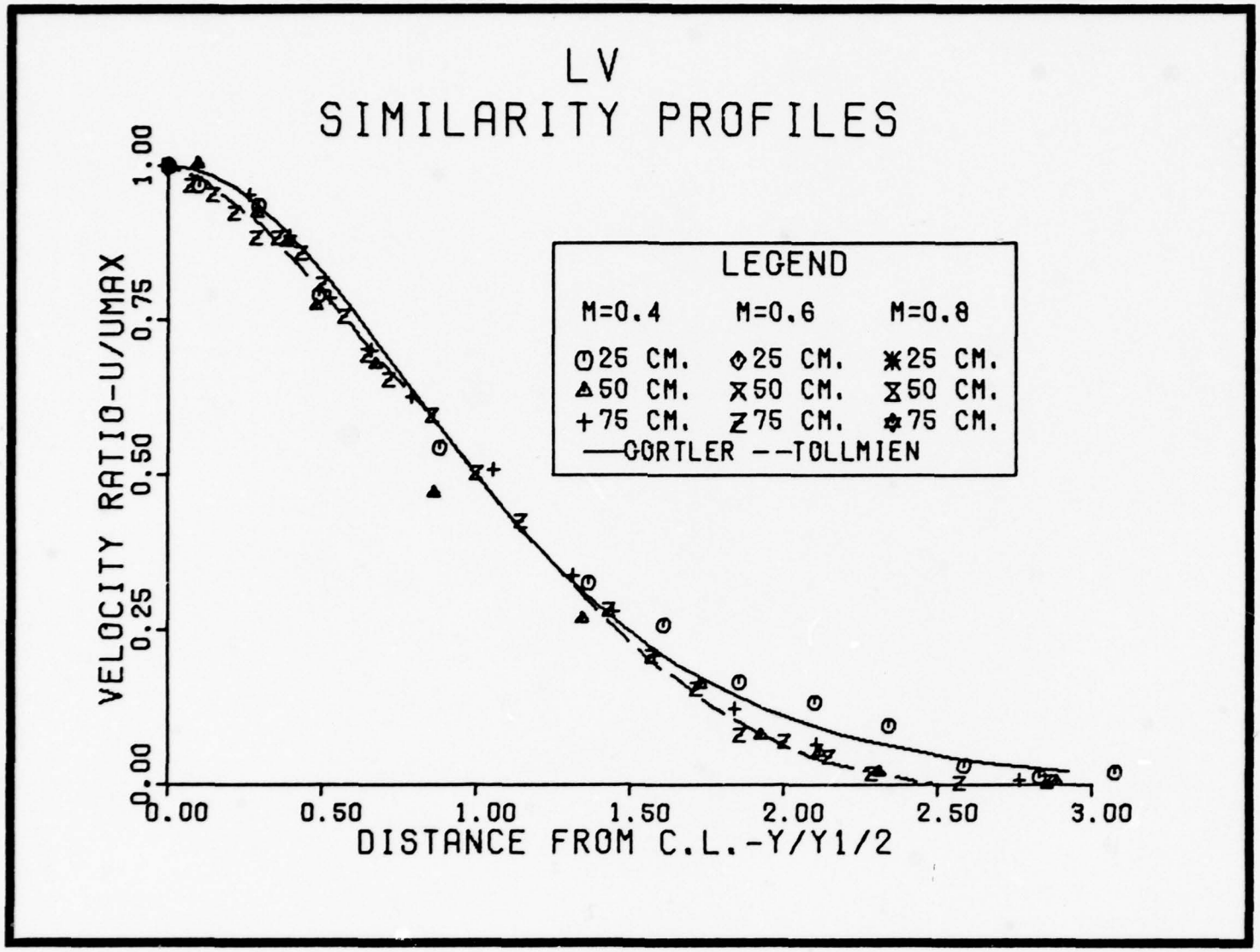

FIG.18 LV MEAN VELOCITY SIMILARITY PROFILES

distances from the centreline. Although there is some scattering of the data, the results are quite good and they also agree well with Shepard's results.

Fig 18 shows the mean velocity profiles arrived at with the LV. The M = 0.8, 25 cm and 50 cm stations and the M = 0.6 and 25 cm station were beyond the capability of this LV system. The available data, however, was quite good. Again, there was some experimental scatter but slightly more than the hot wire for reasons already explained.

From Figs 17 and 18, the spread angle of the jet was calculated to be approximately 40 degrees which is 4 times that calculated by Shepard. Since his mean velocity similarity profiles also agree well with predicted values it is assumed that he made a mathematical error.

Turbulence Intensity Profiles

Fig 19 shows that similar to the mean velocity similarity profiles at each data plane and Mach number, the turbulence intensities, $\frac{u'}{U_{cen}}$, also reduce to one single curve. At M = 0.8 and 25 cm, the curve does not quite agree as well as the others because the velocities were high at this station and the hot wire was near its endurance limit. For this reason the readings had to be recorded quickly and this induced some errors. Also, as the spatial microscale will also show, it is possible that the flow was not quite fully isotropic turbulent flow.

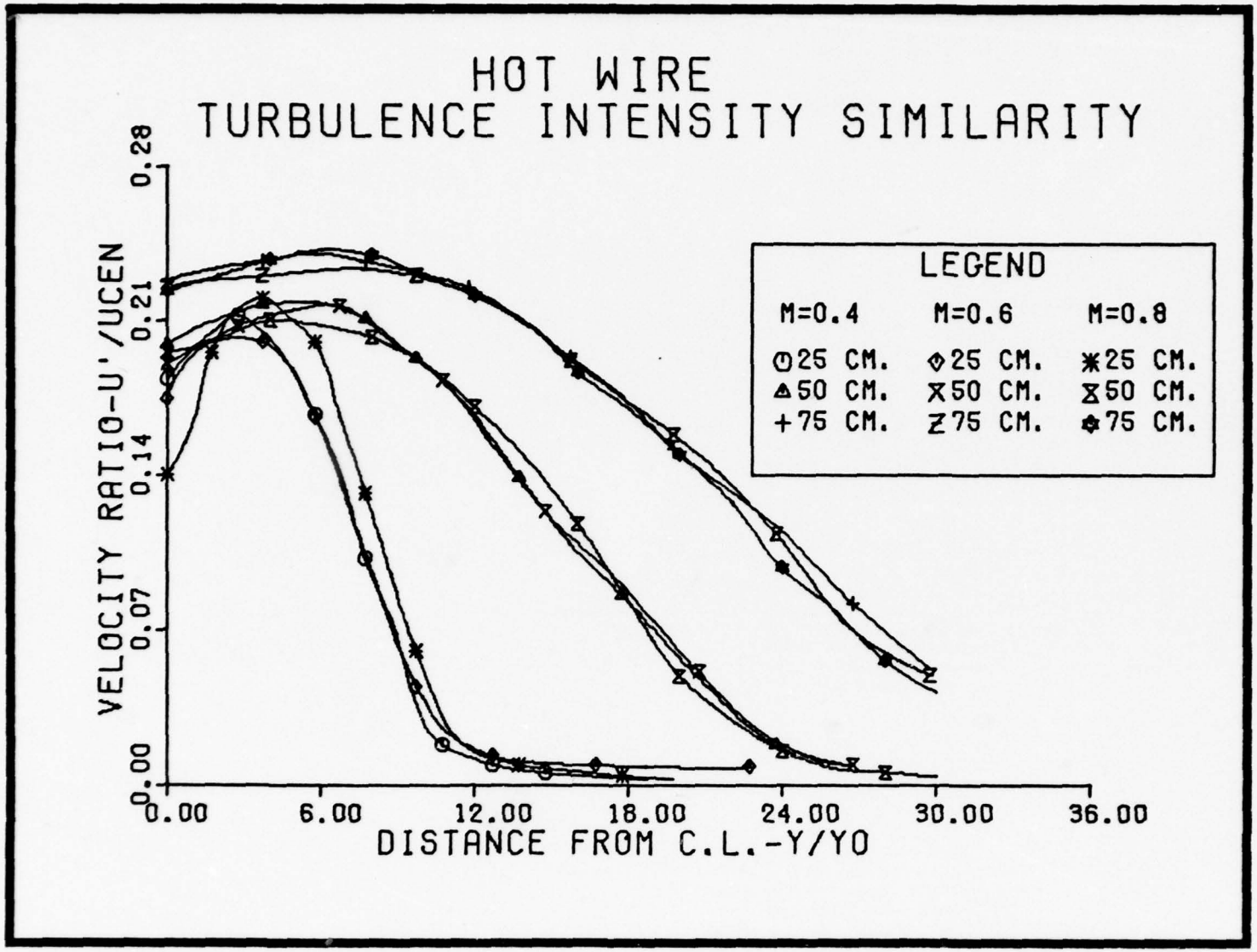

FIG.19 HOT WIRE TURBULENCE INTENSITY SIMILARITY PROFILES

A comparison of Figs 20, 21, 22 in Appendix E, 29, 30 31 in Appendix F, and 38, 39, 40 in Appendix G to the results arrived at by Shepard (Ref 12) showed that the results presented here are slightly higher at the point of peak turbulence intensity and that, as opposed to Shepard, the $\frac{w'}{U_{cen}}$ intensities were very close to those of $\frac{v'}{U_{cen}}$ at all stations and Mach numbers. Shepard found that the $\frac{w'}{U_{cen}}$ were always much smaller than the $\frac{v'}{U_{cen}}$ intensities.

It is also apparent from these figures that all three components remain relatively similar at different Mach numbers and same measurement plane. Although the $\frac{v'}{U_{cen}}$ and $\frac{w'}{U_{cen}}$ were not plotted for similarity as the $\frac{u'}{U_{cen}}$ they appear as if they would reduce just as well, except once again for the 25 cm station. This inconsistency is also probably due to measurement errors. The correction factor for tangential cooling for the turbulence intensities perpendicular to the mean streamwise flow was 1.05928 (Ref 12).

The LV results did not lend themselves to a reasonable comparison between the two systems as the LV did not provide enough data at the different stations as can be seen on the figures provided. Those results available show that as the velocity decreases to a value within the system's limit, it produces values which are more reasonable but still very erratic. Results of turbulence intensities at M = 0.4 and 25, 50 and 75 cm stations very close to the centreline were not plotted as they were so completely erratic that they went

off scale. However, the results in tabular form are available in Appendix H.

Reynold's Shear Stresses

Figures 23, 24, 32 in Appendix E, and 33, 41, 42 in Appendix F show that the $\frac{u'v'}{U^2_{cen}}$ and $\frac{u'w'}{U^2_{cen}}$ resemble each other very closely and are well behaved. Both increased at the centreline as velocity increased, and then decreased slightly at M = 0.8. Generally, they were very much alike in profile and magnitude, which is in agreement with the turbulence intensity values where the v' and w' were very closely matched. The method used to non-dimensionalize is a generally accepted procedure.

The results of $\frac{u'v'}{U^2_{cen}}$ presented here disagree with those of Shepard. They are much higher at the point of peak stresses. The $\frac{u'w'}{U^2_{cen}}$ stresses were also much higher than those reported by Shepard and did not decrease overall as the Mach number was increased but remained constant.

An explanation for this could be that the change in set-up increased turbulence and, hence, the RMS velocity values were increased.

The Reynold's stresses correction factor for tangential cooling used was 1.02922 (Ref 12).

Time and Spatial Microscales

Figures 25, 34 and 43 in Appendices E, F, and G show that the time microscale profiles are well-behaved at all Mach numbers. They are also very small at the centre and seem to

increase exponentially towards the outer edges of the jet. This is to be expected as the size of the eddies is smaller at the centre than at the edges.

At higher Mach numbers, the time microscale tends to remain smaller for a greater distance from the centreline and it always increased with increasing distance from the jet exit. Shepard's results were lower in magnitude but the trend and shape of the curves were similar.

The spatial microscale (Figs 26, 35 and 44) produce some interesting results at M ≈ 0.4 and 0.8 and at 25 cm, and at a somewhat smaller scale at M = 0.8 and 50 cm. The spatial microscale at this station does not gradually decrease as the others do but increases sharply and then decreases. The reason for this behaviour is that the mean velocity and time microscale both increase very rapidly between 1 and 3 cm from the centreline and then, although the time microscale is still increasing rapidly, the velocity decreases at a greater rate.

As has been explained, the spatial microscale was determined by multiplying the time microscale by the local mean velocity and that this was acceptable only as long as the flow was isotropic turbulent flow. It is possible that at the Mach numbers and stations mentioned the flow was not isotropic turbulent flow.

Time and Spatial Integral Scales

The time integral scales (Figs 27, 36 and 45 in Appendices E, F, and G) follow the same trend as the time microscales

except that they are not quite as well-behaved. Some error was induced in the calculation of the areas under autocorrelation function where only 3 points were used in the process of using Simpson's rule.

Shepard's results show the same trend except that they are higher by one magnitude and not quite as well-behaved.

The special integral scales (Figs 28, 37 and 46 in Appendices E, F, and G) decrease in value as the distance from the centreline increases similar to the spatial micro-scales and they are relatively well-behaved. A similar abnormality occurs at M = 0.8 and 0.6 at 25 cm as with the spatial microscales. Again the possible explanation for this occurrence is the same as that for the spatial microscale.

Shepard's results are not well-behaved and tend to remain relatively constant across the flow. Again in this case, the magnitudes of the results are much larger than the results presented here.

The spatial integral scales presented here were arrived at by using Taylor's hypothesis: the time integral scales were multiplied by the local mean velocity.

VII. Conclusions

The Laser Velocimeter was made operational and the turbulence and mean velocity parameters were measured. The results were then compared to those of the hot wire anemometer. In view of the results, the following are the conclusions:

1. Of the three different types of wires used, the most fragile was the TSI 1240 T1.5 X-wire and the TSI 1214 T1.5 the most rugged, in high velocity/high turbulence situations. All the hot wires were found to be very accurate in measuring turbulence intensities and mean velocities. The LV system, while very accurate for mean velocities, did not perform well in the range of turbulence intensities required. The LV, as opposed to the hot wire, could not, however, be affected by the flow with regards to its performance or non-performance.

2. The calibration procedure and the setting of the linearizer constants of the hot wire is considered to be too lengthy a process considering the fragility of the hot wires and the tendency of the linearizer pots to wander. The LV system required no calibration whatsoever and its most stringent requirement was htat it be focused properly. The measurement procedure for the LV was also much easier than the hot wire in that the laser beam could not be damaged by harsh flow conditions and measurements could be made leisurely.

3. The RMS and DC voltage readings from the hot wire fluctuated wildly at high turbulence intensities. This rendered the data taking very difficult. An integrating voltmeter which would provide a mean value over a specified period of observation time, would have helped matters greatly. The LV was even more limited in this respect. High turbulence intensities and/or high velocities rendered the system completely sterile.

4. The hot wire system was easily adaptable within the bounds of this study, and the measurements made were very comprehensive; whereas, the LV was very limited without the use of a complex traversing arrangement and other complementary equipment.

5. The LV system did not require any "seeding". It was also operable with the screens and one paper filter up to a maximum velocity of approximately 70 m/sec.

6. For this set-up the maximum velocity measurable in laminar flow while retaining some reasonable spatial resolution was 260 m/sec. The maximum velocity measurable with some turbulence was in the range of 80 m/sec.

7. The LV system had to be operated in relative darkness which could be restrictive in certain situations.

8. The spatial resolution of the LV system at high values of fringe spacings was not good and this fact coupled with the relatively crude traversing mechanism did not provide the same excellent results of the hot wire system at the jet exit.

9. The relationship between the Doppler frequency shift and the velocity is linear whereas the relationship between the bridge voltage and velocity is not, thereby making the linearization process an integral part of the system. For this reason, the LV is more suited than a hot wire for making velocity measurements in highly turbulent regions provided, of course, that the velocities are within the capabilities of the system.

10. The 50 nanosecond limit of the LV was restrictive in that it limited the range of velocities that could be measured. If the sample time were to be lowered by a factor of 5, for example, the velocity that could be measured would be multiplied by a factor of 5, to approximately 1250 m/sec versus a present capability of only 250 m/sec.

11. The phase modulator frequency shift of approximately 1mHz was not quite sufficient in most high turbulence and high velocity situations experienced in the flow of interest of this study.

VIII. Recommendations

The following are recommendations to bring about possible improvement to the system and recommendations for future study:

1. Since the hot wire linearizer constants were not easily set, a computer interface with the hot wire anemometer could use the calibration curve for the specific hot wire along with the bridge voltage output to provide direct velocity measurements. This would solve the most capricious problem of the hot wire system by obviating the need for the linearizer.

2. The LV system could also easily be adapted with a calculator (a calculator output jack is available on the correlator) to provide direct velocity and turbulence intensity measurements and visually display the data by routing the data to a plotter. This method of data reduction would indicate trends in the flow which could then be interpreted very quickly and with the minimum amount of programming.

3. The availability of a 10 nanosecond correlator would increase the capability of the system in that the maximum velocity measurements could be increased by a factor of 5 over this present system.

4. A different phase modulator with a frequency shift of 50MHz as opposed to the present maximum of 1MHz would also increase the maximum velocity/turbulence intensities measurable.

5. The beamsplitter arrangement and traversing mechanism should be modified so that LV velocity measurements can be made in more than one coordinate direction.

6. The LV system (with phase modulator) was not used to indicate direction of flows as the direction of flow of the jet was readily apparent. This facet of the system should be investigated in a situation where flow reversal occurs at relatively low velocities to evaluate this system's very special capability.

7. This LV system should be evaluated in low velocity hot flows. If the results are accurate, then an attempt could be made to measure and evaluate combustor and after-burner burning irregularities by studying their flow behaviour.

8. The study of flow to inlets of jet engines is very important in that the proper flow characteristics will prevent, amongst other problems, compressor stalls. These results could also be used to increase engine intake efficiencies. The LV system with the above improvements would perform this function very well in that the flow velocities to intakes is usually in the range of M = 0.4 and the LV system would be perfectly adapted for that velocity.

9. The LV system requires more evaluation in actual situations such as wind tunnel measurements before a final verdict as regards its effectiveness can be given.

Bibliography

1. Abbiss, J.B., Chubb, T.W., and Pike, E.R. "Laser Doppler Anemometry". Optics and Laser Technology: 249-261 (Dec 1974).
2. Abramovich, G.N. The Theory of Turbulent Jets. Cambridge, Massachusetts: The M.I.T. Press. 1963.
3. Birch, A.D., Brown, D.R., and Thomas, J.R. "Photon Correlation and its application to the Measurement of Turbulence Parameters in Fluid Flows". Journal of Physics D: Applied Physics, 8: 438-447 (1975).
4. Bradbury, L.S. "The Structure of a Self-preserving Turbulent Plane Jet". Journal of Fluid Mechanics, 23: 31-64 (1965).
5. Bradshaw, P. An Introduction to Turbulence and its Measurement. Oxford, England: Pergamon Press, Ltd., 1971.
6. Foord, R., Harvey, A.F., and Jones, R. "A Solid State Electro-Optic Phase Modulator For Laser Doppler Anemometry". Journal of Physics D: Applied Physics, 7: L36-L39 (1974).
7. Hinze, J.O. Turbulence. New York: McGraw-Hill Book Company, 1959.
8. Keenan, J.H., and Kaye, J. Gas Tables. Wiley and Sons, Inc., New York, 1945.

9. Liepmann, H.W., and Laufer, J. "An Investigation of Free Turbulent Mixing". NACA Technical Note 1257. Washington: U.S. Government Printing Office, 1947.

10. Malvern Instruments, Ltd. Operating and Installation Manual. Spring Lane Trading Estate, Malvern Link, Worcestershire WR14 1AL, England.

11. Pai, S.I. Fluid Dynamics of Jets. Van Norstrand Company, Inc., Canada, 1954.

12. Schlichting, H. Boundary Layer Theory. Fourth Edition. McGraw-Hill Book Co., Inc. New York, 1962.

13. Shepard, W.K. Turbulence Measurements in a Plane Free Jet at High Subsonic Velocities. M.S. Thesis. Wright Patterson Air Force Base, Ohio: Air Force Institute of Technology, Dec. 1974.

14. Tennekes, H., and Lumley, J.L. A First Course in Turbulence. M.I.T. Press, Cambridge, 1972.

15. Thermo-Systems Inc. Instruction Manual for Model 1015C Correlator. St. Paul, Minnesota: Thermo-Systems Inc.

16. Thermo-Systems Inc. Operating and Service Manual for 1050 Series Constant Temperature Anemometer and Related Accessories. St. Paul, Minnesota: Thermo-Systems Inc.

17. White, Frank M. Viscous Fluid Flow. McGraw-Hill Book Co., Inc., New York, 1974.

18. Wygnanski, I., and Fiedler, H.E. "The Two-Dimensional Mixing Region". Journal of Fluid Mechanics, 41: 327-361 (1970).

19. Wygnanski, I., and Fiedler, H.E. "Some Measurements in the Self-Preserving Jet". Journal of Fluid Mechanics, 38: 577-612 (1969).

Appendix A

A Two-Dimensional Turbulent Free Jet - Theory (Ref 11)

Turbulent flow in a free jet resembles closely laminar flow except for the large quantitative differences due to turbulent motion.

Both laminar and turbulent motion are present in the free jet, however, due to their relative magnitudes the laminar portion can be neglected.

For the two-dimensional case, the Navier-Stokes equations reduce to:

$$\rho\left(\frac{\partial u}{\partial t} + u\frac{\partial u}{\partial x} + v\frac{\partial u}{\partial y}\right) = \mu\frac{\partial^2 u}{\partial y^2} \qquad \text{(A1)}$$

for the equation of motion, and

$$\frac{\partial u}{\partial x} + \frac{\partial v}{\partial y} = 0 \qquad \text{(A2)}$$

for the continuity equation.

The pressure term can be neglected as it can be assumed that the pressure remains constant, at least to a first approximation.

Terms which are linear in turbulent components such as $\frac{\partial u'}{\partial t}$ vanish; similarly, for mixed terms such as $(U \cdot u')$.

To obtain the equation for steady flow in the turbulent jet, the flow is separated as follows:

$$u = U + u' \tag{A3}$$

$$v = V + v' \tag{A4}$$

where

$$U = \frac{1}{t_1} \int_{t_o}^{t_1} u\,dt$$

The mean values are taken over a sufficiently long interval of time that

$$\overline{u'} = 0$$

$$\overline{v'} = 0$$

By substituting (A2) and (A3) into (A1) and simplifying

$$U\frac{\partial U}{\partial x} + V\frac{\partial U}{\partial y} = -\frac{\partial}{\partial y}\left(\overline{u'v'}\right) \tag{A5}$$

$$\frac{\partial U}{\partial x} + \frac{\partial V}{\partial y} = 0 \tag{A6}$$

where $\tau'_{yx} = -\overline{\rho u'v'}$ are the apparent or Reynold's stresses of turbulent flow.

Now integrate (A5) over the jet half-width b and arrive at

$$\int_o^b \frac{\partial}{\partial x}(U^2)\,dy = 0 \tag{A7}$$

Since the jet is exiting into still air, the following boundary conditions apply:

$$u = 0 \quad \text{at} \quad y = b$$

therefore

$$\int_o^b \frac{\partial}{\partial x}(U^2)\,dy = \frac{d}{dx}\int_o^b (U^2)\,dy + U^2\Big|_{y=b}^{=0} \frac{db}{dx} - U^2\Big|_{y=o}^{=0} \frac{d(o)}{dx} \tag{A8}$$

where the second and third term of the right hand side are

identically equal to zero.

Therefore, it follows that

$$\int_o^b U^2 dy = \text{CONSTANT} = M_o \qquad \text{(A9)}$$

where M_o is the momentum flux at the jet exit and remains constant everywhere downstream.

From Prandtl's hypothesis and experimental results for free flows such as jets and wakes

$$\overline{u'v'} = \ell^2 \left(\frac{\partial U}{\partial y}\right)^2 \qquad \text{(A10)}$$

where ℓ is the Prandtl mixing length, and

$$\varepsilon = \ell^2 \left(\frac{\partial U}{\partial y}\right) \qquad \text{(A11)}$$

From (A10) and (A11), it follows that the

$$\varepsilon = - \frac{\overline{u'v'}}{\left(\frac{\partial U}{\partial y}\right)} \qquad \text{(A12)}$$

which is almost independent of y. The turbulent shear stress is

$$\tau' = \rho \varepsilon \frac{\partial U}{\partial y}$$

and

$$\varepsilon = \rho X_1 b \left(U_{max} - U_{min}\right) \qquad \text{(A13)}$$

where U_{max} and U_{min} are the maximum and minimum mean velocities in the jet and X_1 is a dimensionless constant.

Therefore,

$$\tau' = \rho \quad X_1 b\left(U_{max} - U_{min}\right)\frac{\partial U}{\partial y} \qquad \text{(A14)}$$

Now if we consider the jet half-width b as proportional to x

$$\frac{Db}{Dt} \sim v' \qquad \text{(A15)}$$

But

$$\frac{Db}{Dt} = U_{max}\frac{db}{dx} + V_{max}\frac{db}{dy} \qquad \text{(A16)}$$

and

$$\frac{\partial b}{\partial y} = 0 \quad \text{as} \quad b = f(x) \text{ only.}$$

$$|\overline{v'}| = \text{CONST} \cdot |\overline{u'}|$$

$$= \text{CONST} \cdot \ell\frac{\partial U}{\partial y} \qquad \text{(A17)}$$

Over the half-width of the jet $\frac{\partial U}{\partial y}$ may be taken to be approximately proportional to $\frac{U_{max}}{b}$.

Therefore, from (A14), (A15) and (A16)

$$\frac{db}{dx} = \text{CONST} \cdot \frac{\ell}{b}$$

But Prandtl theorized that $\frac{\ell}{b}$ is a constant, therefore,

$$b = \text{CONST} \cdot x \qquad \text{(A18)}$$

Now, consider U_{max}

$$M_o = \rho\int_o^b U^2_{max}\,dy$$

$$= \rho\left(U^2_{max}\right)b$$

which implies that

$$U_{max} = \frac{CONST}{\sqrt{x}} \tag{A19}$$

and

$$U_{min} = 0 \tag{A20}$$

By substituting (A18), (A19) and (A20) into (A13), it can be seen that ε is only a function of x.

From (A12)

$$-\overline{u'v'} = \varepsilon(x)\frac{\partial U}{\partial y} \tag{A21}$$

Substituting (A21) into (A5)

$$U\frac{\partial U}{\partial x} + V\frac{\partial U}{\partial y} = \varepsilon(x)\frac{\partial^2 U}{\partial y2} \tag{A22}$$

To summarize

$$b \sim x$$

$$U_{max} \sim \frac{1}{\sqrt{x}} \quad \text{and}$$

$$\varepsilon(x) \sim \sqrt{x}$$

If we choose a fixed characteristic distance s from the orifice

$$U_{max} = U_s\left(\frac{S}{x}\right)$$

$$b = b_s\left(\frac{x}{S}\right)$$

and

$$\varepsilon = \varepsilon_s\left(\frac{x}{S}\right)$$

where

$$\varepsilon_s = X_1 b_s U_s$$

By picking the proper similarity variable

$$\eta = \frac{\sigma y}{x}$$

where is some free constant.

Set the stream function

$$\Psi = \frac{U_s}{\sigma} \sqrt[3]{S} \sqrt{x} \quad F(\eta)$$

where $F(\eta)$ is some function of the similarity variable.

We know that

$$U = \frac{\partial \Psi}{\partial y} \qquad \text{and} \qquad V = -\frac{\partial \Psi}{\partial x}$$

By substituting for U and V into (A22) and simplifying

$$\left(\frac{\varepsilon S}{U_s S}\ \sigma^2\right) F''' + \frac{1}{2} FF'' + \frac{1}{2} F' = 0 \qquad \text{(A23)}$$

Equation (A23) is a third order partial differential equation in $F(\eta)$ with the following boundary conditions

$$F = 0,\ F' = 1 \quad \text{at } \eta = 0$$

$$F' = 0 \quad \text{at } \eta = \infty$$

and

$$F' = \frac{U}{U_{max}}$$

In order to simplify equation (A23) let

$$\sigma = \frac{1}{2} \sqrt{\frac{U_s S}{\varepsilon_s}}$$

and substitute. The result is

$$F''' + 2FF'' + 2F' = 0 \qquad \text{(A24)}$$

This is a simpler version of (A23) which can be integrated to arrive at

$$F' + F^2 = 1 \qquad \text{(A25)}$$

This is the familiar differential equation for the laminar case with solution

$$F = \tanh \eta \qquad \text{(A26)}$$

To arrive at the velocity ratio differentiate with respect to η, $\frac{U}{U_{max}} = \text{sec } h^2 \eta$. From experimental results Reichardt determined that

$$\sigma = 7.67$$

These theoretical results along with the Görtler assumption that $U = \frac{1}{2}U_{max}$ at $Y = Y_{1/2}$ are plotted in Figs 17 and 18 as a basis for comparison between the theoretical and experimental results for both the laser velocimeter and the hot wire anemometer.

Appendix B

Calculation of the Jet Spread Angle
(Ref 16)

From the solution of the equation of motion and continuity in Appendix A, we see that the velocity ratio

$$\frac{U}{U_{cen}} = (1 - \tanh^2 \eta) \qquad (B1)$$

where

$$\eta(Y) = \frac{\sigma Y}{x}$$

and $\sigma = 7.67$ was arrived at from experimental values.

From the mean velocity similarity profiles (Figs 17 or 18), it can be seen that the experimental values arrived at using the hot wire anemometer follow very closely the theoretical curve derived by Görtler. It can also be seen that the profile reaches a constant value at

$$\frac{Y}{Y_{1/2}} \cong 3.0$$

Görtler arrived at the curve by forcing the curve to go through the point $\frac{Y}{Y_{1/2}} = 1.0$ at $U = \frac{1}{2}U_{cen}$. At the outer edge of the jet $Y = b$ where b is the half-width of the jet. Therefore, it follows that

$$b \simeq 3Y$$

Now,

$$\eta(b) = \frac{\sigma\left(\frac{b}{3}\right)}{x}$$

Solving for η from (B1)

$$\eta = 0.881$$

so that

$$\frac{b}{x} = \frac{3\eta(b)}{\sigma} = \frac{3(0.881)}{7.67} = 0.345$$

The spread angle is simply $2 \tanh^{-1}(.345)$ or $\simeq 40°$.

18 June 79

Appendix C

Theoretical Axial Velocity Profile

(Ref 2)

The axial velocity profile of a two-dimensional free jet is a function of the distance from the exit plane.

$$U = \frac{CONST}{\sqrt{x}} \tag{C1}$$

By using the equation of conservation of momentum

$$\rho \int_o^Y u^2 dy = \rho U^2_{cor} Y = M_o \tag{C2}$$

we can arrive at U_{cor} which is the velocity present at the jet exit and then multiplying through by U the ratio of velocities results.

$$\frac{1}{U_{cor}} = \frac{1}{\sqrt{\frac{1}{Y}\int_o^Y u^2 dy}} \tag{C3}$$

$$\frac{U}{U_{cor}} = \frac{1}{\sqrt{\frac{1}{Y}\int_o^Y \left(\frac{u}{U}\right)^2 dy}} \tag{C4}$$

Now, make a change of variable and let

$$\phi = \frac{Y}{ax}$$

where a is some constant and Y_o is the half-width of the jet at the exit

$$F'(\phi) = \frac{u}{U} \tag{C5}$$

The resulting equation allows us to evaluate the value of the integral which is tabulated in Table 2.3 (Ref 2).

$$\frac{U}{U_{cor}} = \frac{1}{\sqrt{\frac{ax}{Y_o}\int_o^{\phi} (F'(\phi))^2 d\phi}} \qquad (C6)$$

The resulting equation was used to compare the theoretical results to the results arrived at experimentally (Figs 15 and 16).

$$\phi = 2{\cdot}4$$

$$\int_o^{2{\cdot}4} (F'(\phi))^2 d\phi = 0{\cdot}685$$

Therefore,

$$\frac{U}{U_{cor}} = \frac{1{\cdot}2}{\sqrt{\frac{ax}{Y_o}}}$$

The value of the constant a which most closely fitted the experimental results from the hot wire anemometer and Laser Velocimeter was

$$a = 0{\cdot}08$$

Other values of the constant a which have resulted from experimental observation have been in the range of 0.09 to 0.12 for plane jets and 0.066 to 0.076 for round jets (Ref 2).

Appendix D

The Autocorrelation Function
(Ref 1)

The autocorrelation function has been referred to very frequently in this thesis and it is from this function that all the information about the flow is derived when using the LV system. Therefore, an explanation on how it is derived is in order.

Basically, the autocorrelation function results from correlating a velocity at a certain time, t, to the velocity at a later time, $(t + \tau)$, at the same point in the flow. That is, the function is a time correlation and not a spatial correlation.

This LV system processes the detected signal and velocity and turbulence intensities information is extracted from the autocorrelation function. Another means of extracting velocity information would be to determine the power spectrum. However, this alternative will not be discussed in this study.

By making appropriate assumptions and invoking the Wiener-Kinchine theorem (Ref 1), the photon correlation function is given as

$$G(\tau) = \langle n(t, T)\, n(t + \tau, T) \rangle$$

where τ is the correlation delay, n is the number of photons absorbed, and T is the sample time.

Expanding the above function for the laminar case and assuming that r_o is much larger than the fringe spacing, S, the correlation function can be approximated by

$$G(\tau) = \left(\frac{a_o}{u}\right) \exp\left\{-\left[\left(\frac{u^2\tau^2}{r_o^2}\right)\left(1 + \frac{1}{2}\cos\frac{2\pi u}{S}\tau\right)\right]\right\}$$

where a_o is a constant.

Normally the fringe visibility across the entire focal volume is not one hundred per cent, therefore, a fringe visibility factor, m, must be included to give

$$G(\tau) = \frac{a_o}{u} \exp\left\{-\left[\left(\frac{u^2\tau^2}{r_o^2}\right)\left(1 + \frac{1}{2}m^2\cos\frac{2\pi U}{S}\tau\right)\right]\right\} \quad (D1)$$

For turbulent flow each particle crossing the focal volume will affect the autocorrelation function described by (D1) and hence, a composite function will result.

$$G(\tau) = a_1 \int_{-\infty}^{\infty} p(u) G_{lam}(\tau)\, du$$

Now, if the shape of p(u) is assumed to be Gaussian such that

$$p(u) = \frac{1}{\sigma\sqrt{2\pi}} \exp\left\{-\left(\frac{(u-U)^2}{2\sigma^2}\right)\right\}$$

where U is the mean velocity and σ the standard deviation of the distribution.

If it is further assumed that

$$\tau^2 << \frac{r_o^2}{2\sigma^2}$$

then the turbulent autocorrelation function reduces to

$$G(\tau) = a_1 \exp\left\{-\left(\frac{U^2\tau^2}{r_o^2}\right)\left\{1 + \frac{1}{2}m^2 \exp\left[-\left(\frac{2\pi^2U^2\eta^2\tau^2\cos 2\pi U}{S^2}\right)\right]\right\}\right\}$$

where

$$\eta = \frac{\sigma}{U} \equiv \text{turbulence intensity}$$

It is important to note that the autocorrelation function derived from the use of the hot wire anemometer system is not the same autocorrelation function derived from using the LV system.

The hot wire does not take into account the intermittency in the flow as "dead" time is also used in the averaging process. The LV does take into account intermittency by not using "dead" time in the flow to arrive at the autocorrelation function.

Appendix E.

Experimental Results at M = 0.4

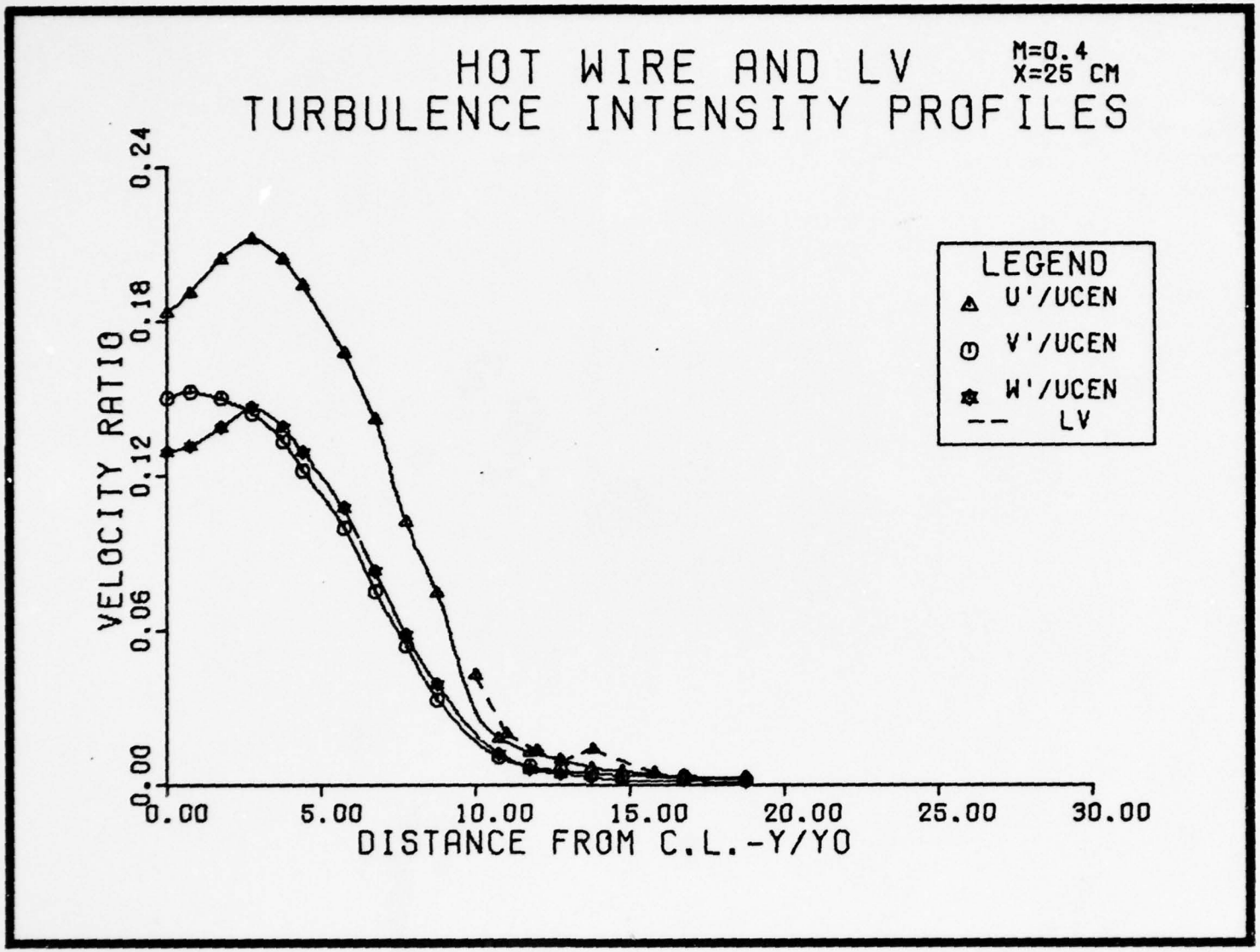

FIG. 20 HOT WIRE AND LV TURBULENCE INTENSITY AT M=0.4 AND 25 CM

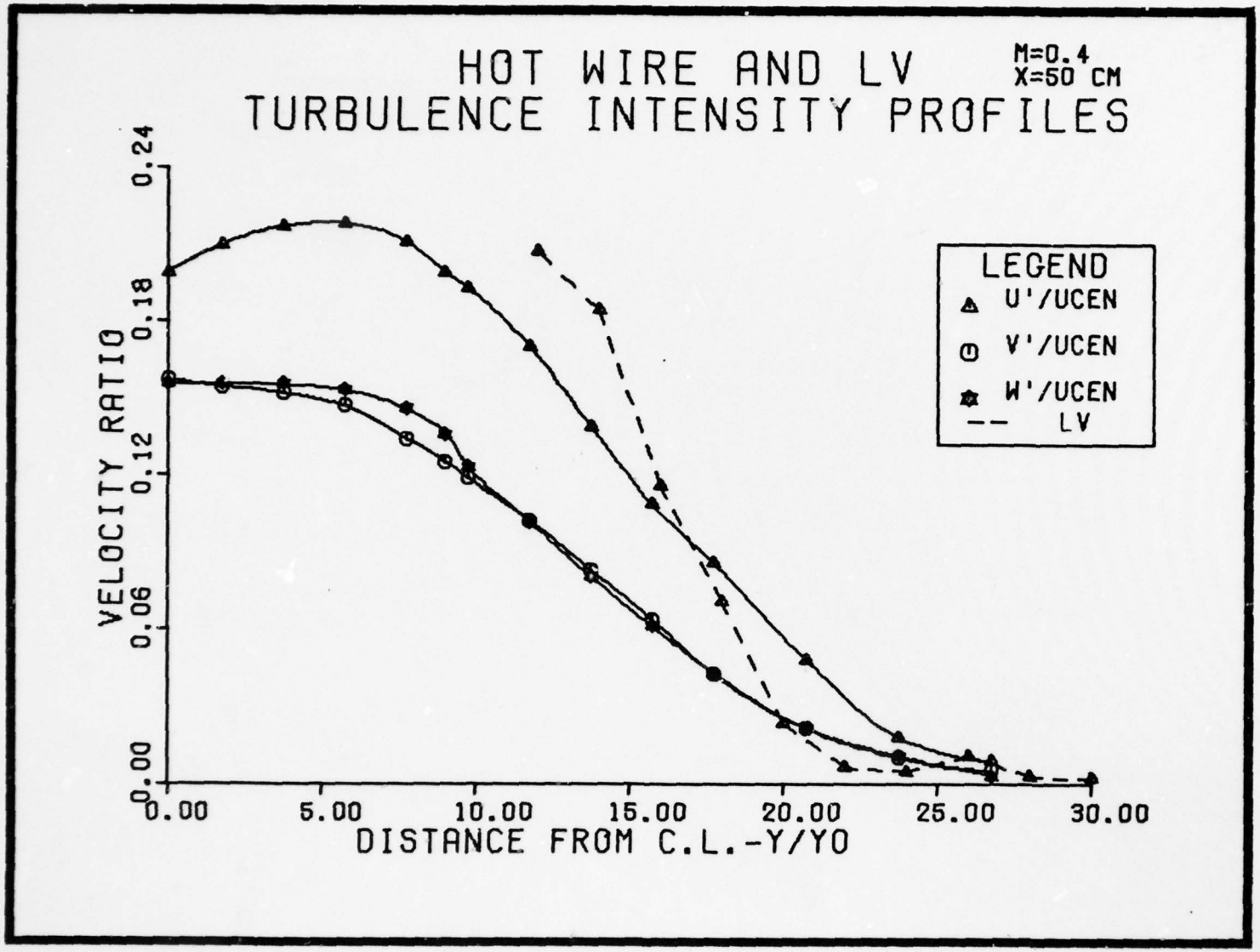

FIG.21 HOT WIRE AND LV TURBULENCE INTENSITY AT M=0.4 AND 50 CM

AD-A070 102 AIR FORCE INST OF TECH WRIGHT-PATTERSON AFB OHIO SCH--ETC F/G 20/4
AN EXPERIMENTAL EVALUATION OF A LASER VELOCIMETER BY THE STUDY --ETC(U)
JUN 79 N G CERULLO

UNCLASSIFIED AFIT/GAE/AA/79J-1 NL

2 OF 2
AD A070102

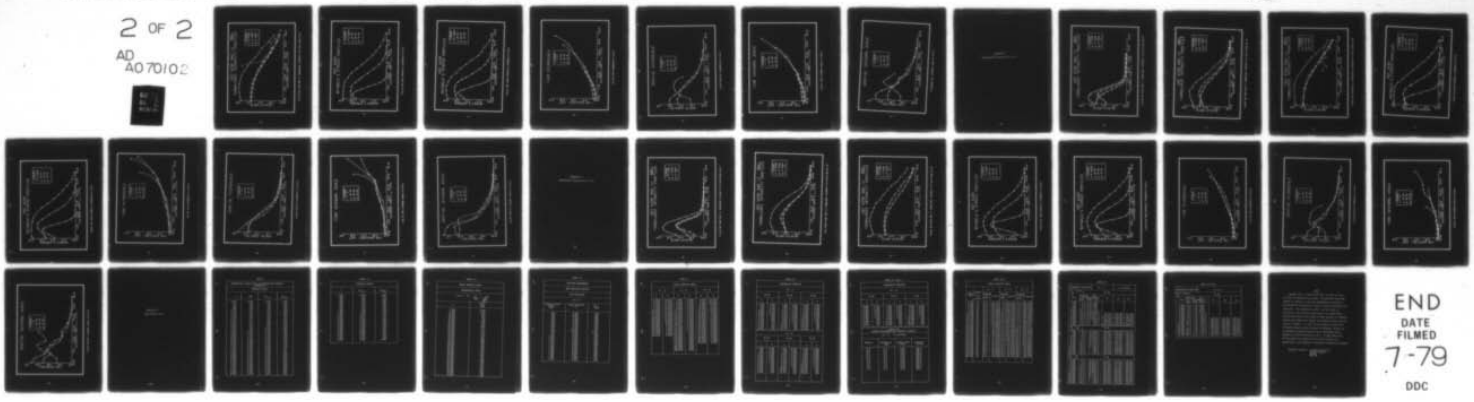

END
DATE FILMED
7-79
DDC

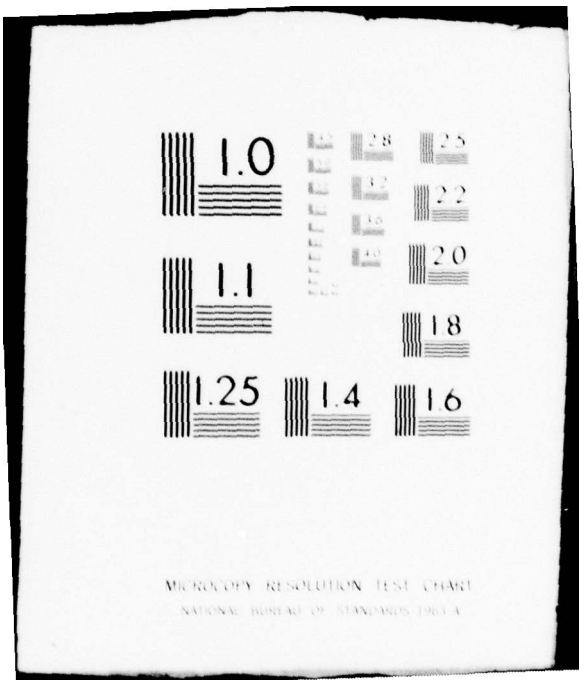
1.0
1.1
1.25
1.4
1.6
2.2
2.0
1.8
MICROCOPY RESOLUTION TEST CHART
NATIONAL BUREAU OF STANDARDS 1963-A

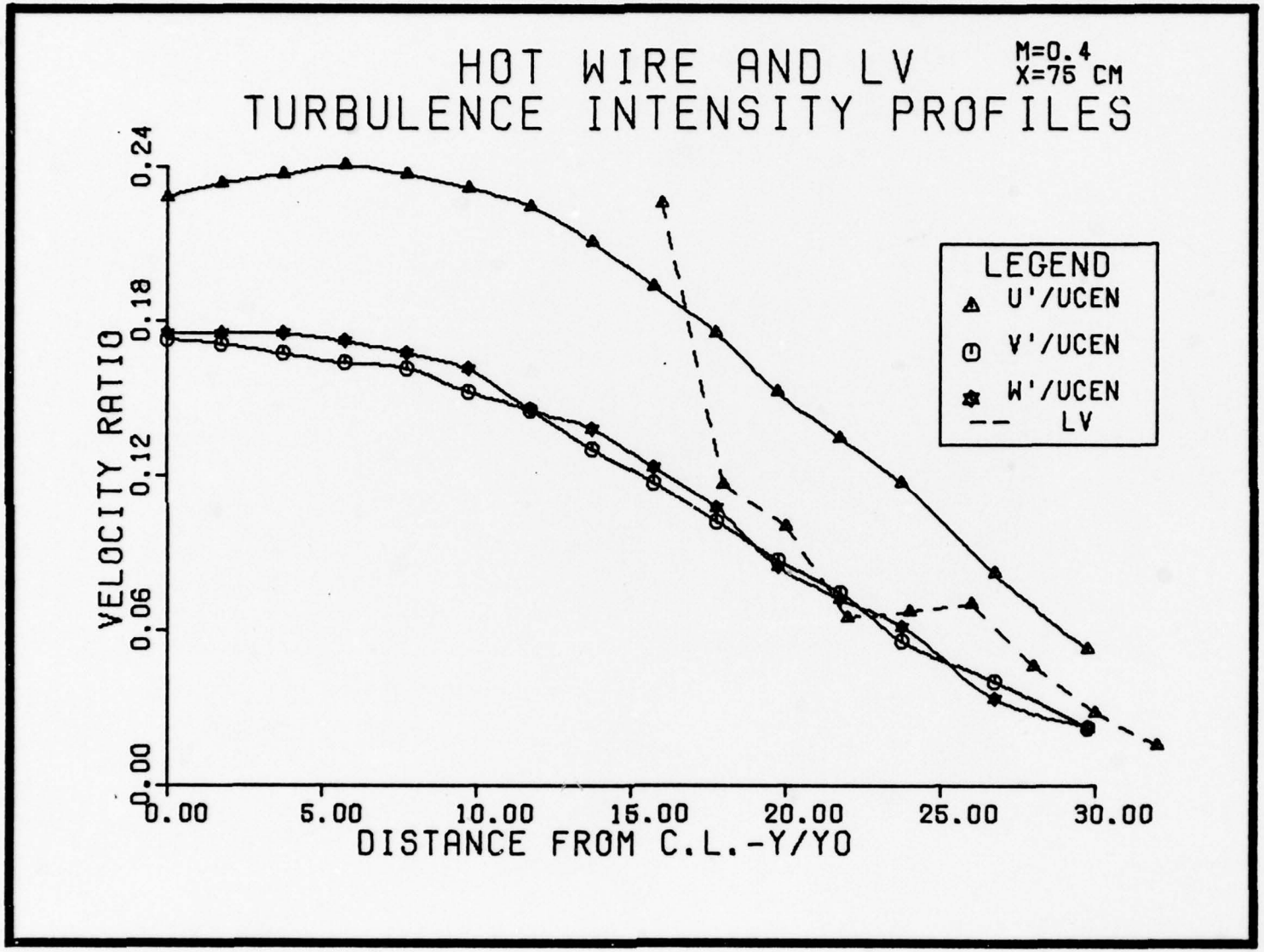

FIG.22 HOT WIRE AND LV TURBULENCE INTENSITY AT M=0.4 AND 75 CM

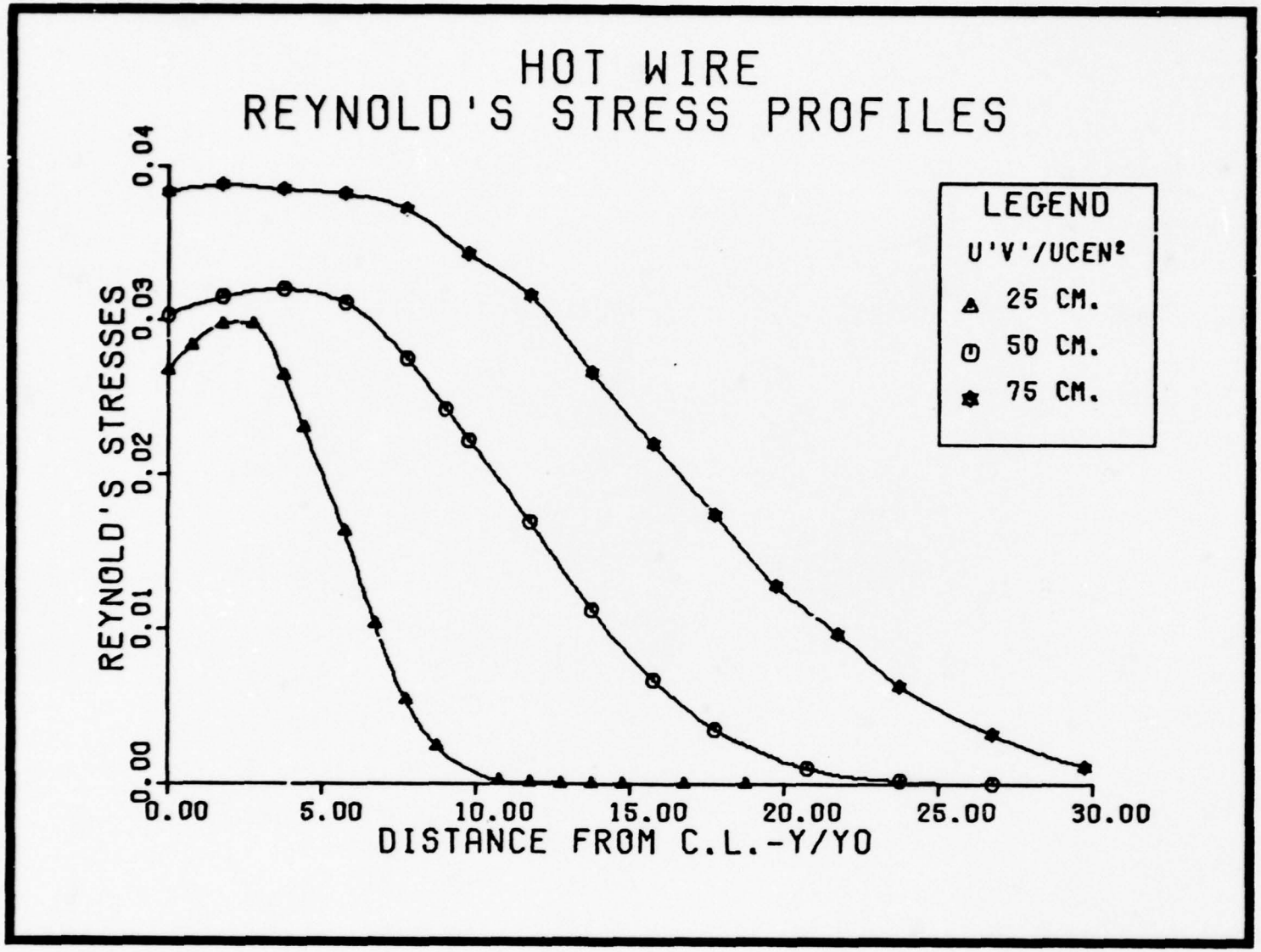

FIG.23 HOT WIRE REYNOLD'S STRESSES AT M=0.4

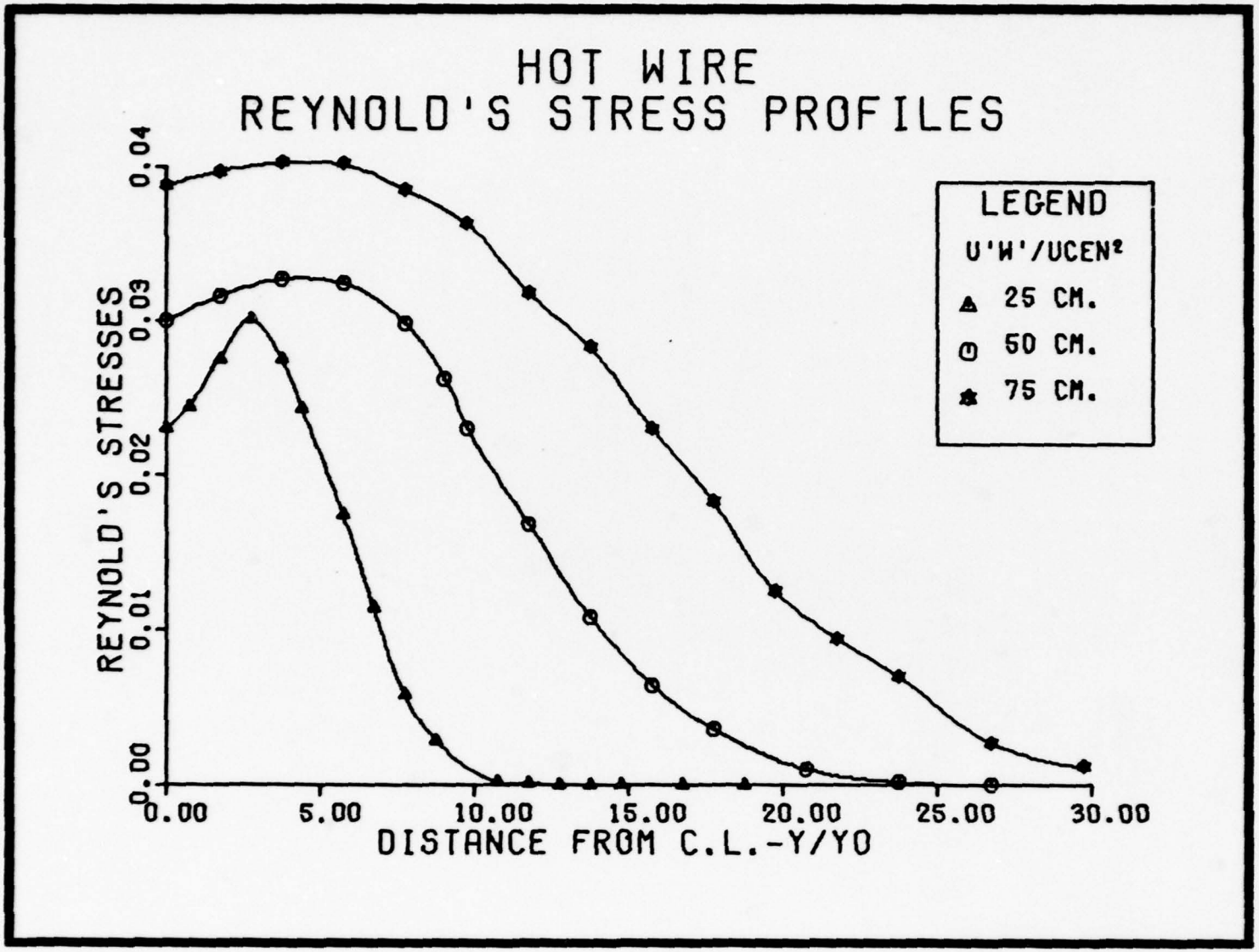

FIG.24 HOT WIRE REYNOLD'S STRESSES AT M=0.4

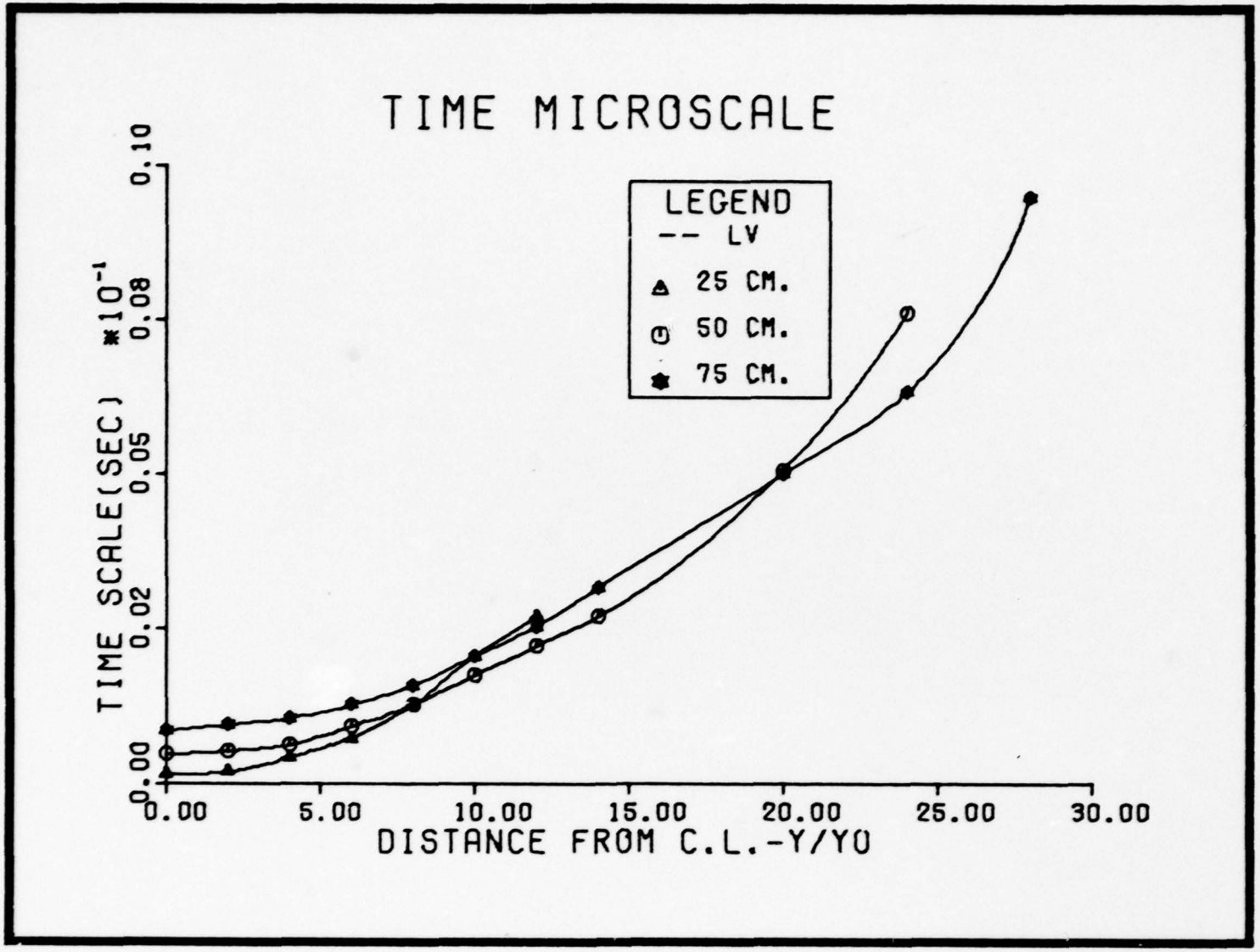

FIG.25 TIME MICROSCALE AT M=0.4

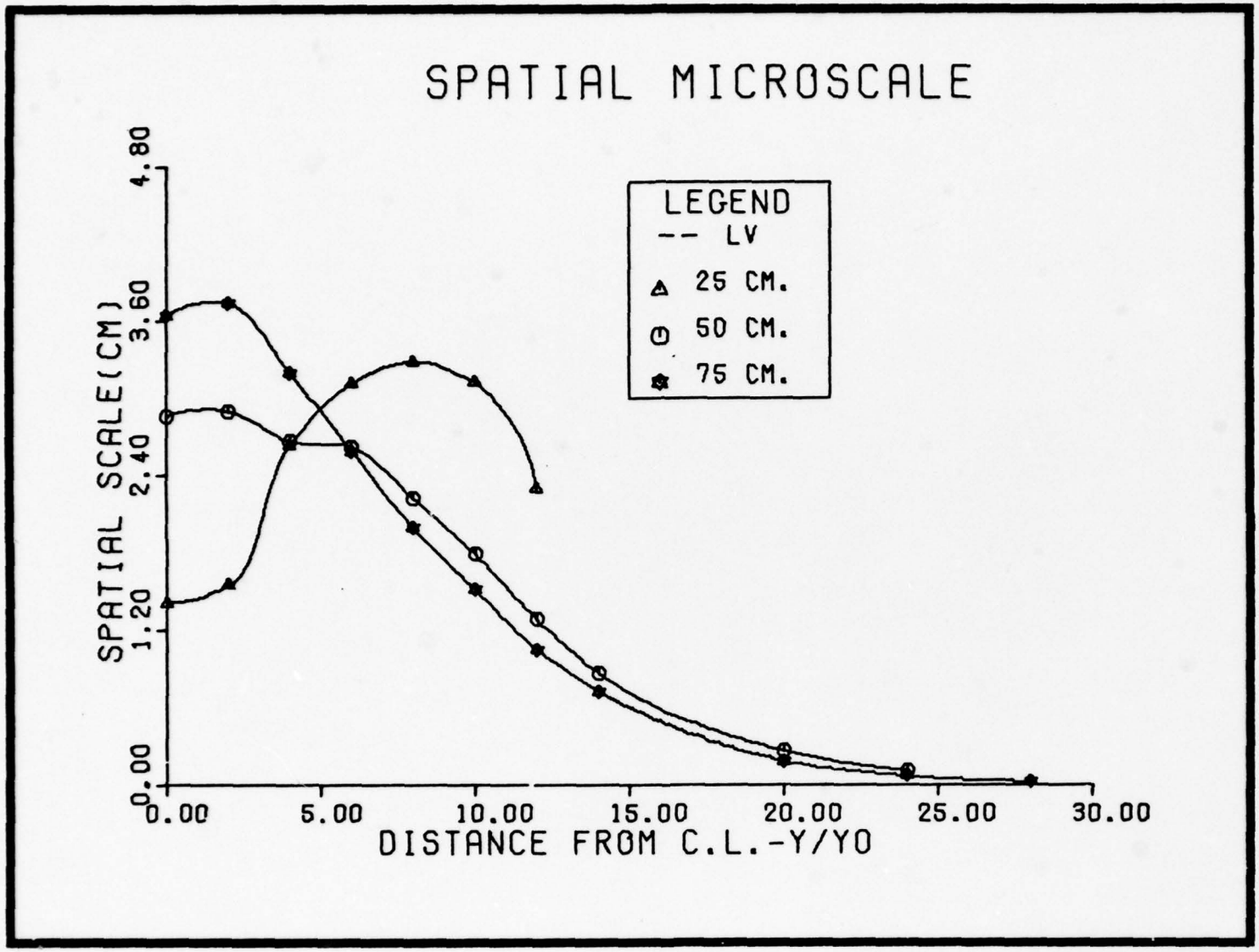

FIG.26 SPATIAL MICROSCALE AT M=0.4

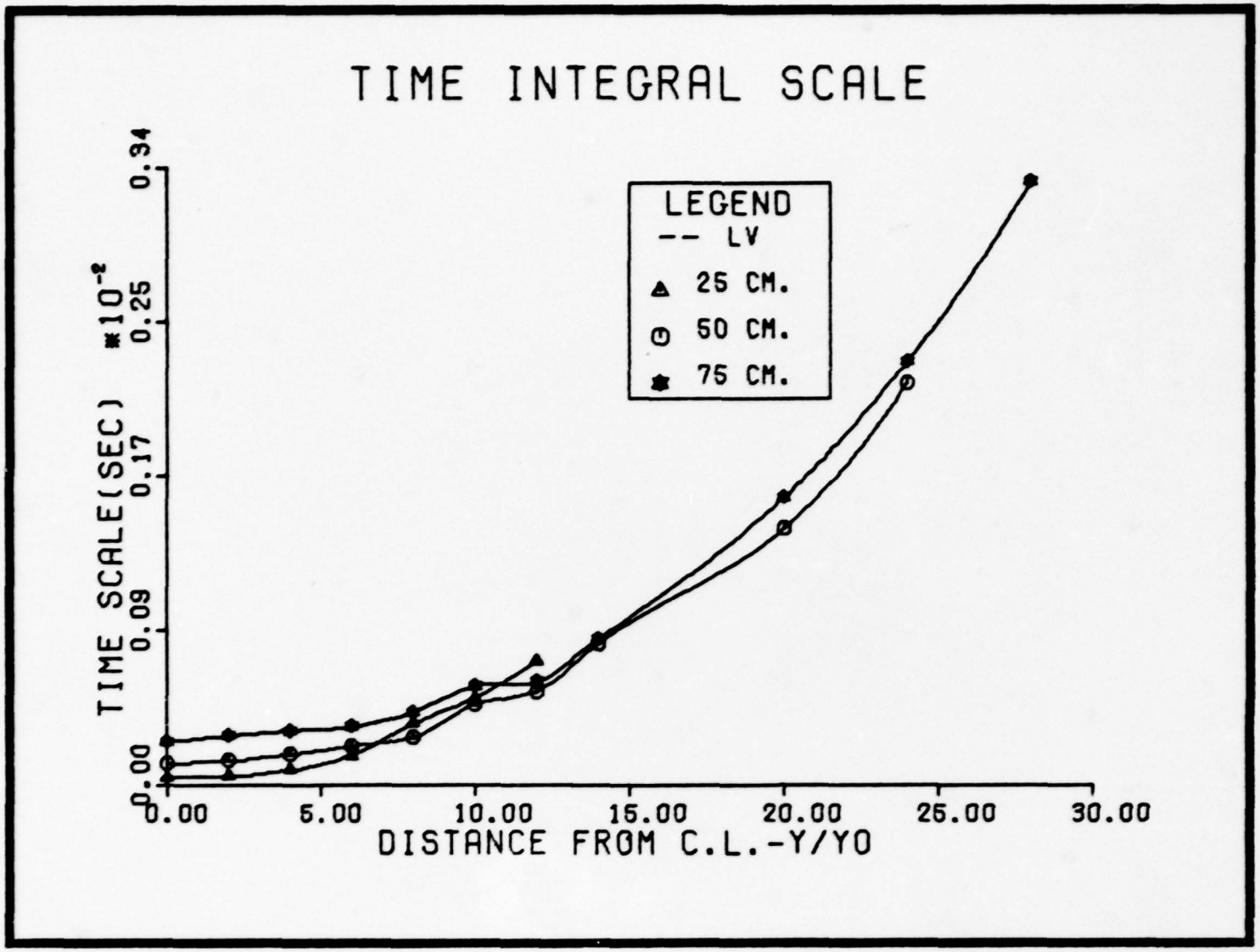

FIG.27 TIME INTEGRAL SCALE AT M=0.4

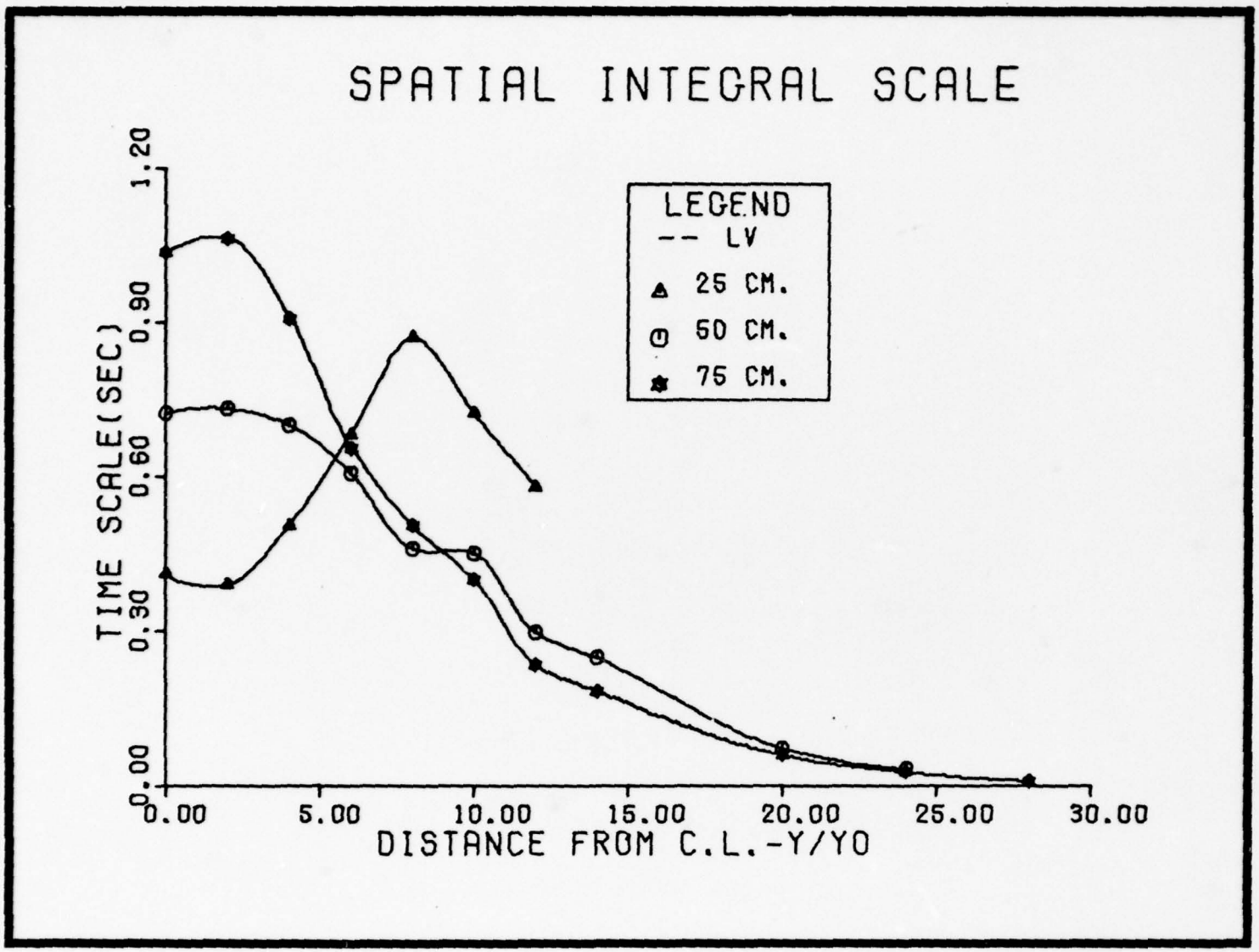

FIG.28 SPATIAL INTEGRAL SCALE AT M=0.4

Appendix F.

Experimental Results at M = 0.6

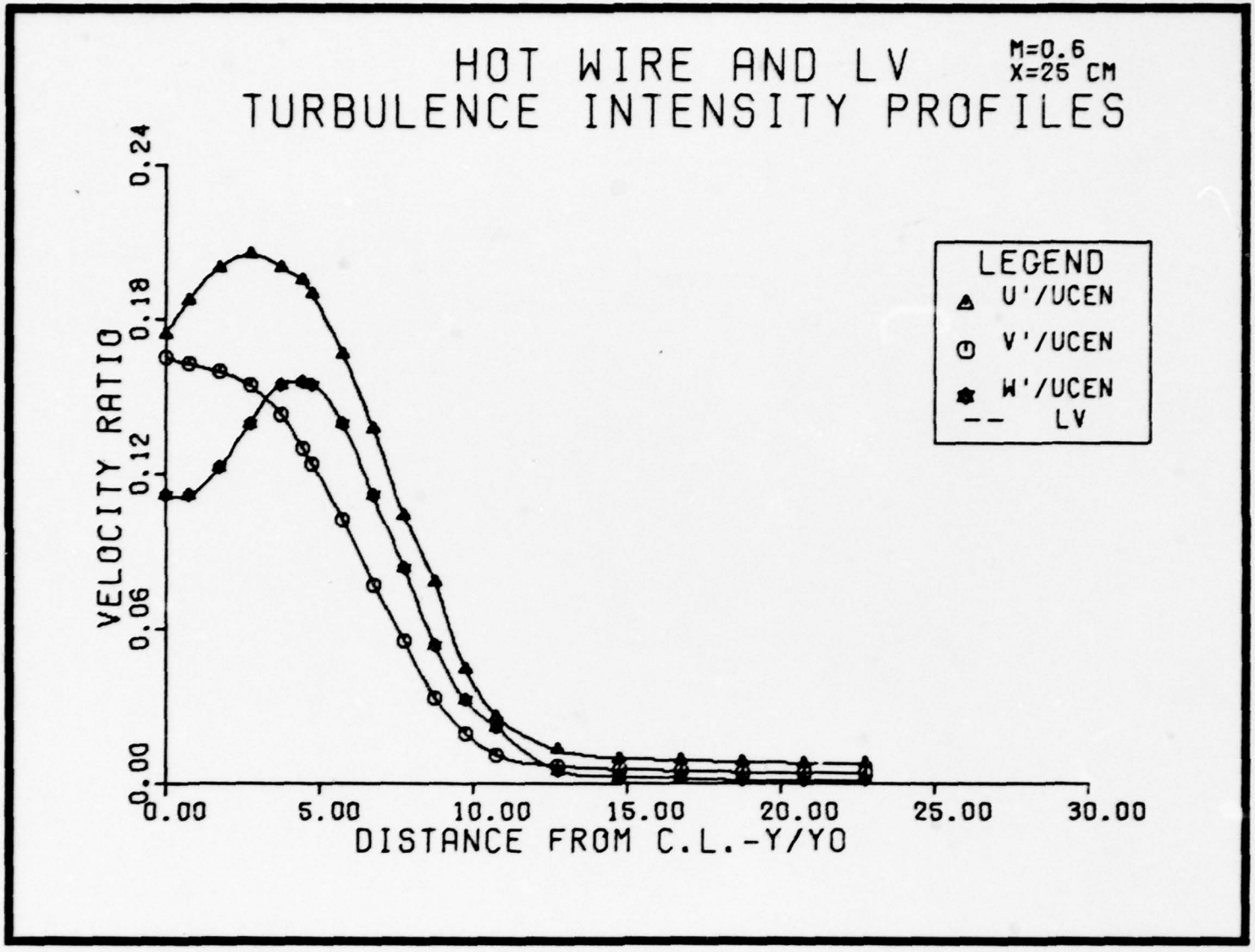

FIG.29 HOT WIRE AND LV TURBULENCE INTENSITY AT M=0.6 AND 25 CM

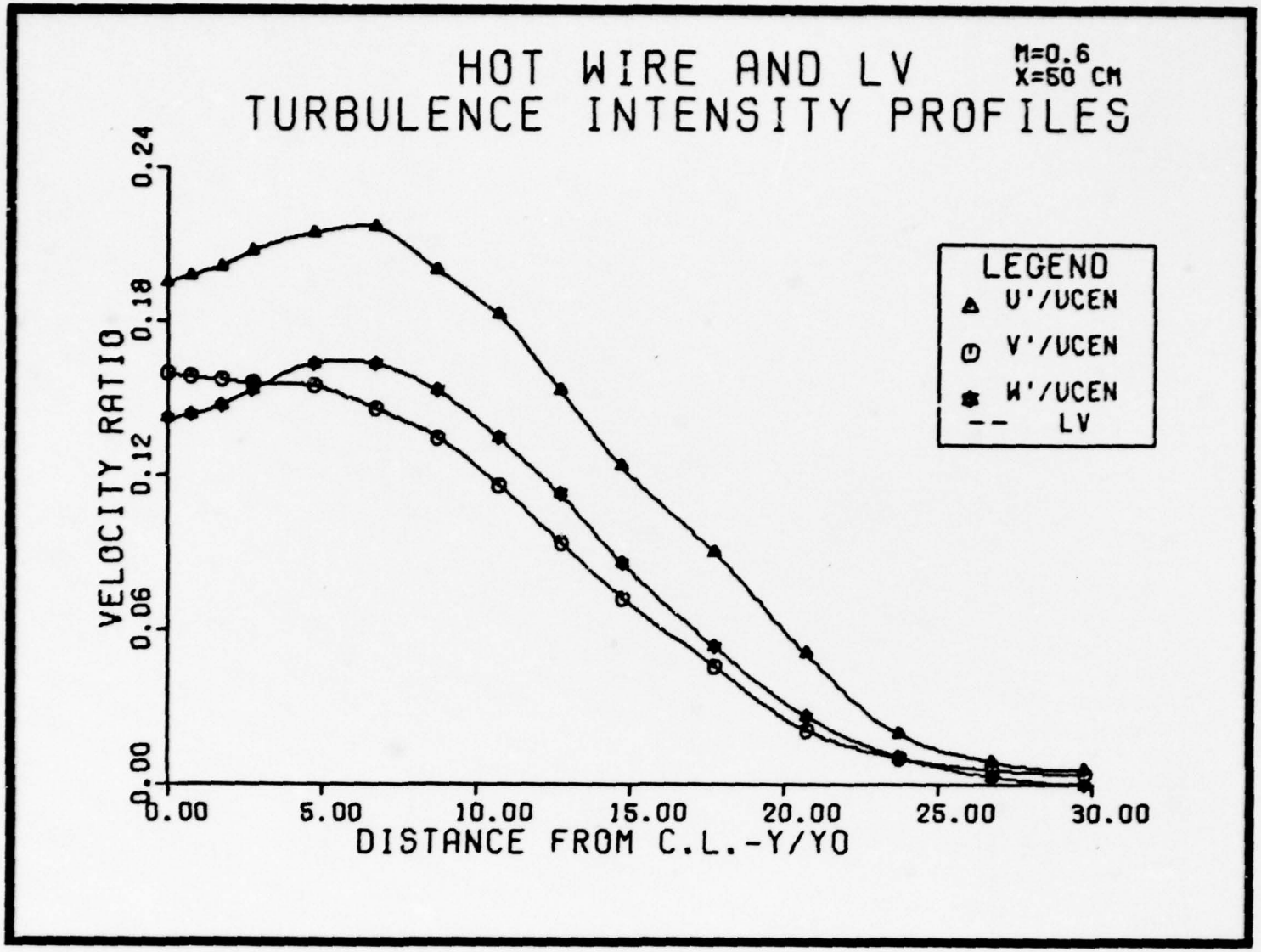

FIG.30 HOT WIRE AND LV TURBULENCE INTENSITY AT M=0.6 AND 50 CM

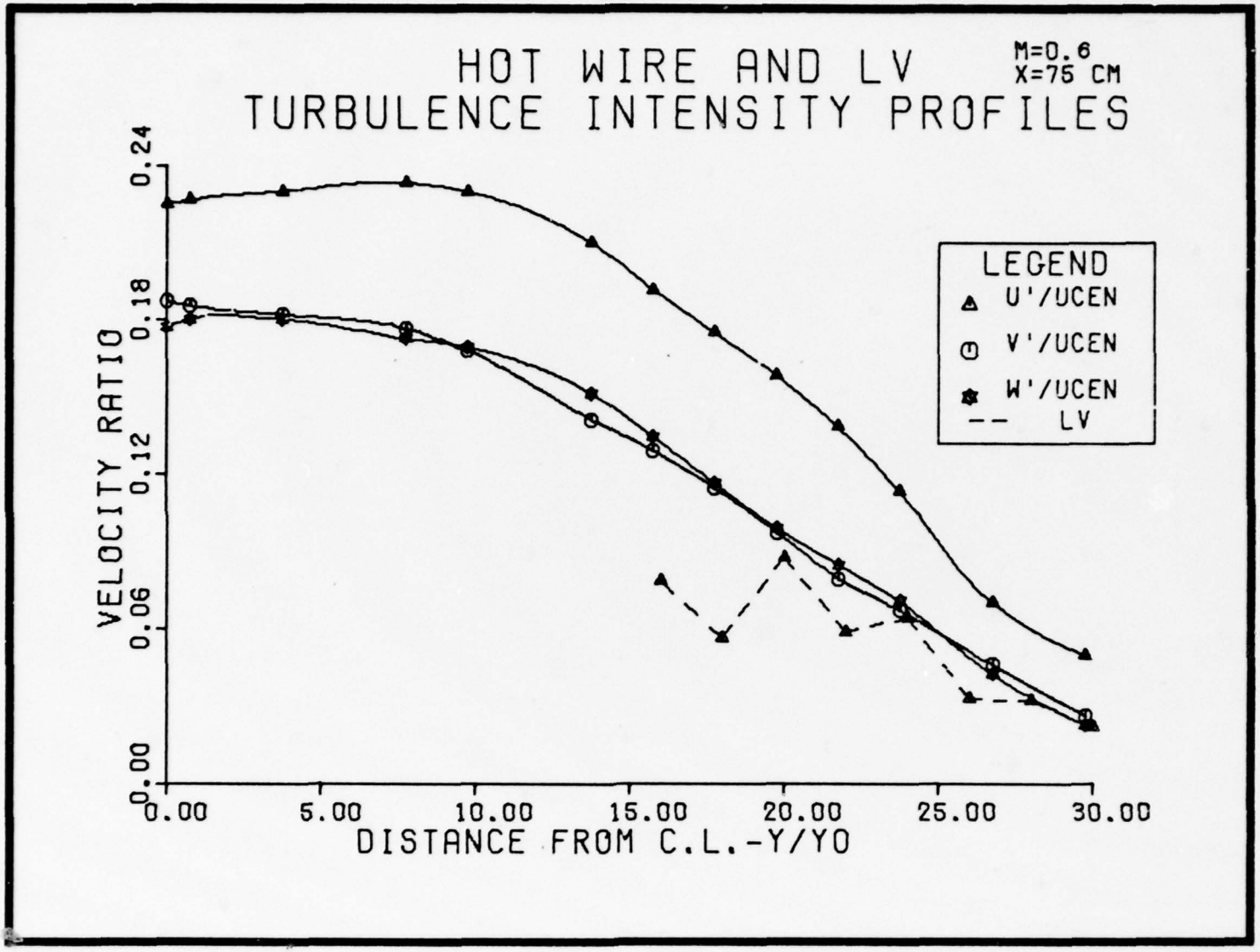

FIG.31 HOT WIRE AND LV TURBULENCE INTENSITY AT M=0.6 AND 75 CM

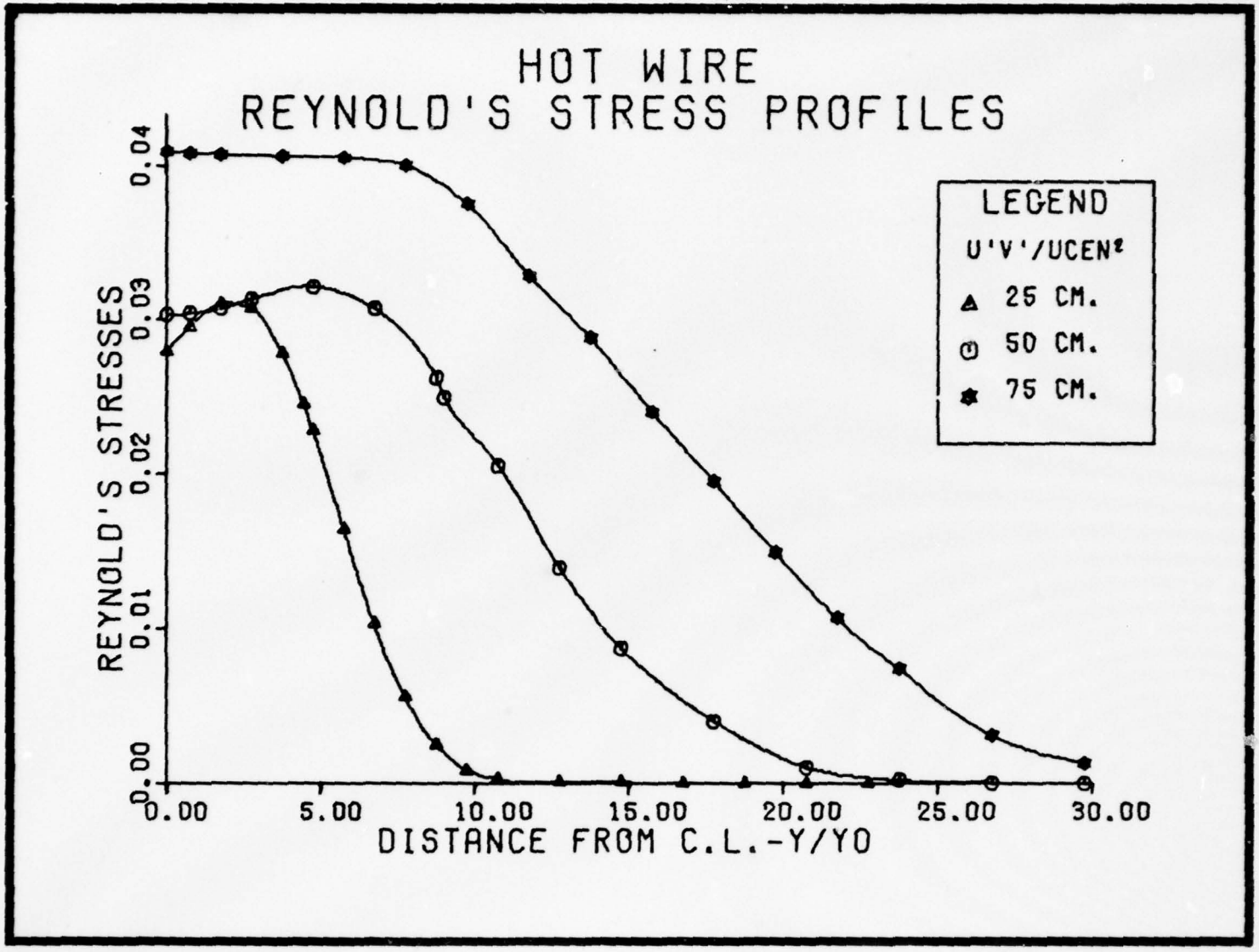

FIG.32 HOT WIRE REYNOLD'S STRESSES AT M=0.6

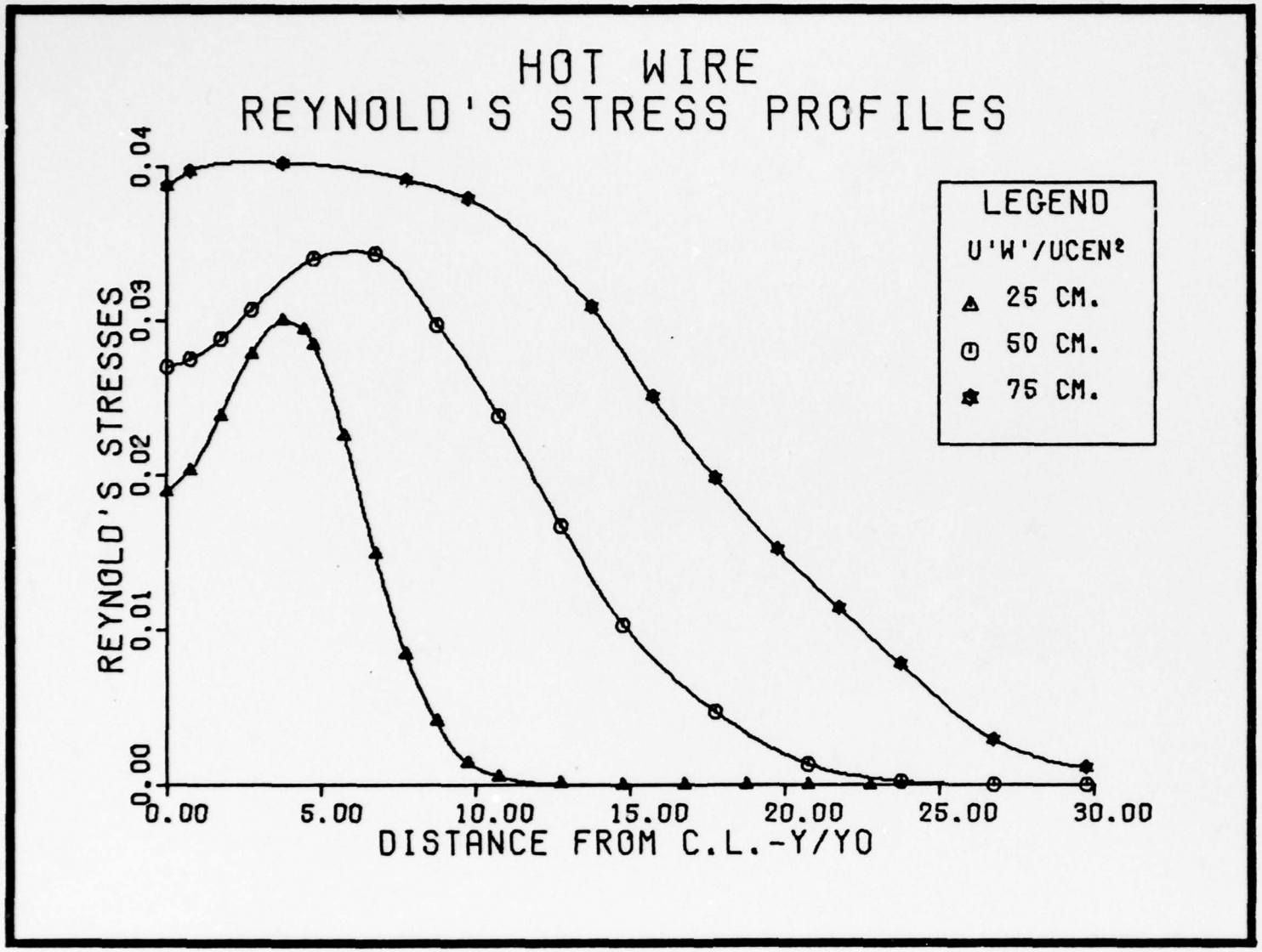

FIG.33 HOT WIRE REYNOLD'S STRESSES AT M=0.6

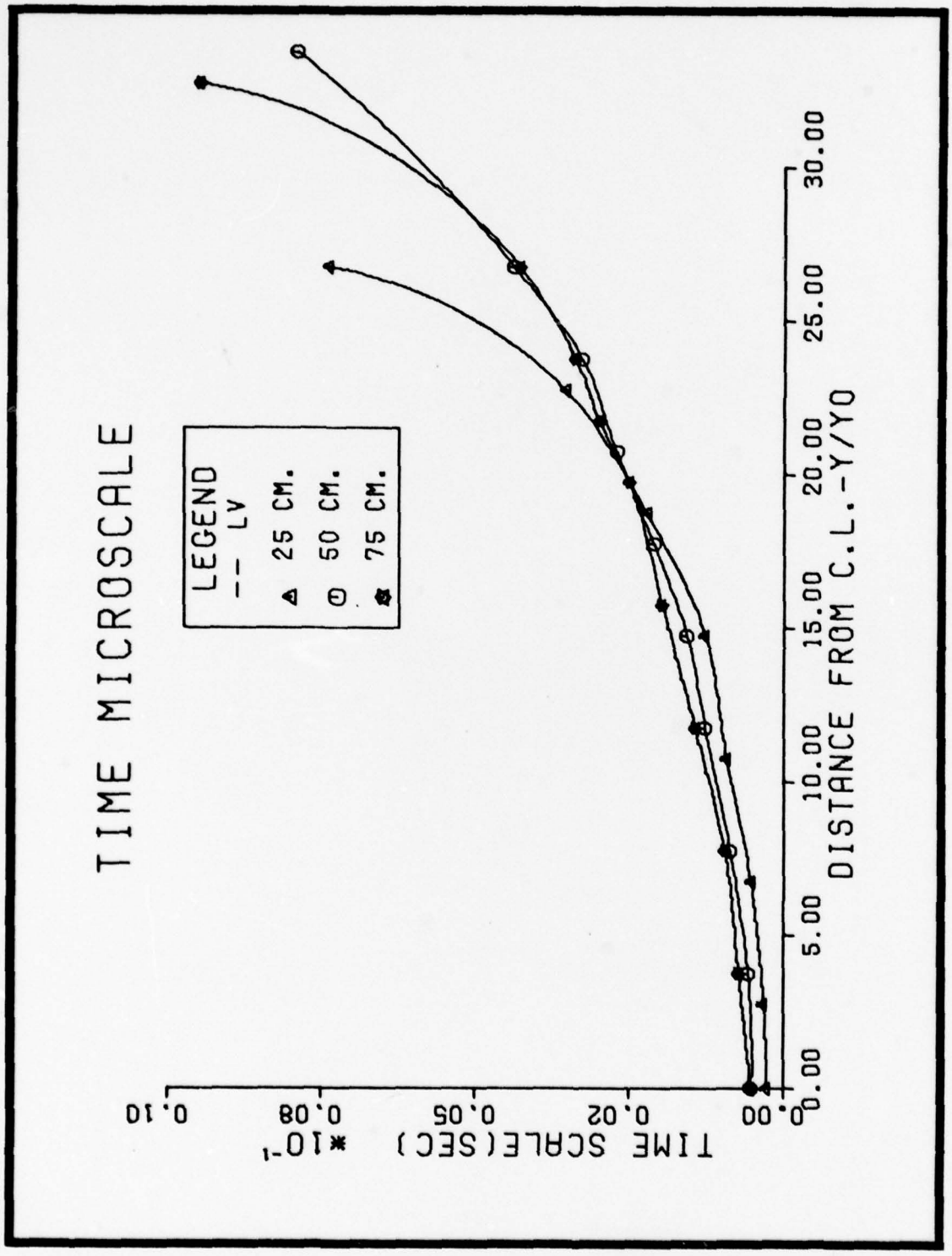

FIG.34 TIME MICROSCALE AT M=0.6

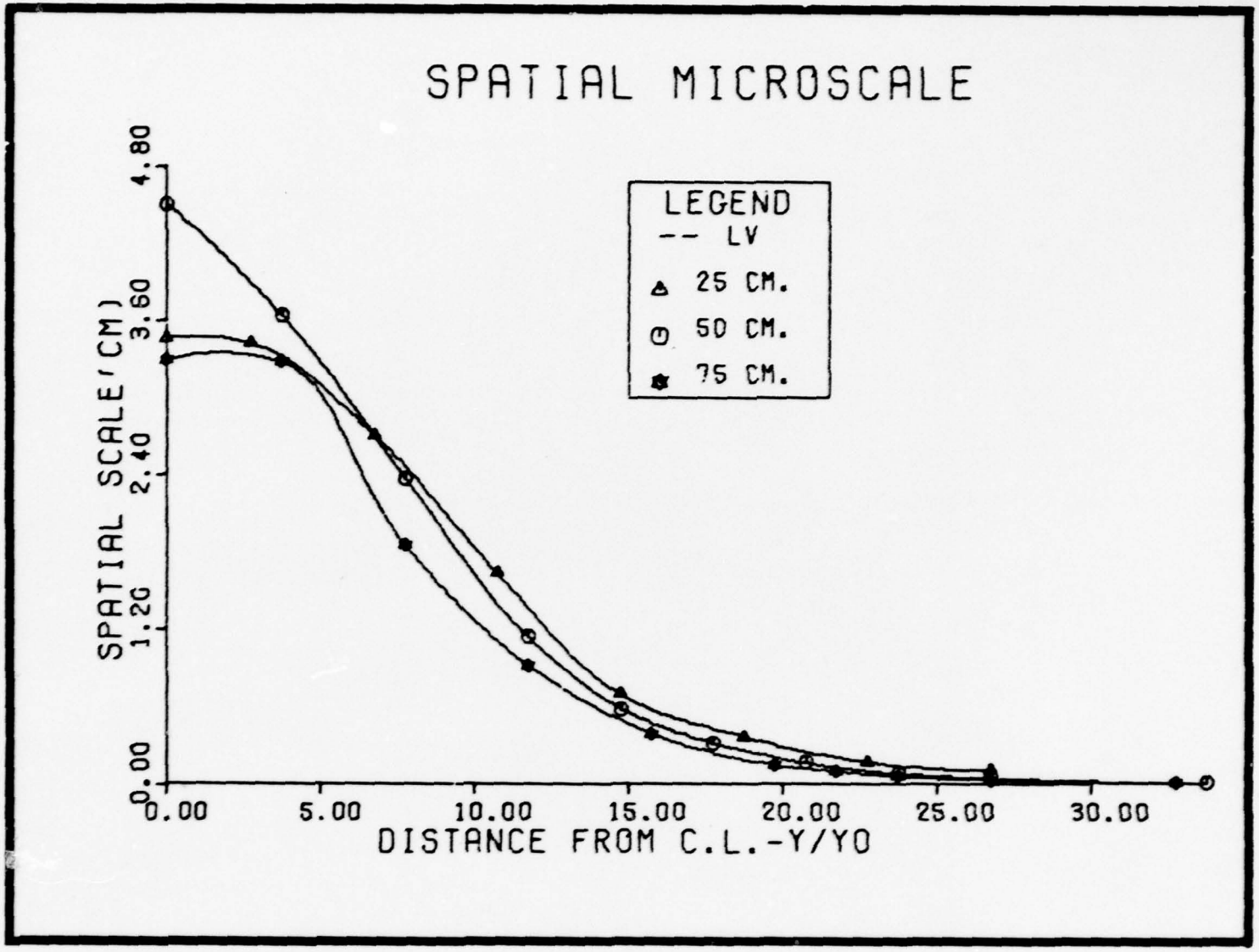

FIG.35 SPATIAL MICROSCALE AT M=0.6

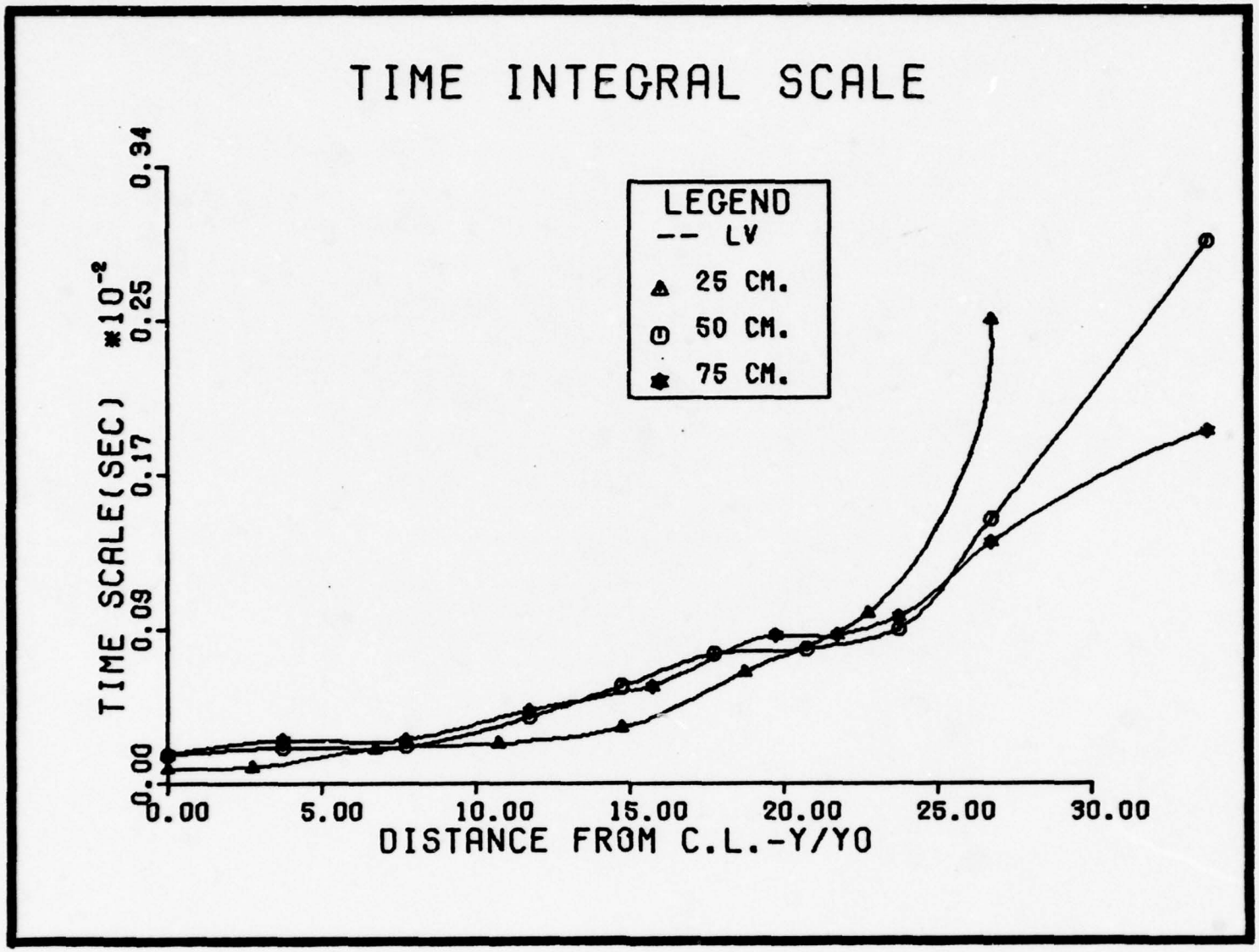

FIG.36 TIME INTEGRAL SCALE AT M=0.6

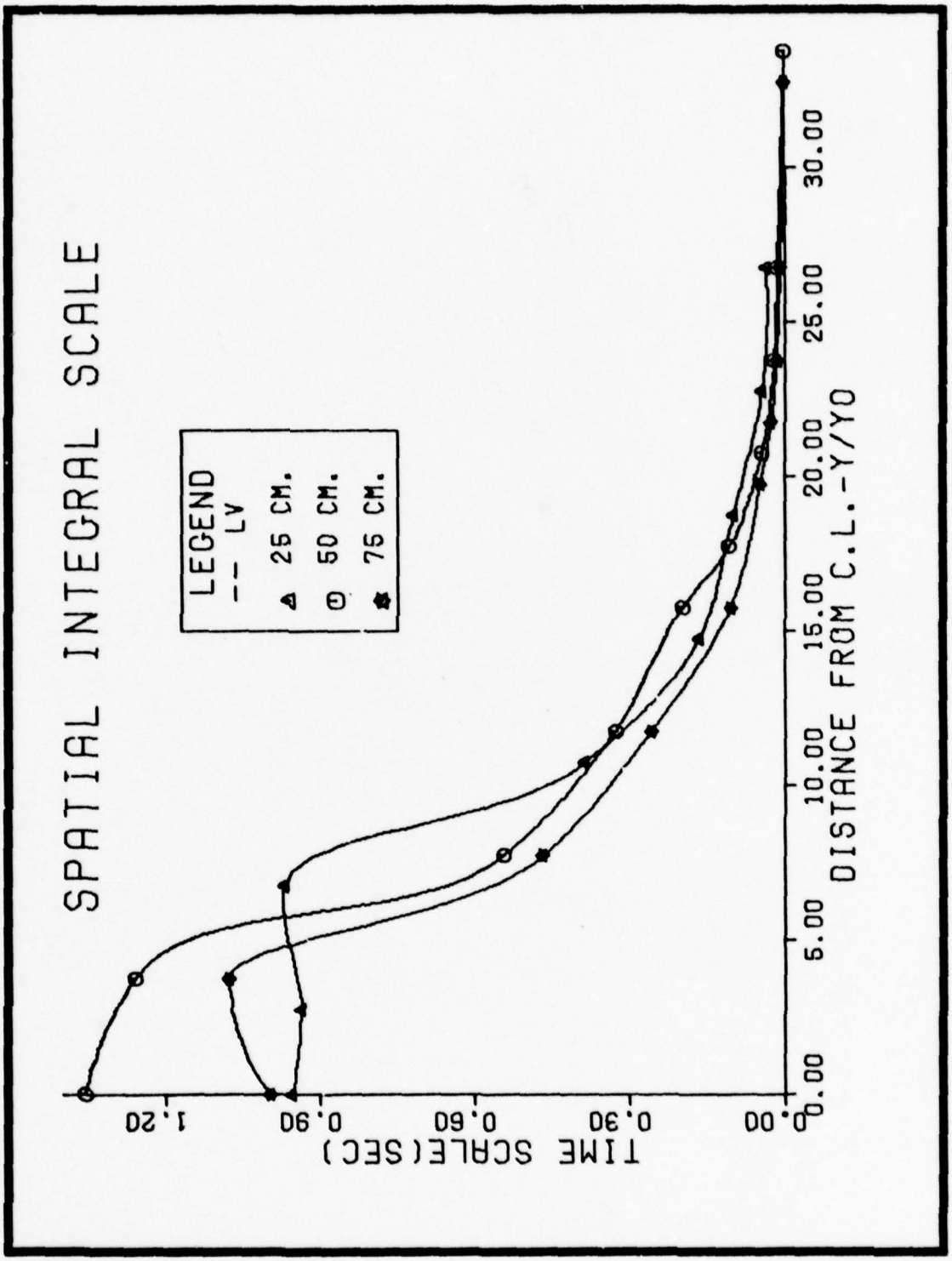

FIG.37 SPATIAL INTEGRAL SCALE AT M=0.6

Appendix G.

Experimental Results at M = 0.8

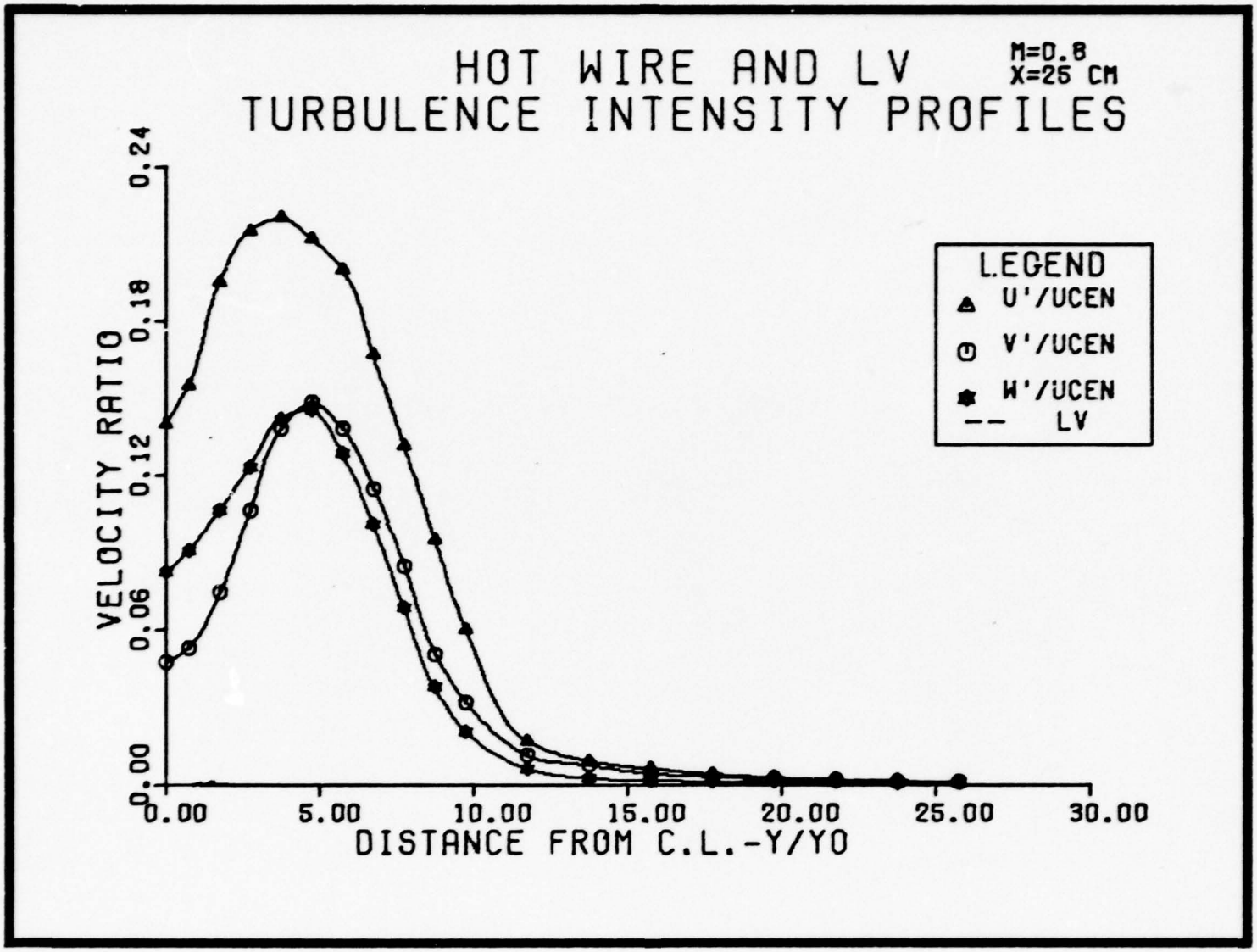

FIG.38 HOT WIRE AND LV TURBULENCE INTENSITY AT M=0.8 AND 25 CM

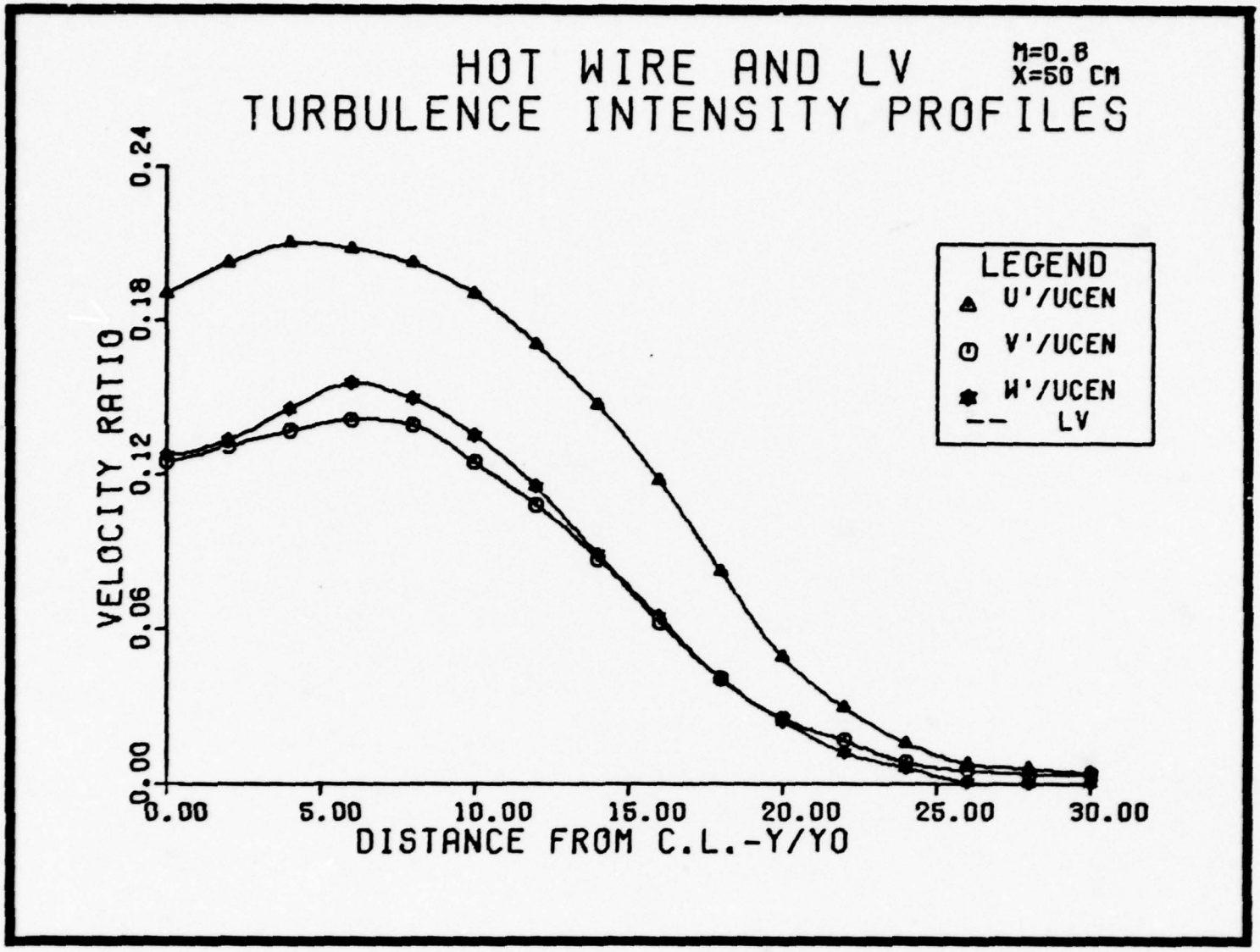

FIG. 39 HOT WIRE AND LV TURBULENCE INTENSITY AT M=0.8 AND 50 CM

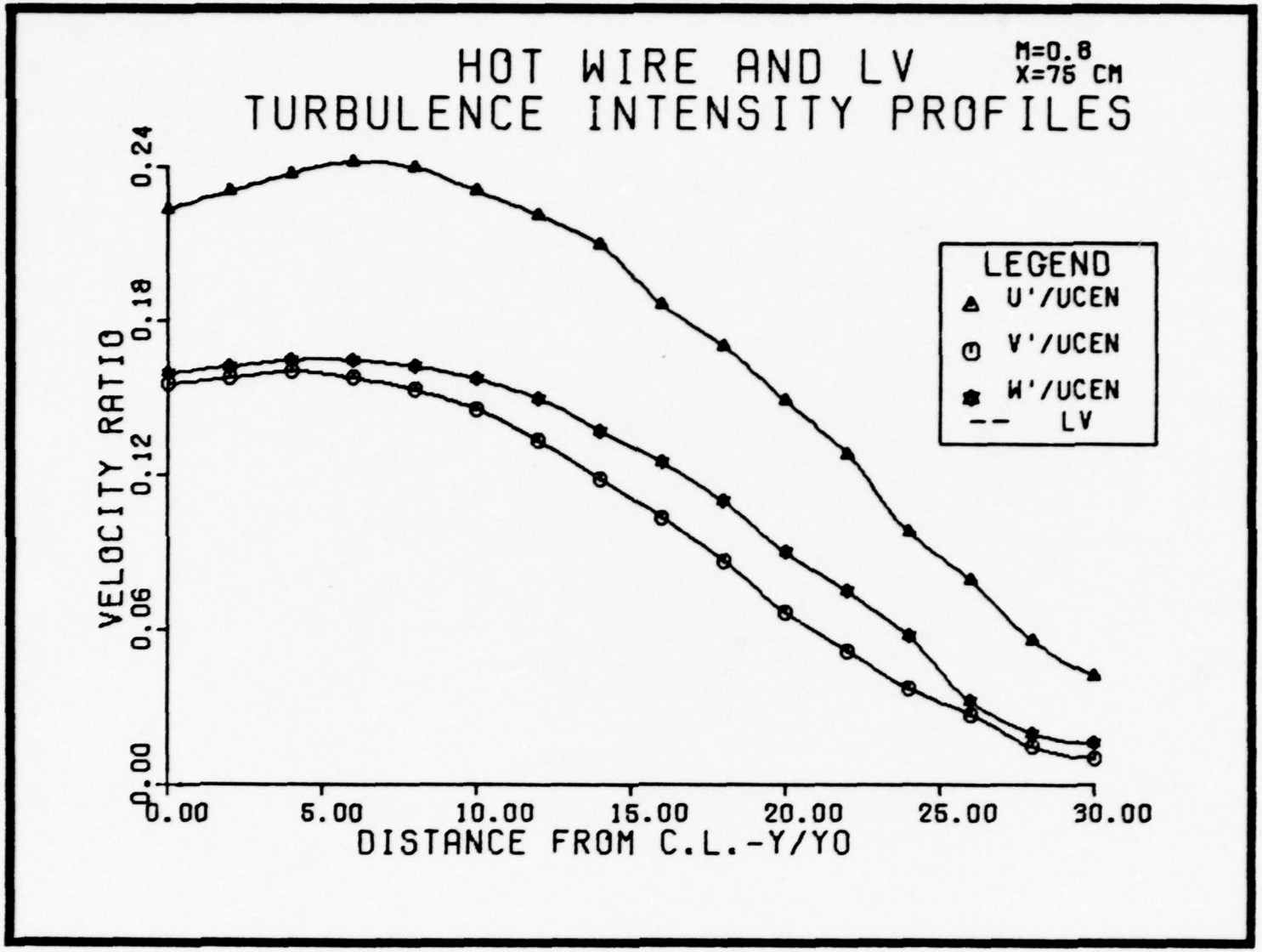

FIG.40 HOT WIRE AND LV TURBULENCE INTENSITY AT M=0.8 AND 75 CM

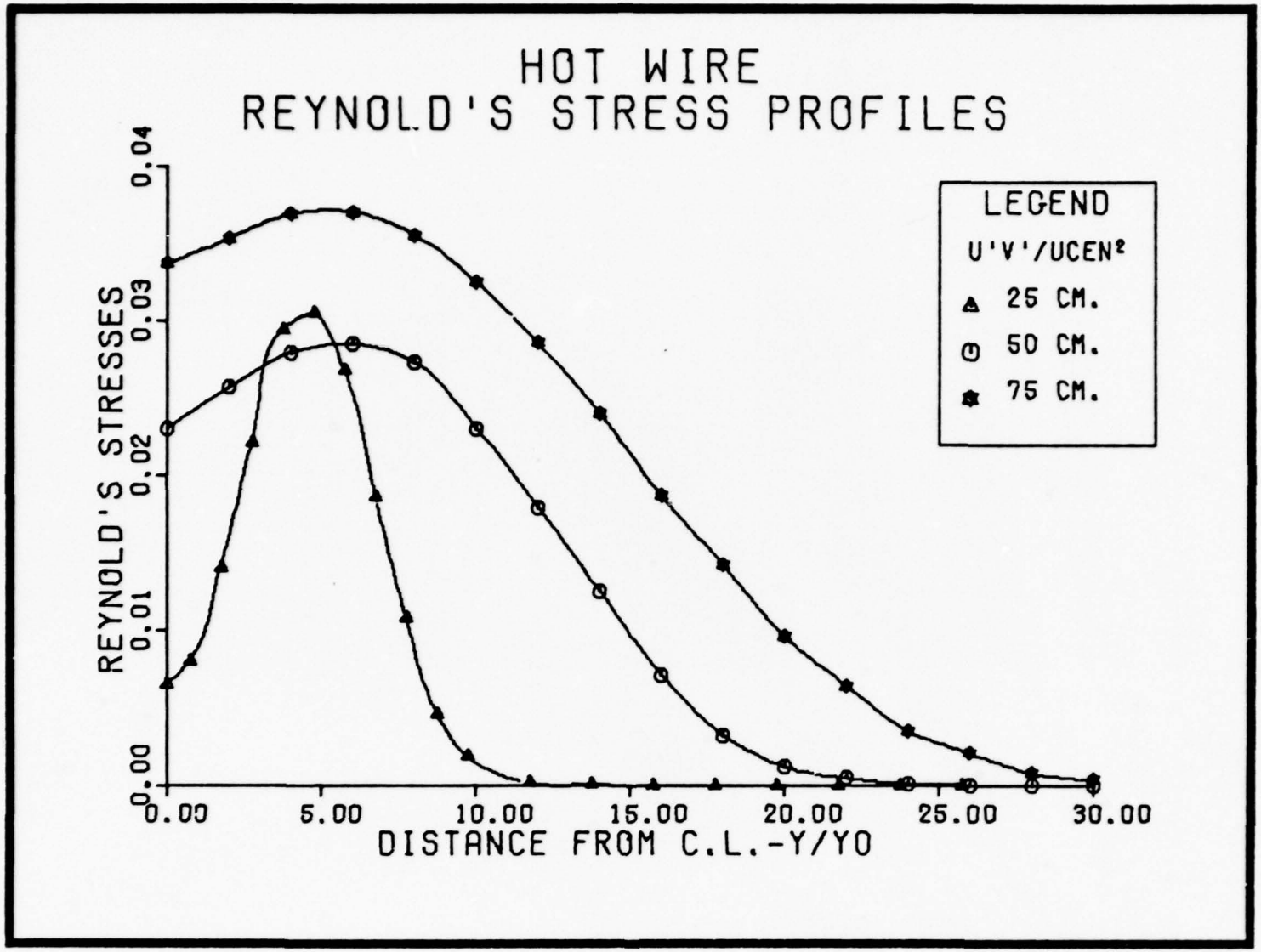

FIG.41 HOT WIRE REYNOLD'S STRESSES AT M=0.8

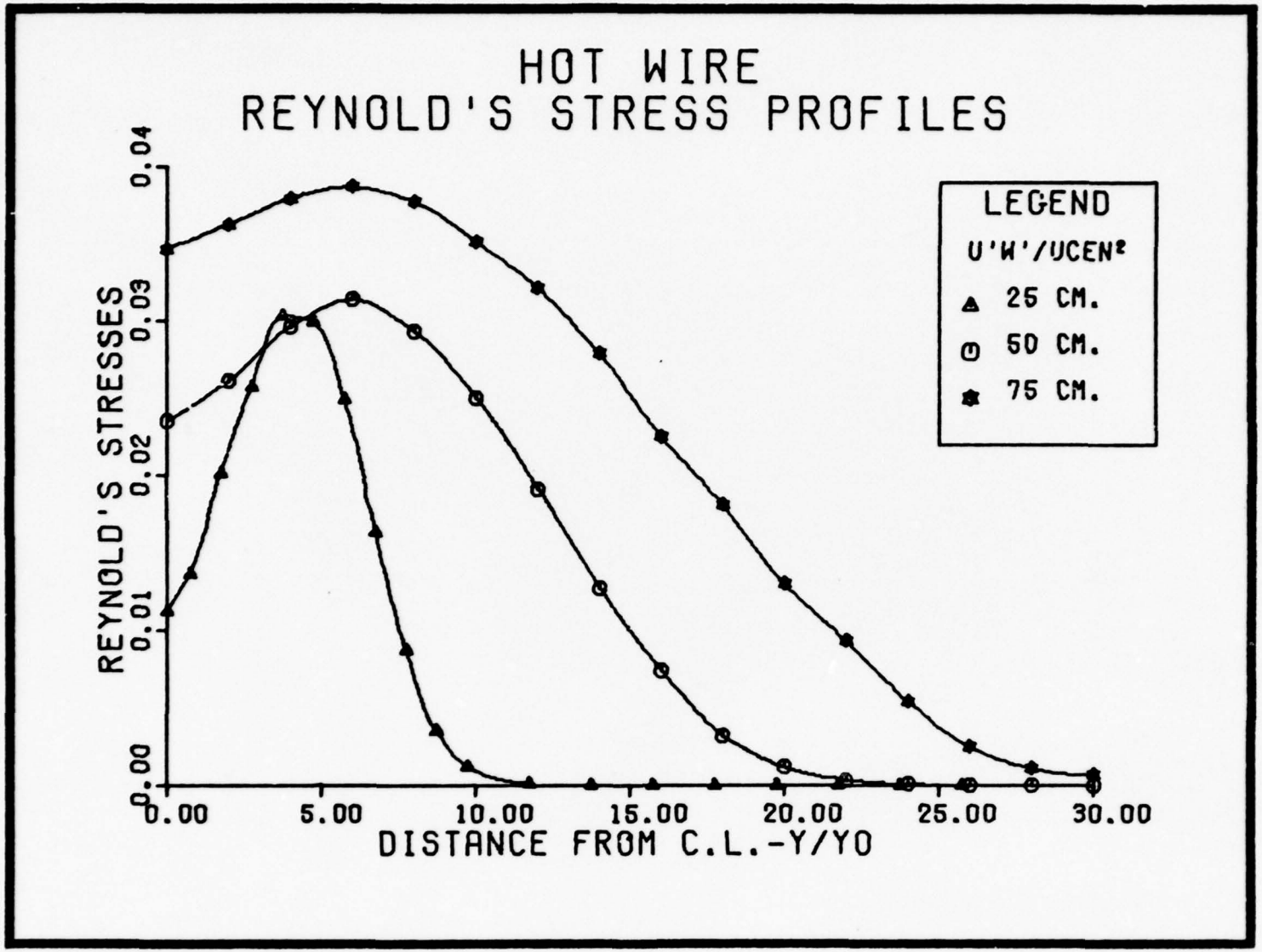

FIG.42 HOT WIRE REYNOLD'S STRESSES AT M=0.8

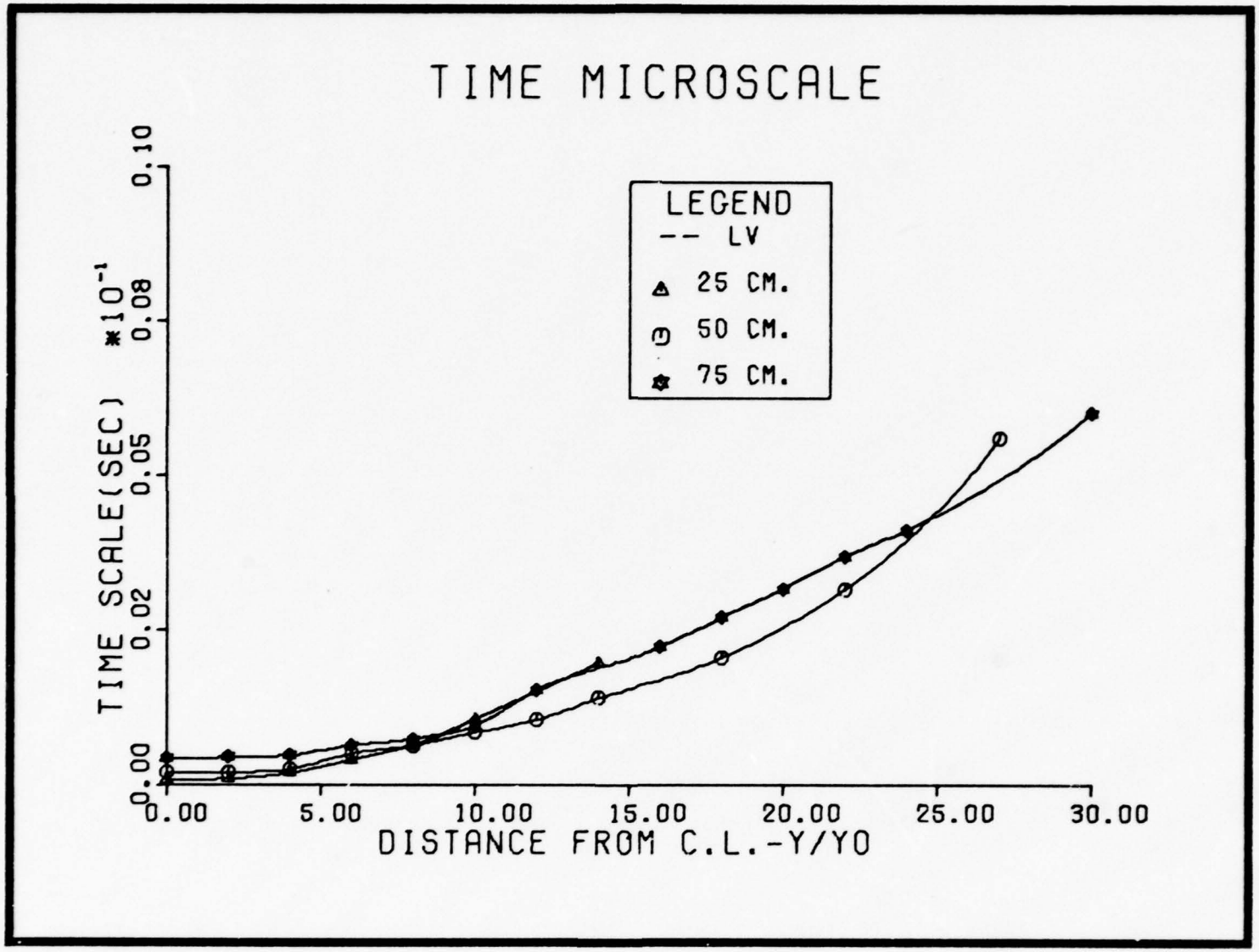

FIG. 43 TIME MICROSCALE AT M=0.8

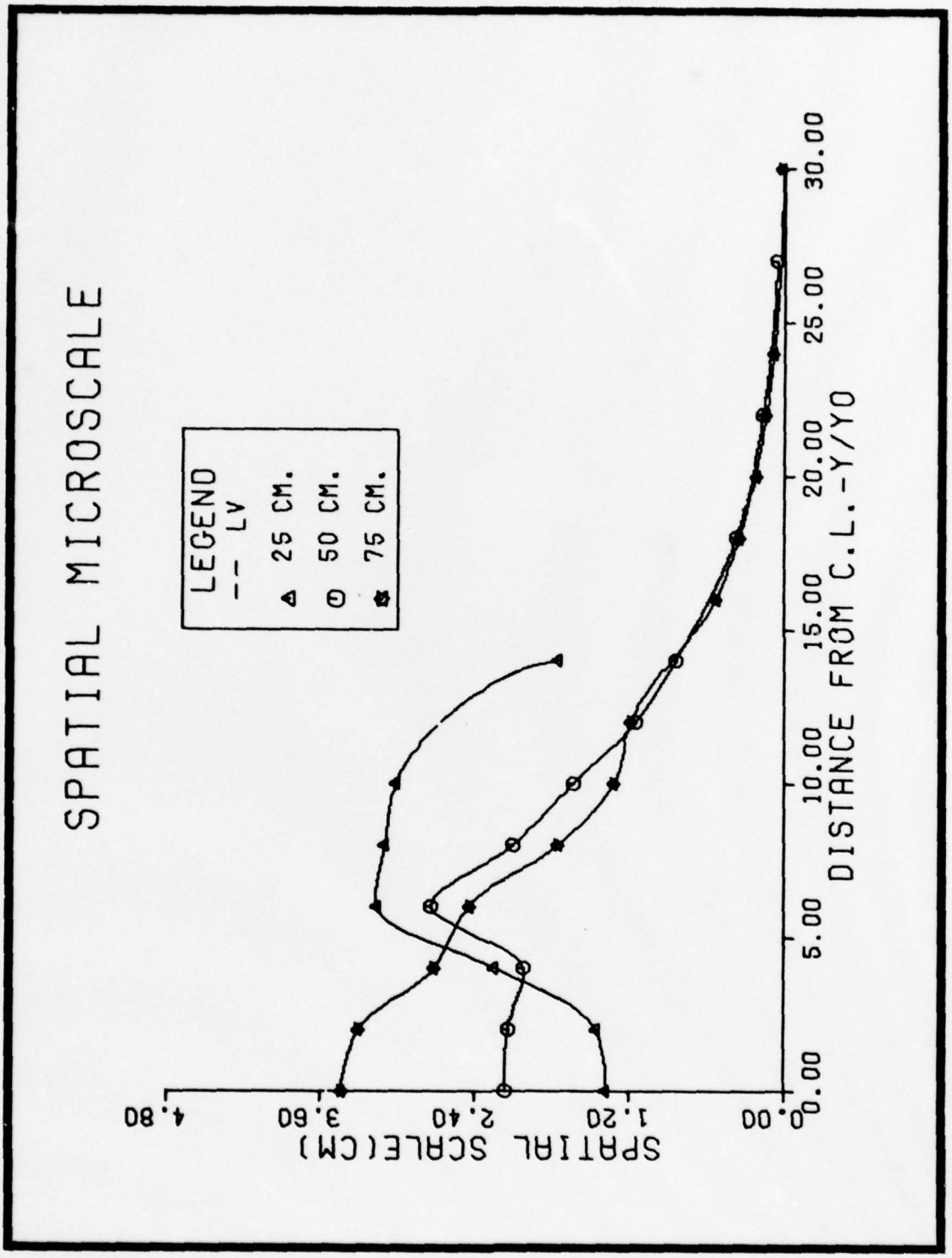

FIG. 44 SPATIAL MICROSCALE AT M=0.8

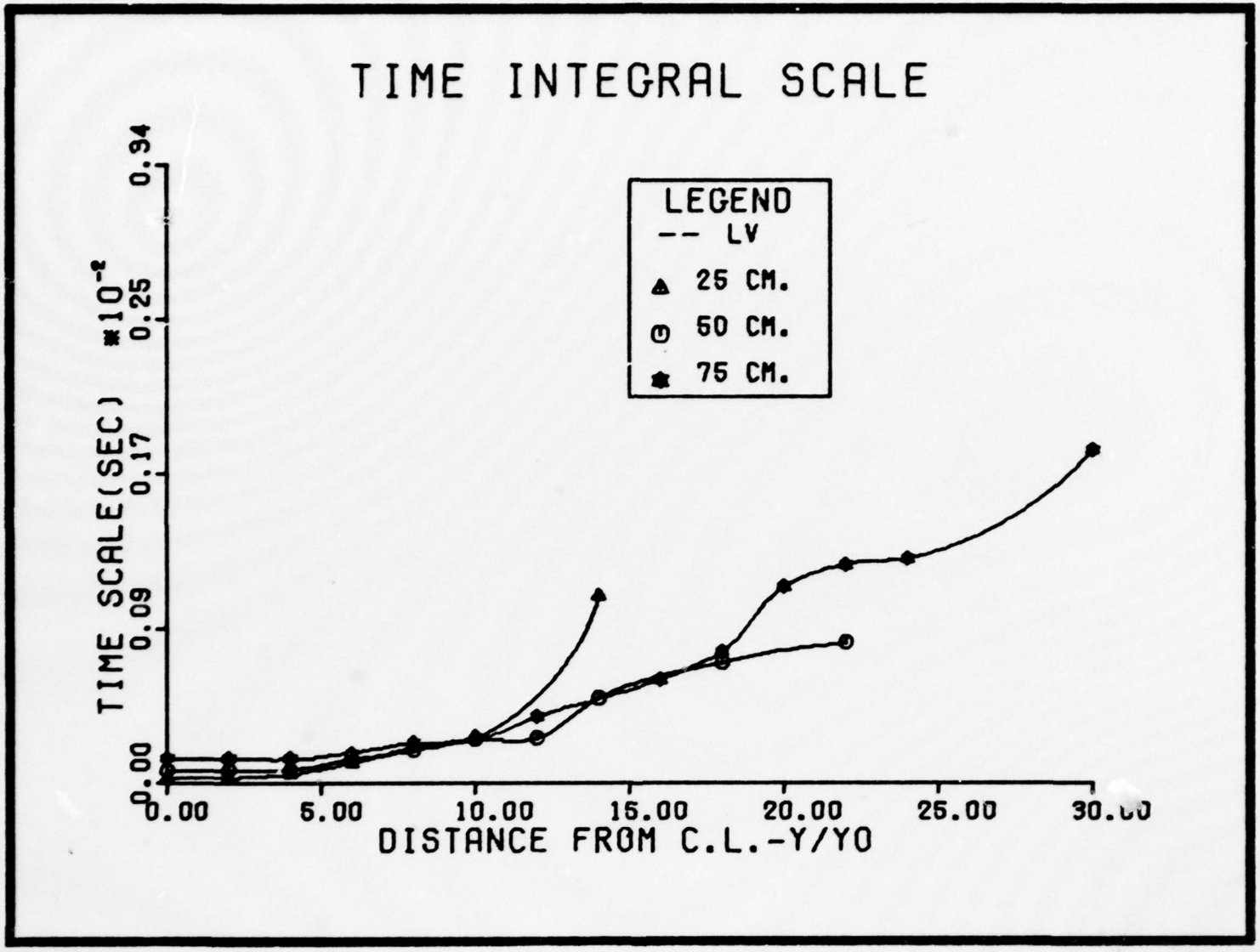

FIG.45 TIME INTEGRAL SCALE AT M=0.8

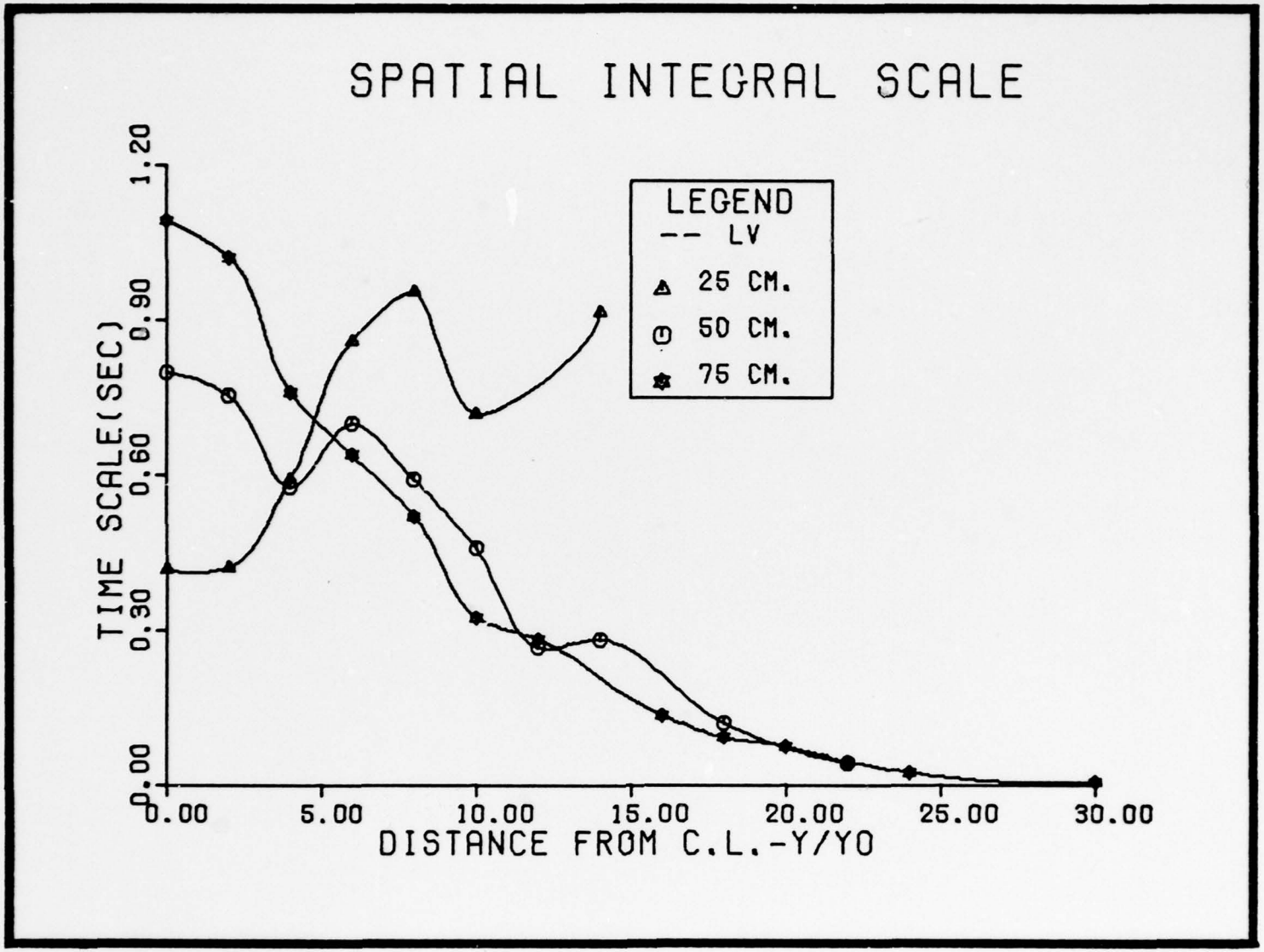

FIG.46 SPATIAL INTEGRAL SCALE AT M=0.8

Appendix H

Experimental Data

Table I

THEORETICAL CURVES USED FOR COMPARISON PURPOSES SIMILARITY			
GORTLER VALUES			
Y	ETA	$Y/Y_{1/2}$	U/U_{CEN}
0.000	0.000	0.000	1.000
.215	.066	.075	.996
.431	.132	.150	.983
.646	.198	.225	.962
.862	.264	.300	.933
1.077	.331	.375	.898
1.293	.397	.450	.858
1.508	.463	.525	.813
1.724	.529	.600	.765
1.939	.595	.675	.715
2.155	.661	.750	.665
2.370	.727	.825	.614
2.586	.793	.900	.564
2.801	.859	.975	.516
3.016	.925	1.050	.469
3.232	.992	1.125	.425
3.447	1.058	1.200	.384
3.663	1.124	1.275	.346
3.878	1.190	1.350	.310
4.094	1.256	1.425	.278
4.309	1.322	1.500	.248
4.525	1.388	1.575	.221
4.740	1.454	1.650	.196
4.956	1.520	1.725	.174
5.171	1.586	1.800	.154
5.386	1.653	1.875	.137
5.602	1.719	1.950	.121
5.817	1.785	2.025	.107
6.033	1.851	2.100	.094
6.248	1.917	2.175	.083
6.464	1.983	2.250	.073
6.679	2.049	2.325	.064
6.895	2.115	2.400	.057
7.110	2.181	2.475	.050
7.326	2.248	2.550	.044
7.541	2.314	2.625	.038
7.757	2.380	2.700	.034
7.972	2.446	2.775	.030
8.187	2.512	2.850	.026
8.403	2.578	2.925	.023

Table II

TOLLMIEN VALUES		
Y	$Y/Y_{1/2}$	U/U_{CEN}
0.000	0.000	1.000
.100	.104	.979
.200	.204	.940
.300	.313	.897
.400	.417	.842
.500	.521	.782
.600	.625	.721
.700	.730	.660
.800	.834	.604
.900	.938	.538
1.000	1.042	.474
1.100	1.147	.411
1.200	1.251	.357
1.300	1.355	.300
1.400	1.459	.249
1.500	1.564	.200
1.600	1.668	.165
1.700	1.772	.125
1.800	1.876	.095
1.900	1.980	.067
2.000	2.085	.046
2.100	2.189	.030
2.200	2.293	.020
2.300	2.397	.009
2.400	2.502	0.000

Table III

AXIAL VELOCITY DECAY	
THEORETICAL CURVE	
For a = .08 $\frac{U}{U_{COR}} = \frac{1.2}{\sqrt{\frac{ax}{Y_o}}}$	
x	$\frac{U_{CEN}}{U_{COR}}$
0.000	1.000
9.000	1.000
11.000	.905
13.000	.832
15.000	.775
17.000	.728
19.000	.688
21.000	.655
23.000	.626
25.000	.600
27.000	.577
29.000	.557
31.000	.539
33.000	.522
35.000	.507
37.000	.493
39.000	.480
41.000	.469
43.000	.457
45.000	.447
47.000	.438
49.000	.429
51.000	.420
53.000	.412
55.000	.405
57.000	.397
59.000	.391
61.000	.384
63.000	.378
65.000	.372
67.000	.367
69.000	.361
71.000	.356
73.000	.351
75.000	.346
77.000	.342

Table IV

HOT WIRE ANEMOMETER		
EXIT VELOCITY PROFILE		
HOT WIRE DATA		
M = .6		
Distance from Nozzle (Y)	Local Velocity (U)	$\frac{U}{U_{COR}}$
.475	4.500	.450
.470	8.000	.800
.465	8.600	.860
.463	9.800	.980
.456	9.840	.984
.450	9.880	.988
.444	9.920	.992
.438	9.960	.996
.432	9.980	.998
.426	10.000	1.000
.325	10.000	1.000
.225	9.900	.990
.125	9.800	.980
0.000	9.800	.980
-.125	9.790	.979
-.225	9.800	.980
-.325	9.800	.980
-.426	9.980	.998
-.432	9.960	.996
-.438	9.910	.991
-.444	9.950	.995
-.450	9.900	.990
-.456	9.850	.985
-.463	9.810	.981
-.470	7.500	.750
-.475	4.400	.440

Table V

AXIAL VELOCITY DECAY					
M = .4		M = .6		M = .8	
X	U	X	U	X	U
0.0000	19.9300	0.0000	2.0400	0.0000	10.1000
4.1660	19.8200	2.1340	2.0400	3.5310	10.0500
5.0550	19.7200	3.6580	2.0400	4.6740	10.0000
6.1980	19.4700	4.4200	2.0300	6.9600	9.7100
7.2140	19.1000	6.4520	2.0100	8.2300	9.4400
8.2300	18.6700	8.2300	1.9500	10.7700	8.8500
10.2620	17.7200	10.7700	1.8300	13.3100	8.4000
12.0400	16.8000	13.3100	1.7100	15.8500	8.0000
17.1200	15.0000	15.8500	1.6000	18.2900	7.6000
22.2000	13.4000	18.3900	1.5100	23.4700	6.9000
29.8200	11.6000	20.9300	1.4400	28.5500	6.3000
37.4400	10.2000	23.4700	1.3500	33.6300	5.8000
46.3300	8.9800	26.0100	1.2900	38.7100	8.3900
51.4100	8.3000	28.550	1.2300	43.7900	5.0000
56.4900	7.7000	32.3600	1.1600	48.8700	4.7000
61.5700	7.0500	36.1700	1.0900	53.9500	4.4000
66.5500	6.6000	39.9800	1.0300	59.0300	4.2000
71.6300	6.3000	43.7900	.9900	64.1100	3.9000
76.7100	6.0000	47.6000	.9300	71.7300	3.6000
86.8700	5.6000	52.6800	.8700	79.3500	3.4000
		57.7600	.8200	81.8900	3.3000
		62.8400	.7600	84.4300	3.2000
		67.9200	.7200	86.9700	3.1000
		73.0000	.6600	89.5100	3.0000
		76.8100	.6400		
		81.8900	.6100		
		84.4300	.5900		
		86.9700	.5700		

Table VI

SIMILARITY PROFILES

M = .4

25 cm		50 cm		75 cm	
Y	U	Y	U	Y	U
0.000	3.820	0.000	8.300	0.000	5.700
.370	3.570	.870	7.900	1.870	5.300
.870	3.280	1.870	7.000	2.870	5.000
1.270	2.770	2.870	5.900	4.870	3.900
1.870	2.280	3.870	4.900	5.870	3.500
2.200	1.910	4.510	4.150	6.870	2.850
2.870	1.290	4.870	4.000	8.870	1.930
3.370	.840	5.870	3.000	10.870	1.330
3.870	.600	6.870	2.100	11.870	1.000
4.370	.300	7.870	1.567	13.370	.667
5.370	.153	8.870	1.000	14.870	.500
5.870	.117	10.370	.500	16.370	.300
6.370	.036	11.870	.300	17.870	.200
6.870	.026	13.370	.220	20.870	.150

M = .6

25 cm		50 cm		75 cm	
Y	U	Y	U	Y	U
0.000	3.850	0.000	8.500	0.000	6.000
.370	3.750	.870	8.100	.870	5.800
.870	3.360	1.370	7.900	1.870	5.600
1.370	2.850	2.370	6.700	2.870	5.200
1.870	2.300	3.370	5.500	3.870	4.600
2.225	1.970	4.370	4.400	5.870	3.600
2.370	1.790	4.490	4.250	7.320	3.000
2.870	1.290	5.370	3.400	8.870	2.100
3.370	.900	6.370	2.500	9.870	1.700
3.870	.590	7.370	1.800	10.870	1.400
4.370	.370	8.870	.967	14.870	.550
4.870	.240	10.370	.567	16.370	.390
5.370	.180	11.870	.333	18.870	.220
6.370	.130	13.370	.290	19.870	.200

Table VI (cont.)

SIMILARITY PROFILES					
M = .8					
25 cm		50 cm		75 cm	
Y	U	Y	U	Y	U
0.000	5.700	0.000	5.100	0.000	4.300
1.000	5.300	2.000	4.500	2.000	4.000
2.000	4.300	3.000	3.900	3.000	3.600
2.960	2.850	4.000	3.300	5.000	2.600
3.000	2.800	5.000	2.550	6.030	2.150
4.000	1.700	6.000	2.000	7.000	1.800
5.000	1.100	7.000	1.500	10.000	.900
6.000	.700	8.000	.990	12.000	.450
7.000	.290	11.000	.240	14.000	.190
8.000	.140	13.000	.130	16.000	.090
9.000	.130	15.000	.100	18.000	.060

Table VII
LASER VELOCIMETER EXIT VELOCITY PROFILE

M = .6 S = 62.43μm

Station	Channel of Peak	Sample Time (μsec)	Velocity (m/sec)
-0.6	9.2	0.05	201.4
-0.5	9.3	0.05	198.2
-0.4	9.3	0.05	198.2
-0.3	9.3	0.05	198.2
-0.2	9.2	0.05	201.4
-0.1	9.2	0.05	201.4
0.0	9.2	0.05	201.4
0.1	9.1	0.05	204.7
0.2	9.1	0.05	204.7
0.3	9.1	0.05	204.7
0.5	9.1	0.05	204.7
0.7	9.0	0.05	208.1

Table VIII

AXIAL VELOCITY DECAY							
X Station (cm)	Sample Time (μsec)	M = .4		M = .6		M = .8	
		Channel of Peak	U m/sec	Channel of Peak	U (m/sec)	Channel of Peak	U (m/sec)
0.000	.05	12.0	138.7333	9.5	192.0923	8.0	249.7200
2.030	.05	12.0	138.7333	9.5	192.0923	8.0	249.7200
4.060	.05	12.0	138.7333	9.5	192.0923	8.0	249.7200
6.090	.05	12.5	131.4316	9.5	192.0923	8.0	249.7200
7.110	.05	12.8	127.4082	9.8	183.6176	8.0	249.7200
8.380	.05	13.0	124.8600	10.0	178.3714	8.0	249.7200
9.650	.05	13.0	124.8600	10.0	178.3714	8.2	240.1154
10.920	.05	13.0	124.8600	10.0	178.3714	8.4	231.2222
12.190	.05	13.5	118.9143	10.3	171.0411	8.5	227.0182
13.460	.05	14.0	113.5091	10.5	166.4800	8.8	215.2759
14.730	.05	14.0	113.5091	10.8	160.0769	9.0	208.1000
17.270	.05	15.0	104.0500	11.0	156.0750	9.0	208.1000
19.810	.05	15.5	99.8880	11.5	146.8941	9.5	192.923
22.350	.05	16.0	96.0462	12.0	138.7333	9.8	183.6176
24.890	.05	16.8	90.4783	12.5	131.4316	10.0	178.3714
27.430	.05	17.0	89.1857	12.8	127.4082	10.5	166.4800
29.970	.05	17.5	86.1103	13.0	124.8600	10.8	160.0769
32.510	.05	18.5	80.5548	13.5	118.9143	11.0	156.0750
35.050	.05	19.0	78.0375	14.0	113.5091	11.3	150.4337
37.590	.05	20.0	73.4471	14.5	108.5739	12.0	138.7333
42.670	.05	21.0	69.3667	15.2	102.3443	12.5	131.4316
47.750	.05	22.0	65.7158	16.2	94.5909	13.0	124.8600
52.830	.05	24.0	59.4571	17.5	86.1103	14.0	113.5091
57.910	.05	25.0	56.7545	18.0	83.2400	14.6	107.6379
62.990	.05	26.5	53.1319	19.0	78.0375	15.5	99.8880
68.070	.05	28.5	48.9647	20.4	71.7586	16.2	94.5909
73.150	.05	20.0	46.2444	21.5	67.4919	17.0	89.1857
78.230	.05	31.5	43.8105	22.5	64.0308	18.0	83.2400
83.310	.05	33.7	40.6710	24.0	59.4571	18.5	80.5548
88.390	.05	35.0	39.0188	25.0	56.7545	19.0	78.0375

Table IX

SIMILARITY PROFILES		M = .4		S = 16.07μm	
$Y_{\frac{1}{2}}$ = 2.05	25 cm				
Y(cm)	Channel of Peak	Sample Time	Frequency kH_z	g_1	g_2	g_3
0.000	6.3	0.05	682.			
.200	6.4	0.05	684.			
.600	6.5	0.05	686.			
1.000	7.0	0.05	747.			
1.800	8.5	0.05	722.			
2.800	10.0	0.05	1108.5			
3.300	11.0	0.05	1109.7	619,094	628,489	617,546
3.800	13.0	0.05	1110.2	450,247	518,289	503,392
4.300	14.0	0.05	1110.4	1,015,210	1,093,996	1,050,306
4.800	15.3	0.05	1109.4	456,965	509,183	476,803
5.300	15.0	0.1	676.4	649,080	726,351	672,566
5.800	16.5	0.1	670.0	1,453,331	1,554,948	1,517,826
6.300	17.0	0.1	607.5	1,021,559	1,138,160	1,068,216
$Y_{\frac{1}{2}}$ = 5.2 cm	50 cm					
0.000	8.0	.05	1112.4	860,691	1,278,195	1,212,791
.500	8.0	.05	1108.0	178,986	205,036	192,721
1.500	8.3	.05	1113.0	241,029	276,806	262,665
2.000	8.5	.05	1112.9	518,796	590,028	565,964
2.500	9.0	.05	1110.9	486,772	551,372	530,506
3.500	10.0	.05	1115.5	113,256	123,350	121,135
6.000	13.0	.05	639.6	246,833	266,072	258,656
8.000	16.5	.05	707.6	353,221	379,509	368,647
9.000	22.0	.05	587.5	121,897	130,534	126,653
10.000	14.0	.1	681.9	301,532	318,016	306,782
11.000	15.0	.1	681.9	433,154	465,530	437,220
12.000	16.0	.1	710.4	251,392	278,892	254,166
15.000	20.0	.1	573.4	256,854	314,978	260,405
$Y_{\frac{1}{2}}$ = 7.6 cm	75 cm					
0.000	9.0	.05	1113.1	111,077	120,272	118,163
2.000	9.2	.05	1112.9	108,291	117,769	115,061
3.000	9.5	.05	1112.9	257,299	277,758	274,230
4.000	10.0	.05	1112.7	536,643	574,251	563,300
5.000	10.5	.05	1112.5	312,642	331,589	328,574
6.000	11.0	.05	1112.4	347,933	364,056	360,975
8.000	12.0	.05	1095.1	152,853	158,957	156,432
10.000	15.0	.05	919.5	205,253	218,302	211,215
11.000	16.0	.05	917.6	110,107	117,872	112,976
12.000	20.0	.05	708.3	110,007	119,755	114,362
14.000	13.0	.1	726.9	188,178	206,494	195,381
16.000	17.0	.1	572.9	269,550	300,913	276,796
21.000	20.0	.1	570.0	146,243	163,608	146,695

Table IX cont.

SIMILARITY PROFILES			M = 0.6			
$Y_{\frac{1}{2}}$ = 7.0cm			75 cm			
Y(cm)	Channel of Peak	Sample Time	Frequency (KH_z)	g_1	g_2	g_3
0.000	8.2	.05	-498.			
1.000	8.5	.05	-499.			
2.000	9.0	.05	-499.			
2.500	9.0	.05	-499.			
3.500	8.0	.05	497.0			
4.000	8.3	.05	497.0			
4.500	8.7	.05	497.0			
5.000	9.0	.05	498.0	448,946	474,020	460,211
6.000	9.5	.05	498.0	492,202	522,860	514,619
7.000	10.0	.05	680.0	880,701	931,482	917,531
10.000	13.0	.05	772.0	445,875	465,698	456,673
11.000	.0	.05	767.0	882,444	920,080	900,917
12.000	17.0	.05	759.0	579,853	609,157	596,009
14.000	22.0	.05	750.0	452,930	479,041	464,817
17.000	27.0	.05	755.0	452,999	500,779	461,796
19.000	29.0	.05	756.0	451,746	522,262	456,353
21.000	22.0	0.10	503.0	628,723	723,198	634,155

Vita

Captain Nino G. Cerullo was born in Italy in 1946. In 1958, he emigrated to Canada. He graduated from high school in Toronto in 1965 and subsequently enrolled in an Aeronautical Technology course at Ryerson Polytechnical Institute. He graduated in 1968. In June 1968, he enrolled in the Canadian Armed Forces as a Maintenance Engineering Officer and served in that capacity at Canadian Forces Base Bagotville, Quebec and Canadian Forces Station Val D'Or, Quebec. In 1975, he was chosen to attend the Canadian Forces Military College in Kingston, Ontario as an academic upgrading process and he graduated with a Bachelor of Science degree in 1977. In that same year, he was chosen to attend the Air Force Institute of Technology in the Graduate Aeronautical Engineering program.

Permanent address: 60 Hamptonbrook Dr.
Weston, Ontario
Canada
M9P 1A1